Development of Aluminium-Based Lewis Acids as Catalysts for Organic Transformations

Dissanayake Mudiyanselage Deepamali Dissanayake

Bachelor of Science (Honours), Master of Science.

A thesis submitted for the degree of *Doctor of Philosophy* at

Monash University in 2022

(*School of Chemistry*)

Copyright notice

Abstract

Catalysis is a key component in organic synthesis and Lewis acid catalysis is one of the major features of it. This thesis focuses on the development of aluminium based Lewis acid complexes as catalysts for various transformations.

The main aspect of this thesis is to structurally modify one of our published achiral aluminium based Lewis acid complexes in order to form a series of chiral complexes. In addition, we also intend to widen the applications of the published achiral system to new organic reactions.

Chapter 1 of this thesis chronicles the development of Lewis acid compounds used for (a)chiral catalysis. This is then followed by our proposal about the target structural variations of the existing complex in order to convert it into a series of chiral complexes.

Chapter 2 describes the synthesis of the chiral complexes with the focus on modifying the steric features away from the chiral carbon atom (achiral end) of the supporting ligand. The influence of these ligand's steric modifications on catalytic properties of the prepared aluminium complexes is then investigated with the focus on difficult-to-execute asymmetric Diels-Alder transformations.

Chapter 3 presents the synthesis of the target chiral complexes with the focus of modifying the ligand's structural features adjacent to the chiral centre (chiral end) followed by exploring the complexes' abilities for enantioinduction towards selected asymmetric Diels Alder reactions.

Chapter 4 of this thesis focuses on using the existing achiral and newly-developed chiral aluminium complexes in symmetric and asymmetric hydrosilylation reactions, respectively.

Chapter 5 brings in the possible future directions of the project, while the appendix section contains all the experimental details and data relevant for this study.

Declaration

This thesis is an original work of my research and contains no material which has been accepted for the award of any other degree or diploma at any university or equivalent institution and that, to the best of my knowledge and belief, this thesis contains no material previously published or written by another person, except where due reference is made in the text of the thesis.

Name: D.M. Deepamali Dissanayake

Date: 27/10/2022

Publications

- **Dissanayake D**.; Forsyth C.; Vidović D. 'Synthesis, Characterisation and Reactivity studies of Chiral β-Diketiminate Supported Aluminium Lewis Acid Complexes towards Difficult Diels Alder Cycloadditions - *A study of structure vs. ability of enantioinduction'*; *manuscript in preparation.*

Presentations

- **Dissanayake D**.; Vidović D., 'Synthesis of well-defined chiral aluminium based catalysts'. Oral presentation, RACI national congress- Brisbane, QLD, Australia, July 2022.

- **Dissanayake D**.; Vidović D., 'Synthesis of Chiral Aluminium Based Complexes for catalysis of asymmetric Diels Alder Reactions'. Oral presentation, OZOM13, 13th Australasian Organometallics Meeting, Cairns, QLD, Australia, July 2022.

- **Dissanayake D**.; Vidović D., 'Synthesis of well-defined chiral aluminium based catalysts'. Poster, Inorganic Chemistry Symposium–RACI Victorian branch, Melbourne, VIC, Australia, December 2019.

- **Dissanayake, D**.; Zhai, S.; Liu, Z.; Draper, A.; McAllister, W.; Vidović D., 'Lewis acids: Versatile catalysts for fundamental transformations and polymerisations'. Poster, OZOM12, 12th Australasian Organometallics Meeting, Melbourne, VIC, Australia, July 2019.

Acknowledgements

I would never have imagined getting this far in my life, if not for the tremendous amount of support I have received from great many people. Therefore, I extend my sincere gratitude,

to my parents, who are my great pillars of success, without their sacrifices, unconditional love and support, completing this thesis or simply being the person, I am today, would not be possible.

to Ryan, for his love, care, unwavering support and patience throughout these long years I have spent studying and chasing my dreams.

to my supervisor Dr. Drasko Vidović, for giving me the opportunity to join his lab, his continuous support and encouragement throughout this time specially when the chemistry was not very cooperative. I could not ask for a better supervisor than you and am forever grateful for your inspiration, guidance and very many things I have learnt from you.

to Vidović group members of the past, Dr. Zhizhou Liu, Alysia Draper, Will McAllister, for your warm welcome and help during the initial settle down-period in the lab.

to the present Vidović group members, Mike (Siyuan Zhai), Mostafa Kamal, Dr. Palak Garg, and Neelofur Jaunnoo for all their support and being excellent colleagues.

to Dr. Vicki Blair and Blair group members for sharing their glove box and to all professional and research support staff at Monash School of Chemistry, including Phil Holt, Dr. Alasdair McKay, Anna Severin, Dr. Boujemaa Moubaraki, Dr. Craig Forsyth, Scott Blundell and our librarian Romney Adams for their immense support throughout.

to my friends at Monash, Iyomali, Sneha, Manjiri, Dr. Minoli Aponso, Tania, Dr. Yudhi Kuniawan, Meri, and many more for their great friendship, lovely memories and support.

to Derek Hewitt for his time and invaluable support in reading and correcting grammatical mistakes in this thesis.

to my dear brother, in-laws, all other family members, friends, and anyone I could not mention by name due to limited amount of space, for their great love and support.

Finally, to the Australian Government Research Training Program (RTP) Scholarship, for the financial support provided for the past few years.

Abbreviations

Å	Angstrom
°	Degrees
°C	Degrees Celsius
β	Beta
δ	Chemical shift
2D	Two dimensional
3D	Three dimensional
Ac	Acetyl
ac-ac	Acetylacetonate
Ar	General aryl functional groups
Ar^{Cl}	3,5-$Cl_2C_6H_3$
BINAP	1,1′-binaphthalene]-2,2′-diyl)bis(diphenylphosphane)
BINOL	1,1’-binaphthol
br.	Broad
c	Concentration in g/ 100 mL
Cat.	Catalyst
Cp	Cyclopentadienyl
$CDCl_3$	Deuterated - chloroform
d	Doublet
dd	Doublet of a doublet
DA	Diels Alder cycloadditions
dba	Dibenzylideneacetone
DCM	Dichloromethane
DIOP	2,3-*O*-isopropylidene-2,3-dihydroxy-1,4 bis(diphenylphosphino)butane)
Dip	2,6-diisopropylphenyl
ee	Enantiomeric excess
Et	Ethyl
eq. / equiv.	Equivalent

GLC	Gas Liquid Chromatography
h	Hours
HBA	Hidden Brønsted Acids
HOMO	Highest Occupied Molecular Orbital
HPLC	High Performance Liquid Chromatography
HRMS	High Resolution Mass Spectrometry
i-Pr	*Iso*-propyl
i-PrOH	*Iso*-propanol
J	Coupling constant
L	Ligand, laevorotatory
LUMO	Lowest Unoccupied Molecular Orbital
M	Metal
m	Multiplet
m	Meta
Me	Methyl
Mes	Mesityl = 1,3,5-trimethylphenyl
min	Minutes
MS	Molecular sieves
^{n}BuLi	*N*-butyllithium
NBS	*N*-bromosuccinimide
NMR	Nuclear Magnetic Resonance
Nu	Nucleophile
o	Ortho
OTf	Triflate = CF_3SO_3
p	Para
Ph	Phenyl
ppm	Parts per million
PYBOX	Pyridine-bisoxazolines
R, R_x (x=1,2,3…), R’	Alkyl functional groups
(*R*)	Rectus- right, clockwise
rac	Racemic
RT	Room Temperature
(*S*)	Sinister- left, anticlockwise

s	Singlet
salen	Salicylaldehyde-ethylenediamine
t	Triplet
TADDOL	Tetraaryl-1,3-dioxolane-4,5-dimethanol
Taxol	Paclitaxel
t-Bu	*Tertiary*-butyl
tert	Tertiary
THF	Tetrahydrofuran
TLC	Thin Layer Chromatography
TMP	2,2,6,6-tetramethylpiperidine
TON	Turn Over Number
TOF	Turn Over Frequency
t_R	Retention time
Ts	*Para*-toluenesulfonyl
TMS	Trimethylsilyl
Xyl	2,6-dimethylphenyl
q	Quartet

Table of content

Chapter 1

1. Introduction

1.1 Lewis acid catalysis in organic synthesis

Lewis acids are typically known as electron deficient species which can accept a pair of electrons.[1] This definition encapsulates a wider range of classical acids (including H^+), non-metallic and metallic species, expanding its applicability into a much broader field. The versatile range of species categorised as Lewis acids, which can easily bind to many substrates, reagents, and intermediates with their ability to accept a pair of electrons, arguably creates the most extensive class of man-made catalysts.[2] Crowned as one of the most prominent type of catalysts, Lewis acid species are well known to play a vital role in classical as well as modern synthetic organic chemistry.[3,4]

There are a number of elements such as Al, Au, Sb, B, Cd, Ce, Co, Cu, Eu, Ge, Hf, Fe, Ln, Li, Mg, Mo, Ni, Pd, P, Si, Ag, Ru, S, Tl, Sn, Ti, V, Yb, Zn, and Zr [2,4,5] known to show Lewis acidic properties, which, as salts or when coordinated with suitable ligands, can be developed into very useful catalytic systems. Many types of organic reactions such as C-C bond formation reactions, reductions, oxidations, catalytic rearrangements, cyclisation reactions and polymerisations are known to be catalysed by these electron deficient species.[2,4] While many of the early discoveries of Lewis acid catalysis featured relatively simple species such as, $AlCl_3$, $TiC1_4$, $BF_3 \cdot OEt_2$, and $SnCl_4$ for conventional organic synthesis applications, in most of the cases, significant regio-, stero-, and chemo-selectivities were not displayed.[2] On the other hand, these classic Lewis acids were also incapable of asymmetric synthesis. Having supporting ligands coordinated to the metal/element centres had certainly brought the potential of "trying to mimic" the core of different functional groups in an enzyme binding site, via tuneable electronic, steric and structural properties (such as chiral centres), allowing these systems/compounds to be utilised as catalysts in reactions considered important in modern organic synthesis.[4]

C-C bond formation reactions are considered as the most popular application of both classical and modern Lewis acid catalysis fields. Given their electron deficiency, Lewis acids are well known to bind to heteroatoms (O or N) of various substrates, enhancing the substrates' reaction feasibility by lowering the energy of the LUMO level.[6] Thus, reactions of carbonyl compounds in transformations such as aldol reactions, Mukaiyama aldol reactions (using $TiCl_4$, $BF_3 \cdot Et_2O$, $B(C_6F_5)_3$, **A** (Figure 1.1)), and Michael additions (using $BF_3 \cdot Et_2O$, LiAlBINOL (BINOL = 1,1′-bi-2-naphthol), $Bu_2Sn(OTf)_2$ (OTf = triflate = CF_3SO_3), $SnC1_4$, and Et_3SiClO_4), have been reported to be catalysed by Lewis acids.[4] The famous Friedel Crafts alkylations and acylations (catalysed by BF_3, $AlCl_3$, $AlBr_3$, copper triflates (for indole derivatives)), allylations (catalysed by **B**, Figure 1.1), (*S*)-BINAP $\cdot$AgOTf (BINAP = [1,1′-Binaphthalene]-2,2′-diyl)bis(diphenylphosphane)) and carbonyl-ene reactions (catalysed by **C**, Figure 1.1) are also among the many useful C-C bond formation reactions known to be catalysed or mediated by various Lewis acid catalysts.[4]

Furthermore, oxidation and reduction reactions such as Baeyer-Villiger oxidation by $Me_3SiOSO_2CF_3$, Oppenauer oxidation by $Al(i\text{-}PrO)_3/C_6F_5B(OH)_2$, acetal reductions by $TiCl_4$, together with rearrangement reactions such as, epoxide rearrangements with $BF_3 \cdot Et_2O$, pinacol rearrangements with $SbCl_5$-$AgSbF_6$ system, Claisen rearrangements (with **D**, Figure 1.1) are also among the types of organic reactions catalysed by Lewis acids.[4] Other important reactions such as, Diels Alder cycloadditions (catalysed with $BF_3 \cdot Et_2O$, $MgBr_2$, $ZnCl_2$) and olefin polymerisation (catalysed by $B(C_6F_5)_3$) demonstrate the enormous versatility of Lewis acid catalysis as applied in organic synthesis.[2,4]

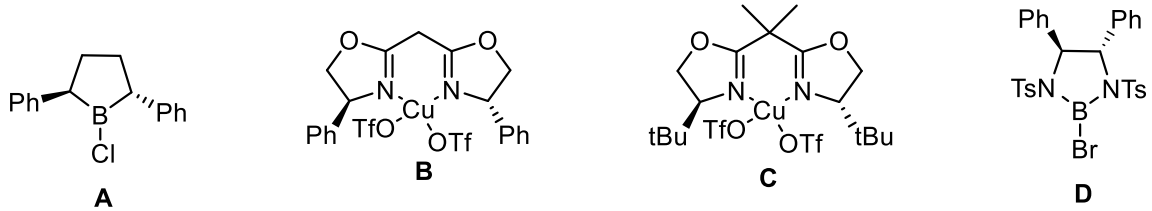

Figure 1.1: Examples of Lewis acid catalysts

More recent advancements in the field of Lewis acid catalysis, also allowing for the currently growing need of developing environmentally sustainable reaction processes, include the development of recyclable yet effective species such as Lewis acids supported on solid surfaces.[7]

1.2 Aluminium based Lewis acids in catalysis

Aluminium, being a member of group 13 in the periodic table, is naturally capable of accepting a lone pair of electrons in its neutral, three coordinated state. Complimented by its high abundancy as the richest metal in Earth's crust (~ 8 by weight)[8] and electron deficient nature, Al is one of the most widely used elements in the field of Lewis acid catalysis. It is also desired in commercial applications as it appears in the lower region in terms of toxicity and price, compared to many other metals such as Ag, Au, Ti, Pt, Pd, Cr, Ru etc.[4,9] One of the most well-known and earliest discoveries in Al based catalysis in organic chemistry dates back to as early as 1877, where aluminium chloride was used in Friedel Crafts reactions.[4,10] Another similarly renowned discovery is the use of inexpensive alkylaluminium compounds as versatile co-catalysts in olefin polymerisation reactions with $TiCl_4$. This reaction later became famously known as "Ziegler and Natta polymerisation", for which the two scientists Karl Ziegler and Giulio Natta received the 1965 Nobel prize.[4,11] Followed by these discoveries, other simple Al compounds such as aluminium alkoxides were used as efficient catalysts in Meervein-Ponndorf-Verley reduction, allylic alcohol epoxidations and hetero Diels Alder reactions, while alkylaluminium compounds were effectively used in reactions such as Beckmann rearrangement and alkylation reactions.[4,12–14]

A more recent use of Al based Lewis acid complexes included the exploration of their catalytic properties for reductions of various substrates such as carbonyls, alkenes, alkynes and imines. For instance, hydroborations by Al-H containing complexes (**E** by Roesky and co-workers[15], **F** by Nembenna and co-workers[16] Figure 1.2), cyanation reactions (**G** by Roesky and co-

workers[17], **H** by Verkade and co-workers[18,19] Figure 1.2), hydrosilylations by cationic Al complexes (**I** by Bergman and co-workers[20], **J** by Venugopal and co-workers[21], **K** by Nembenna and co-workers[22] Figure 1.2), hydrophosphonylations (using Et_2AlCl, $AlEt_3$ or $Al(O\textit{i}\text{-}Pr)_3$ with tridentate Schiff base ligands by Feng and co-workers[23]), hydrophosphinations (using $^{i}Bu_3AlPPh_2Li(THF)_3$ by Mulvey and co-workers[24]), and hydroaminations (**L** by Bergmann and co-workers[25] Figure 1.2) are some examples of the reactions catalysed by Al-based complexes. Moreover, several other reactions such as oxidations (eg: Oppenauer oxidations of both primary and secondary alcohols by $AlMe_3$ as demonstrated by Nguyen co-workers[26]), conjugate additions (by salen based Al systems[11] (salen = tetradentate C_2-symmetric ligands synthesised from salicylaldehyde (sal) and ethylenediamine (en))), Mukaiyama Aldol reactions (by **H** Figure 1.2), and several different cyclisation reactions such as Diels Alder cycloadditions (using cationic Al complex **M** by Vidović and co-workers[27] Figure 1.2) have also been reported as reactions catalysed by Al based Lewis acidic complexes. Evidently, the number of Al based Lewis acid catalytic systems and their applicability in both classical and modern organic synthesis is tremendous.

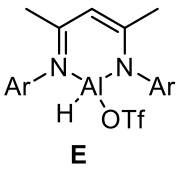

E

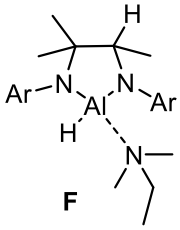

F

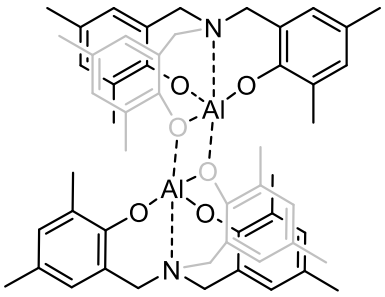

H

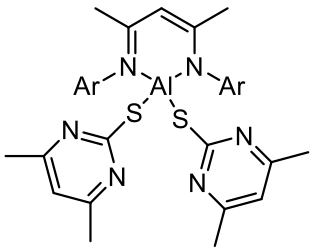

G

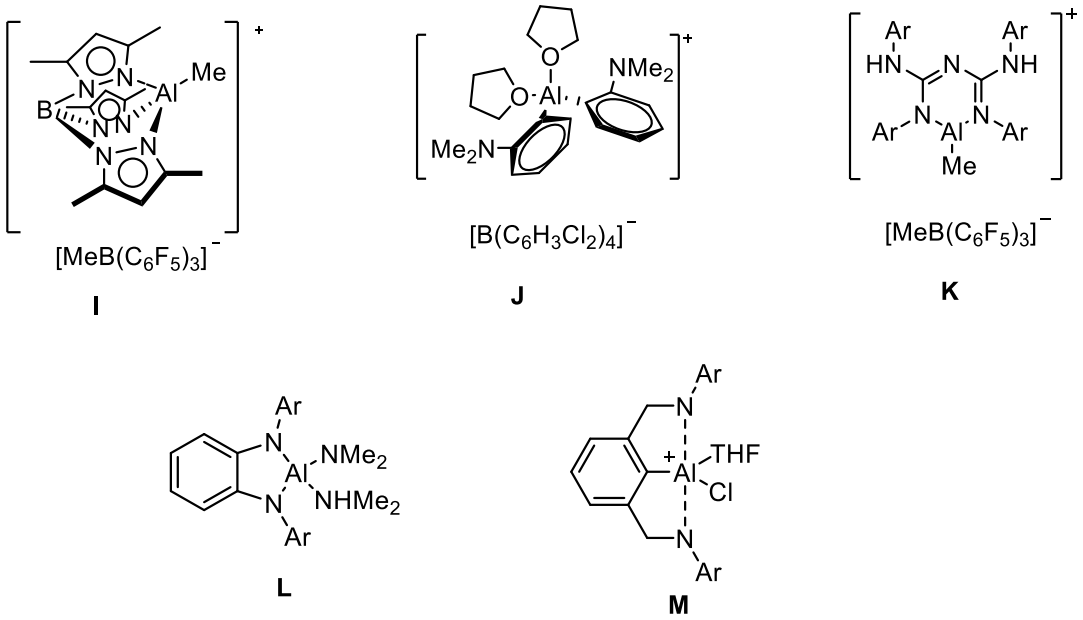

Figure 1.2: Examples of Al based Lewis acid catalysts

1.3 Hidden Brönsted acids (HBA)

As mentioned earlier, given the popularity of Lewis acids in the world of catalysis, an extremely large number of Lewis acid compounds have been studied for this particular purpose producing many important scientific reports. However, a vast majority of these early reports did not dedicate any significant attention to how (reaction conditions) these reactions were carried out nor they discussed the structural properties of the catalytically active species. In fact, most of these reactions were done under atmospheric conditions while *in situ* preparation and use of Lewis acid compounds as catalysts in these transformations were also very common. This had not been identified as an issue until recently, when the ability of Lewis acids to create hidden Brønsted acids *in situ* had been experimentally observed.[28–32] Some recent publications showed that, the catalytic activity of most of the claimed but unidentified Lewis acidic active species could have been due to their ability to create hidden Brønsted acids (HBAs) and not due to their Lewis acid properties. For example, Fringuelli et al. reported catalytic activity of [$AlCl_3$ + 2 THF] towards Diels Alder cycloaddition reactions, under atmospheric conditions.[33]

However, $AlCl_3$ (i.e. Al_2Cl_6), being an extremely air and moisture sensitive compound, could have easily hydrolysed creating HBA (presumably HCl) sites, which in this case, most probably had been the active catalyst responsible for the observed reaction. A similar example is AgOTf, discussed by Hintermann and co-workers as it could easily convert into an HBA (HOTf).[28] This confirmed the ability of most of these "so called Lewis acid catalysts" to nurture Brønsted acids by *in situ* hydrolysis or reaction with solvent molecules. As identifying active species gives the key idea about the underlying mechanisms of catalytic reactions, one must agree that these hidden mechanisms and uncontrolled active site formation make the reproducibility of these catalytic systems highly questionable.

Therefore, in order to confirm that the actual catalytically active species responsible for catalysis is truly a Lewis acid, these catalytic reactions need to be carried out strictly under air and moisture free atmosphere i.e. by adhering to standard Schlenk and glove box techniques. In addition, avoiding the preparation and use of *in situ* catalytic systems and defining the active species responsible for the catalytic activity, at least in its solid state by means such as single crystal X-ray diffraction, is also crucial. Moreover, as Bates and co-workers elaborated, the need of testing for the presence of these hidden Brønsted acids in a catalytic system by carrying out relevant control experiments was also important. For example, testing the catalytic activity in the presence of a proton scavenger such as, 2,6-di-tert-butylpyridine or Me_3SiPh is highly recommended.[29] Additionally, choosing substrates that are known to be difficult to convert with HBAs/Brønsted acids can provide additional evidence for true Lewis acid activity of the examined complex(es) and hence eliminate the possibility of HBA presence. For instance, using 2,3-dimethylbutadiene or 1,3-cyclohexadiene in Diels Alder cycloaddition reactions (which are around 250 and 500 times less reactive than the commonly used cyclopentadiene, respectively) should also give the researchers and the readers a reasonable idea about the potential presence of HBAs in a Lewis acid catalytic system.[11] However, it is considered that

at least a few of the above recommended precautions have to be accommodated in a study in order to adequately support the claim of "true Lewis acid catalytic activity".

1.4 A well-defined, "true" aluminium based Lewis acid catalyst

Under these circumstances, attempts have been taken by our group to synthesise well-defined, "true" Al-based Lewis acid complexes that can act as efficient catalysts in organic transformations. As a result, a collection of Al complexes supported by β-diketiminate backbones and triflate groups were successfully synthesised. These were first reported in 2015 (see Figure 1.3 and Figure 1.4).[31] The expectation was to have triflates acting as good leaving groups providing the incoming substrates sufficient space to bind to the Al centre. In addition, β-diketeiminato ligands, also known as "nac-nac" ligands, were incorporated to have different substituents on the nitrogen atoms such as substituted aryl groups allowing us to tune both electronic and steric properties of the explored electron deficient compounds for an optimal level of catalytic activity. As anticipated, multinuclear NMR spectroscopic data and single crystal X-ray diffraction analyses revealed that the basic structure of these complexes in their molecular form contained an Al centre coordinated by two weakly bound electron-withdrawing triflate groups.

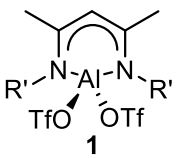

1

1a $^{Dip}LAl(OTf)_2$: R' = 2,6-iPr_2-C_6H_3

1b $^{Xyl}LAl(OTf)_2$: R' = 2,6-,Me_2-C_6H_3

1c $^{Ph}LAl(OTf)_2$: R' = C_6H_5

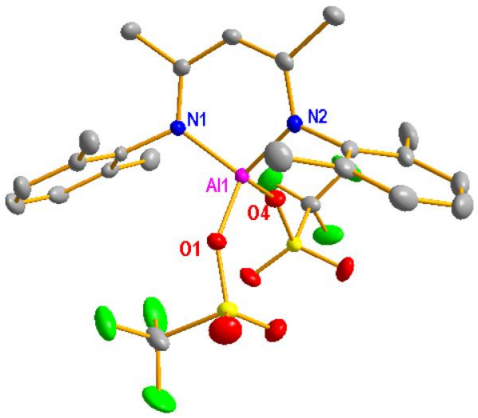

Figure 1.3: β-diketiminate supported aluminium bistriflate complexes by our group; example for crystal structure, **1b** (right)

On the other hand, β-diketiminato supporting ligand formed strong bonds with the metal in a bidentate fashion, facilitating tuneable steric and electronic properties (Figure 1.3). When the catalytic activity of these complexes towards Diels Alder cycloaddition reactions was initially tested, it was observed that the targeted transformations were not achieved, even though coordination of the dienophile to the Al centre was evident via ^{1}H NMR spectroscopy.[31] Therefore, the complexes were further activated by addition of 1 equivalent of $Na[BAr^{Cl}{}_4]$ (Ar^{Cl} = 3,5-$Cl_2C_6H_3$). It has been shown that the complexes were substantially more efficient in the presence of $Na[BAr^{Cl}{}_4]$, while $Na[BAr^{Cl}{}_4]$ alone did not exhibit any catalytic activity. Since defining the active species and the structure is of extreme importance, the catalytic system was characterised using single crystal X-ray crystallography (Figure 1.4). This confirmed that the triflate groups extend their coordination further into the Na atom of $Na[BAr^{Cl}{}_4]$ keeping their primary bond with the Al centre intact. This finally gives rise to a dimeric unit which, in the solid state, forms a 2D coordination polymer. Although this solid-state structure with a weakly binding Na atom was not expected to be preserved in solution, it still showed that this catalyst

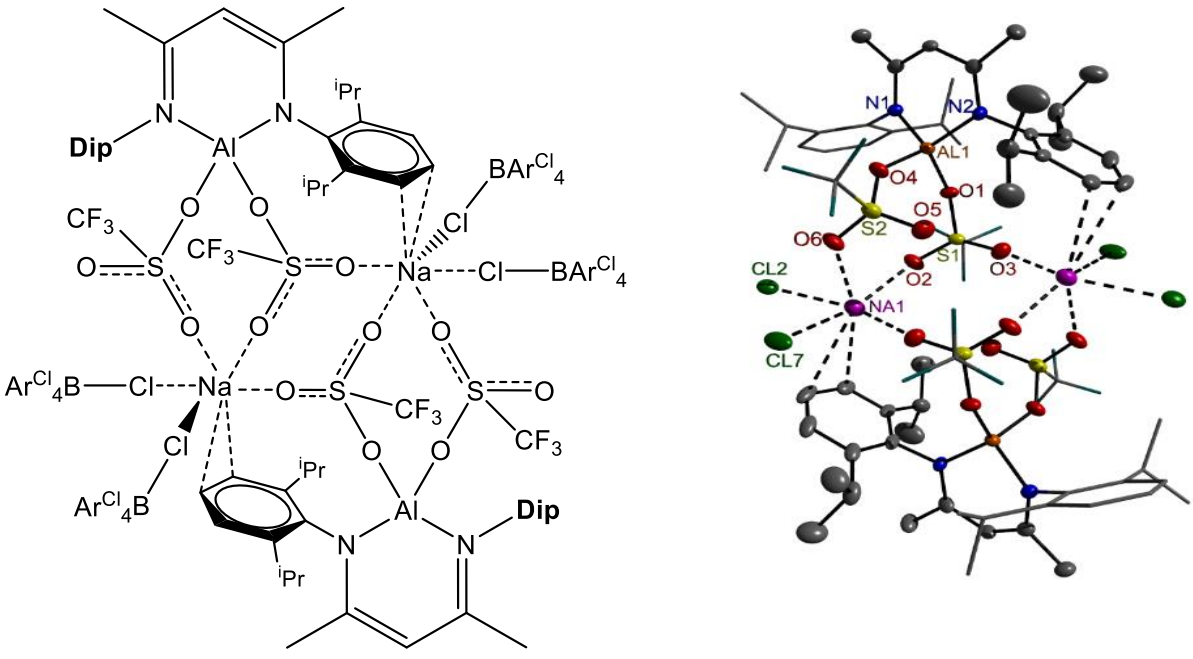

Figure 1.4: Single crystal structure of the active catalytic system[31]

was truly a Lewis acid. Most importantly, following Hintermann and co-workers' suggestions, the presence of HBAs has also been experimentally investigated and ruled out for this catalytic system. In addition, all the catalytic experiments and complex syntheses were done under inert conditions, excluding the possibility of HBAs formation through hydrolysis.

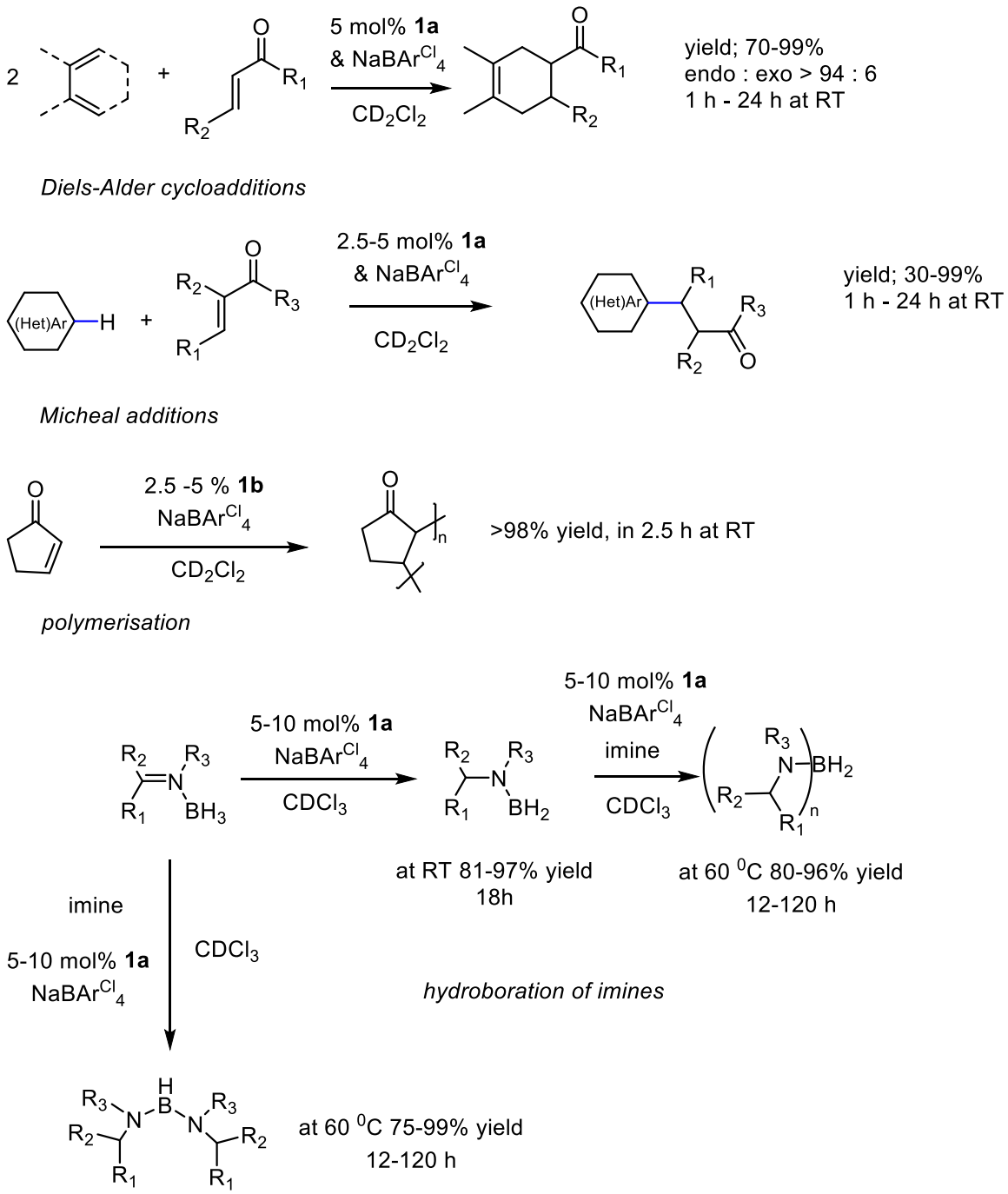

Figure 1.5: Reported applications of organic synthesis by the catalytic system designed by our group

This system demonstrated excellent catalytic activity towards Diels Alder transformations of challenging i.e. less reactive substrates such as dienes 1,3-cyclohexadiene and 2,3-dimethylbutadiene,[31] Michael addition reactions,[34] hydroborations of imines,[35] and polymerisation reactions (Figure 1.1).[36]

1.5 Asymmetric Catalysis

Stereochemistry has become one of the most important concepts in modern organic chemistry, as a significant number of organic molecules which are of academic and industrial significance are chiral. These molecules do not possess an improper axis of rotation or, in layman's terms, these molecules, when reflected in a mirror plane, do not generate superimposable mirror images. The two distinct mirror images are known as enantiomers. Interestingly, these enantiomers are known to possess identical physical properties except for the direction of optical rotation although the magnitude is still the same. Optical rotation, is one of the most discussed and widely investigated properties of chirality – and is defined as the direction of rotation of plane polarised light by a molecule (Figure 1.6).

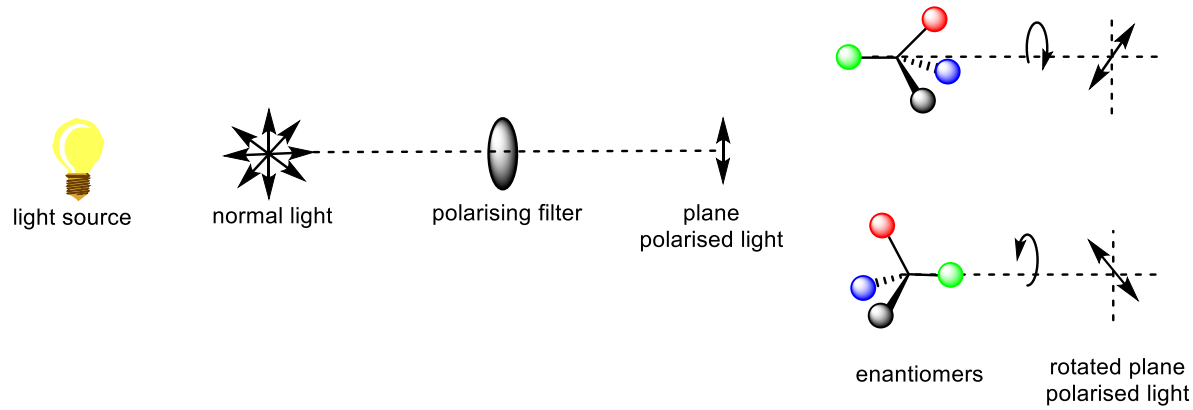

Figure 1.6: Activity of chiral molecules against plane polarised light

When it comes to the chemical properties of enantiomers, they share almost all of the ordinary chemical properties, but most importantly, the rates, orientations and modes of reactions of one enantiomer with another molecule, specially another chiral molecule is completely different and opposite to the other enantiomer. Another important aspect is that the biological properties of enantiomers are also different in nature.[37,38] A classic example is racemic-Thalidomide, a drug used to alleviate nausea and vomiting in pregnant women, which was withdrawn due to dangerous side-effects of limb deformities in newborn babies. In the late 1970s it was established that the (*R*)-enantiomer was the only enantiomer responsible for the expected therapeutic effects while the (*S*)-enantiomer was responsible for the deformities.[39] This explains why most pharmaceutical, agricultural, and even cosmetic industries focus on the use of optically pure compounds.[40] Although chiral resolution was considered as a practical solution in the past, due to intricate, time consuming procedures involved, modern industrial requirements stipulate direct synthesis of optically pure materials. Thus, asymmetric synthesis and catalysis have become widely studied topics in both the organic and inorganic chemistry fields as indicated by an outstanding number of scientific works published in this particular field. In fact, the 2001 Nobel prize for chemistry was jointly awarded to scientists Noyori, Knowles and Sharpless, in recognition of their work on asymmetric catalysis.[41]

In general, asymmetric catalysis is the type of catalysis in which "a chiral catalyst catalyses the transformation of a prochiral substrate into one enantiomer as a major product".[42] This type of catalysis is basically driven via the way of interaction of catalysts with the target substrates. This only becomes possible if the catalyst possesses a chiral feature, orienting target substrates into a restricted 3D space controlling the exposure of it towards other substrates or reagents, ultimately resulting in a single enantiospecific product. This could be achieved via a few key activation modes such as, *Lewis acid activation*-which proceeds via the combination of a Lewis acidic metal/element with a chiral Lewis basic ligand constructing a Lewis acidic chiral species

capable of interacting with/biding to substrates (Figure 1.7, **a**), *Brønsted acid activation*-which is similar to the prior but the metal is replaced by a proton instead (Figure 1.7, **b**), *ion pairing or electrostatic activation*-where enantioselectivity is passed on to the substrate via an electrostatic-ion paring/ionic bond formation process with the chiral catalyst (Figure 1.7, **c**), and *activation via hydrogen bonding interaction*-where catalysts such as organocatalysts, (usually) form multiple H bonds with substrate ensuring the enantio-restricted environment for catalysis (Figure 1.7, **a**).[40,43] Out of these modes, the study discussed in this thesis is mainly focused on chiral Lewis acid catalysts.

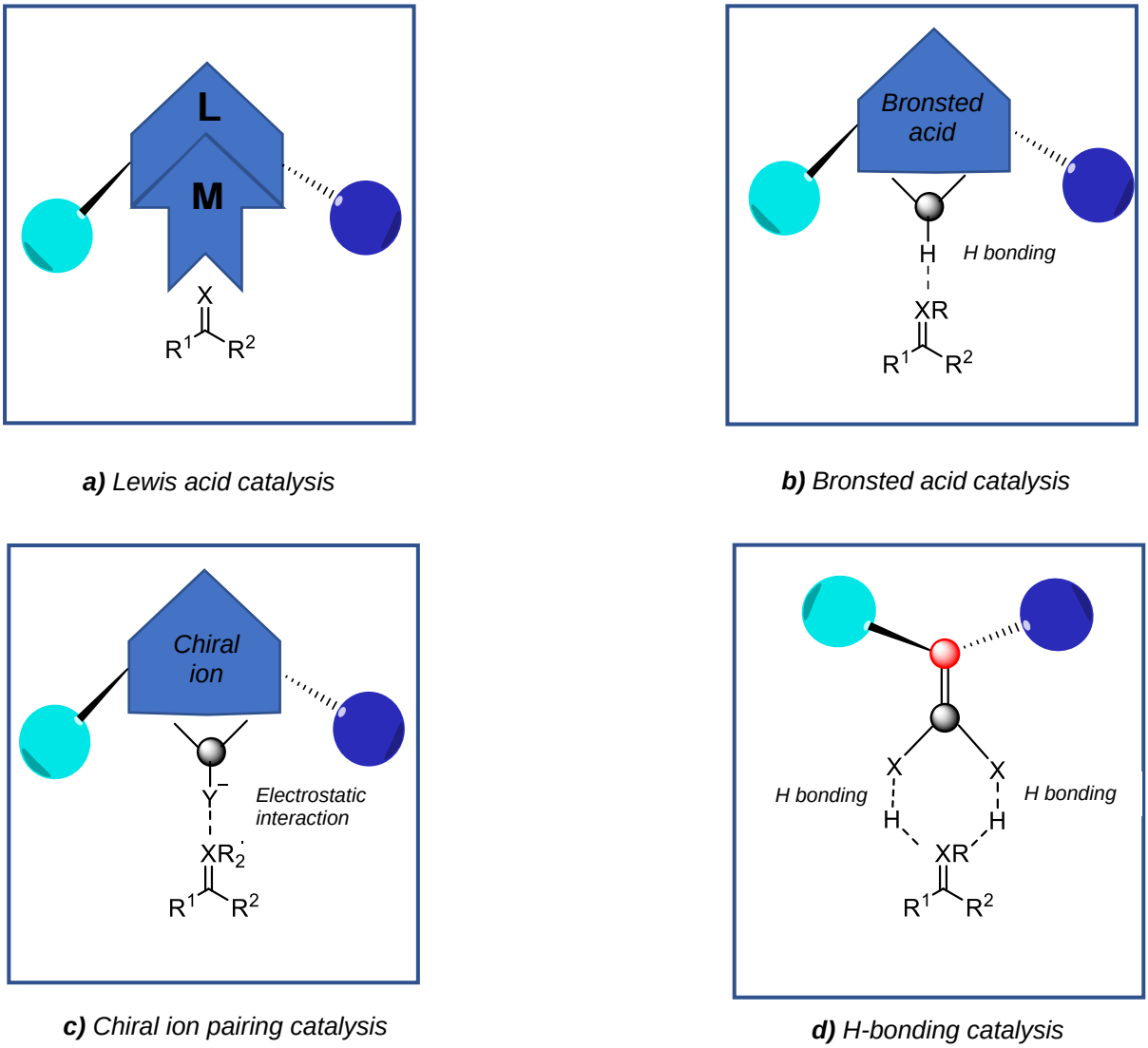

a) *Lewis acid catalysis*

b) *Bronsted acid catalysis*

c) *Chiral ion pairing catalysis*

d) *H-bonding catalysis*

Figure 1.7: Some activation modes of chiral catalysis[43]

1.6 Chiral Lewis acid catalysis

As briefed in section 1.5, a chiral Lewis acid catalyst is normally prepared by combining a Lewis acid metal/element (**M**) with a chiral Lewis base ligand (**L**). This **M**-**L** combination forms a chiral species possessing a net Lewis acidity.[43] During the reaction, this chiral Lewis acid species is coordinated directly (to a reacting atom) or indirectly (to a non-reacting atom) by a net electrophile such as a carbonyl or an imine group, making the whole unit chiral, while at the same time activating the substrate towards a nucleophilic attack.[43,40] Since the substrate itself now has become a chiral entity due to the temporary binding to the chiral Lewis acid catalyst, the reaction proceeds favouring a single enantiomeric product (Figure 1.8).

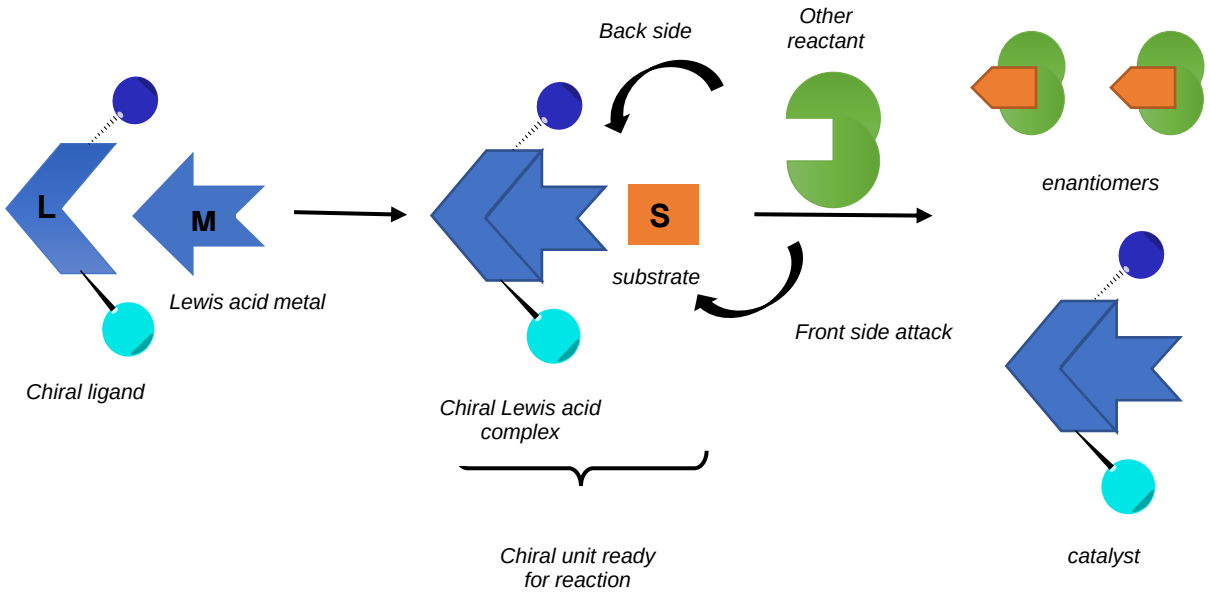

Figure 1.8: A Graphical interpretation of chiral Lewis acid catalysis

These enantio-directive i.e. asymmetric Lewis acid catalysts of transition metals such as Cu, Pd, Au, Fe, Rh, Ag, Ti and Zn as well as main group elements Al, Mg and B are abundantly reported.[41,44] As they are responsible for bringing stereospecific information to the overall chiral Lewis acid catalysts, the ligands serve an important aspect in this type of catalysis. Bisoxazolines such as PYBOX (PYBOX = pyridine(PY) based bisoxazolines (BOX)), BINAP,

its hydroxyl counterpart BINOL, TADDOL (tetraaryl-1,3-dioxolane-4,5-dimethanol), and chiral salen molecules are among the popular choices of ligands.[41] These chiral molecules combined with different Lewis acidic metals/elements have been reported to catalyse numerous asymmetric reactions such as cycloadditions (e.g. Diels Alder and hetero Diels Alder transformations),[45,46] carbonyl-ene[47] and condensation reactions (e.g. Aldol , Mannich, Michael addition and Friedel-Crafts reactions).[48,49]

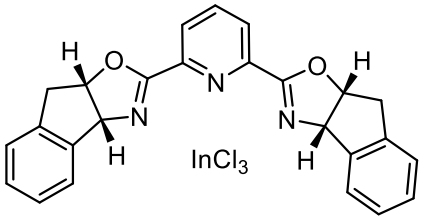

Chiral In (III)- PYBOX complex prepared and used in situ capable of driving asymmetric hetero-DA reactions

Same ligand/metal combination showed ability of catalysing enantioselective carbonyl-ene reaction of trifluoropyruvate in the presence of $AgSbF_6$

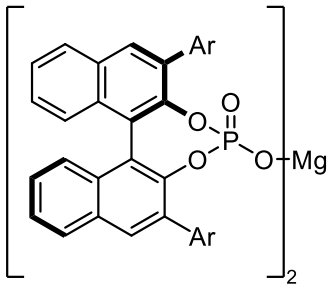

BINOL-phosphate ligand containing Mg complex capable of catalysing asymmetric DA reactions

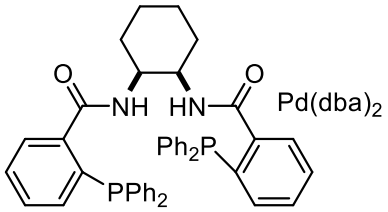

in situ reaction of this chiral salen type ligand with $Pd(dba)_2$ showed activity towards asymmetric Friedel-Crafts reactions

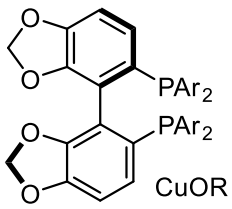

This modifed BINAP type ligand and CuOR, followed by addition of AgOTf showed activity towards asymmetric Aldol and Michael adiition reactions

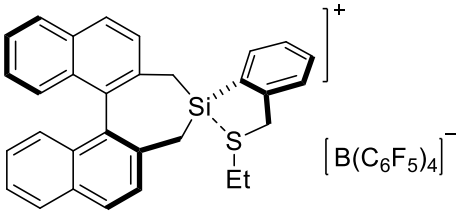

a BINAP containing S stabilised Si cationic Lewis Acid shows activity towards DA cycloadditions

Figure 1.9: Examples for different types of chiral ligands used and asymmetric catalysis by chiral Lewis acid catalysts

1.6.1 Aluminium based chiral Lewis acid catalysts

The first report on asymmetric aluminium containing Lewis acid catalysis was published around 70 years ago involving asymmetric Meerwein-Ponndorf-Verley reduction of ketones which was followed by a few scattered reports on polymerisations.[4] After almost three decades, Koga and co-workers' report on an aluminium chloride catalysed asymmetric Diels-Alder reaction appeared which was believed to instigate the inspiration responsible for the enormous growth of Al based chiral catalysis (Figure 1.10).[41,50] An extremely larger number of studies have followed targeting various different asymmetric organic transformations.[4]

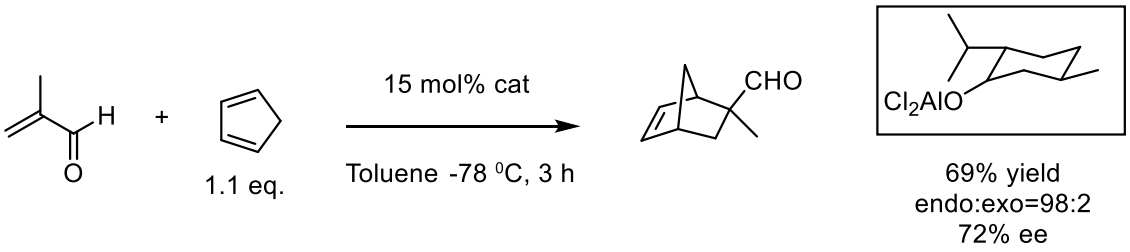

Figure 1.10: Asymmetric DA reaction catalysed by Al based catalyst published by Koga et al.

To mention a few, asymmetric Muikaiyama aldol reactions, catalysed by **N (**in Figure 1.11), were reported to reach up to 66% enantiomeric excess (*ee*), and with a few modifications to the catalyst, the *ee* value was improved to 90% for certain substrates.[51] Catalyst **O** (in Figure 1.11) with different Ar substituents such as Ph, *t*-$BuMe_2$ was reported to generate 93% *ee* towards certain substrates in Claisen rearrangement reactions of *trans*-cinnamyl vinyl ethers.[52] In addition, the same catalyst was also reported to be effective towards different asymmetric cycloaddition reactions.[52] Further, asymmetric [3+2] cycloadditions of aldehydes to 2-aryl-5-methoxyoxazoles were reportedly catalysed by **P (**in Figure 1.11**)** with *ee* values of up to 90% for certain substrates.[53] $AlCl_3$ together with the PYBOX ligand in **Q** (Figure 1.11) was able to generate > 90% *ee* towards Michael addition reactions.[54] Catalytic cyclopropanation reactions

of allylic alcohols have been reported to be catalysed by **R** (Figure 1.11) producing *ee* values up to 70%.[55] These only represent a handful of numerous different Al based chiral compounds capable of driving asymmetric catalysis of a wide collection of different organic transformations.[4]

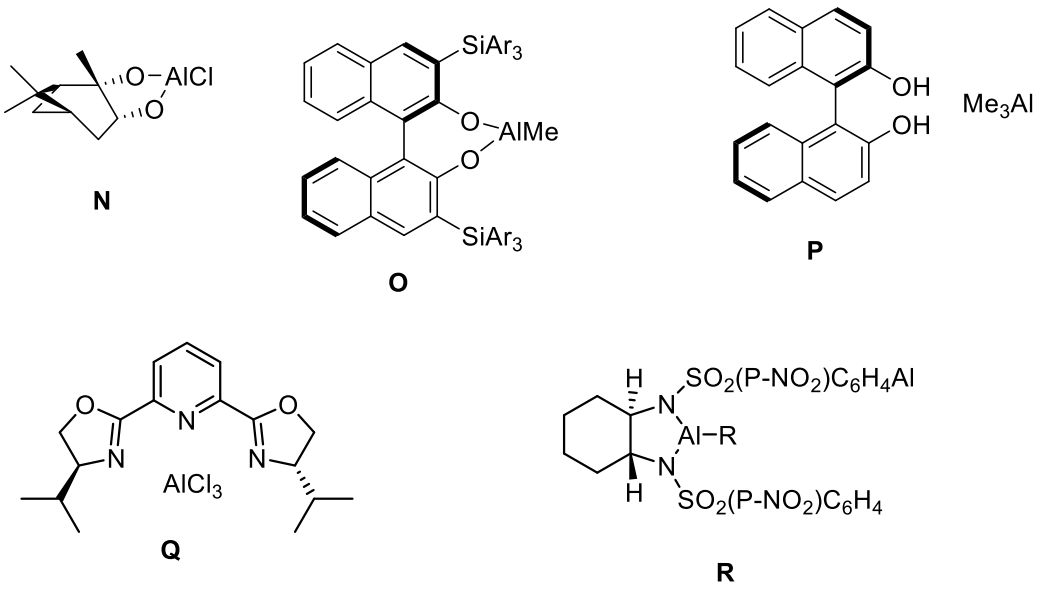

Figure 1.11: Few of reported chiral Al Lewis acid catalysts

1.6.2 Chiral Lewis acids of Al with β-diketiminato supporting ligands

As discussed, supporting ligands play an important role in Lewis acid catalysis, improving regio-, chemo-, stereo- and enantio-selectivities, therefore, ligand design will always play a vital role in any type of catalysis. Thus, ligand synthesis is considered to be an extremely important task in designing adequate catalytic systems. β-difunctional, monoanionic, chelating ligands shown in Figure 1.12 are among the various ligands used to support many Lewis acids. These β-diketonato (I), β-enaminoketonato (II), β-ketiminato ligands (III) (Figure 1.12) also known as "ac-ac", "ac-nac", and "nac-nac" ligands respectively, have been investigated and successfully utilised as spectator ligands dating back a few decades ago.[56–59] However, β-diketiminato III ligands or "nac-nac" ligands, have demonstrated their wide appeal due to the

ability of having different bulky-substituents on both N atoms. These bis-chelating, monoanionic, β-difunctional, bulky supporting ligands are specially well known to stabilise unsaturated coordination centres and unusual oxidation states.[60] Given their ability to bind strongly with metals in a bidentate manner and pass tuneable steric and electronic properties, it is quite surprising that their chiral counterparts have not been developed as progressively as expected.[61] Perhaps, this may be due to fact that most of β-diketiminato ligands are perfectly symmetric in nature.

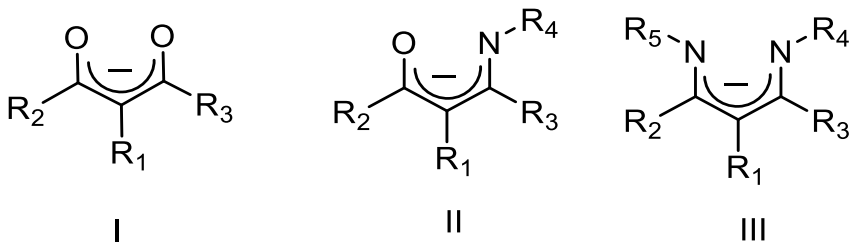

Figure 1.12: different types of β-difunctional, monoanionic, chelating ligands which are known as β-diketiminato ligands

One can argue that this comparatively less versatile exploration of chiral β-diketiminato ligands is not simply because they are demonstrating less potential in asymmetric catalysis but the field is yet to be explored, specially within of the field of small molecule synthesis. However, as discussed below, a few chiral β-diketiminato ligand containing catalytic systems were reported and some of them show excellent capabilities in asymmetric catalysis in large molecule synthesis such as polymerisations.

First ever chiral β-diketiminato ligand along with its copper complexes was introduced about a decade ago by Schaper and Oguadinma (**S**, Figure 1.13).[60] This was quickly followed by two similar works by the same group (**T** and **U**, Figure 1.13), which represented the first examples of complexes containing chiral β-diketiminato ligand(s) used in asymmetric catalysis (i.e. for lactide polymerisation reactions).[62,63] In 2011, Guodong Du and co-workers published a library

of β-ketiminato-like ligands,[64] and followed up their work by synthesising different complexes using a few ligands from their collection.[65–67] This work included catalytic activity of Al based complexes towards ring opening polymerisation of *rac*-lactide[66] and zinc complexes for asymmetric alternating copolymerisation of CO_2 and cyclohexene oxide.[67] In addition, another report by Jingping Qu and co-workers elaborated structure analysis and asymmetric ring-opening polymerisation of ε-caprolactone by another Al based complex containing a chiral β-diketiminato ligand (**V**, Figure 1.13).[68] Another couple of reports on Mg based complexes containing chiral β-diketiminato ligands were reported recently, but any significant application in catalysis was not accompanied in these reports.[69,70] Surprisingly, there is not much evidence for the use of chiral β-diketiminato ligand containing chiral complexes in small organic molecule synthesis and the ability of the chiral analogues of these versatile ligands to drive asymmetric organic reactions is yet to be reported.[61]

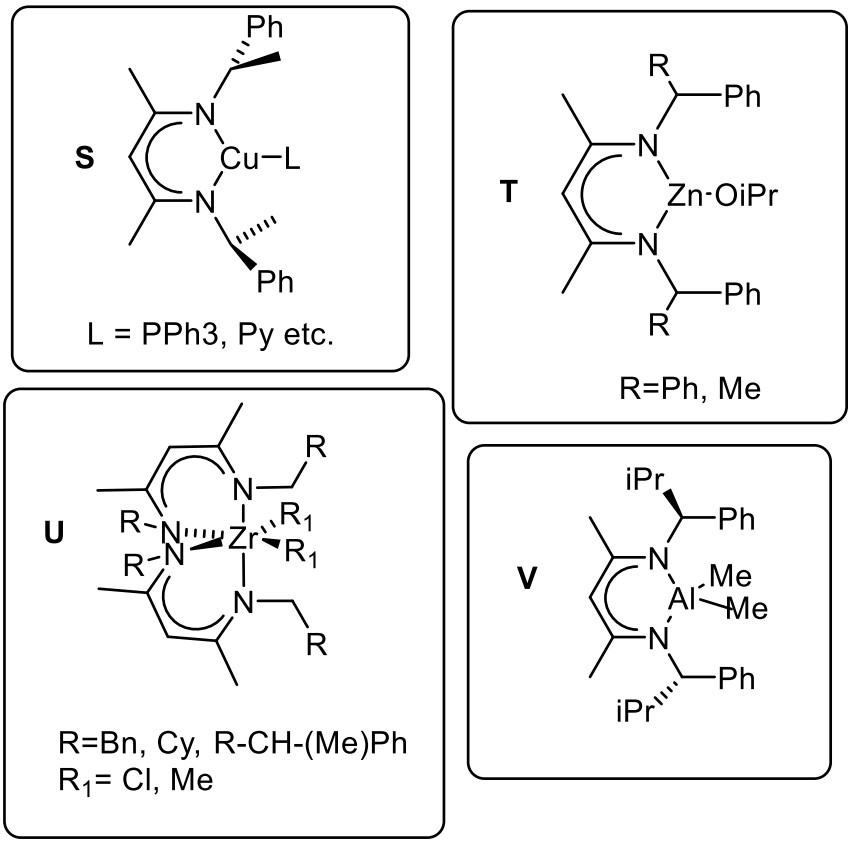

Figure 1.13: Some of the reported chiral β-diketiminato ligand containing complexes

1.7 This Study

As discussed, the already reported, β-diketiminate supported aluminium bistriflate Lewis acid complex by our group, has shown the ability to catalyse Diels Alder cycloadditions of a less reactive substrate combination i.e. between cyclohexadiene simple α,β-unsaturated ketones such as chalcones, as well as Michael addition reactions, and an example of a polymerisation reaction.[31,34] Driven by this, our main goal in this thesis project is to structurally alter this achiral Al complex into a novel chiral complex in order to explore their ability of performing asymmetric catalysis. As majority of early reports on Lewis acid catalysis and chiral Lewis acid catalysis are mostly done *in situ*, lacking proper evidence to back "true" Lewis acid activity, as well as compelled by recent findings on HBA catalysis, producing well-characterised, chiral-Lewis acid complexes with adequate structural information will also be one of our main goals.

We propose to introduce chirality at the β-diketiminate supporting ligand by inserting a five-membered oxazoline ring motif (with a chiral C atom) between one of the N atoms and ligand backbone such as the ones reported by Du and co-workers[64] We believe that these ligands closely resemble the β-diketiminato ligands we already used to prepare achiral complexes, and that these structural modifications would not compromise the already achieved catalytic activity of these systems. We also believe that this ligand framework will allow us to systematically alter the structural features of these complexes as variations can be done at two sites, namely, at **Ar** and **R** positions (Figure 1.14). We recognise these two positions as the "*achiral end"* (**Ar**) and the "*chiral end"* (**R**) and plan to investigate how these systematic changes in structural features at these two ends can affect the properties of these complexes when used as catalysts for enantioselective organic transformations. Thus, the effects of the proposed structural modifications of β-diketiminate-like ligands as depicted in Figure 1.14 on the enantioselective activity of the target aluminium-based complexes will be studied.

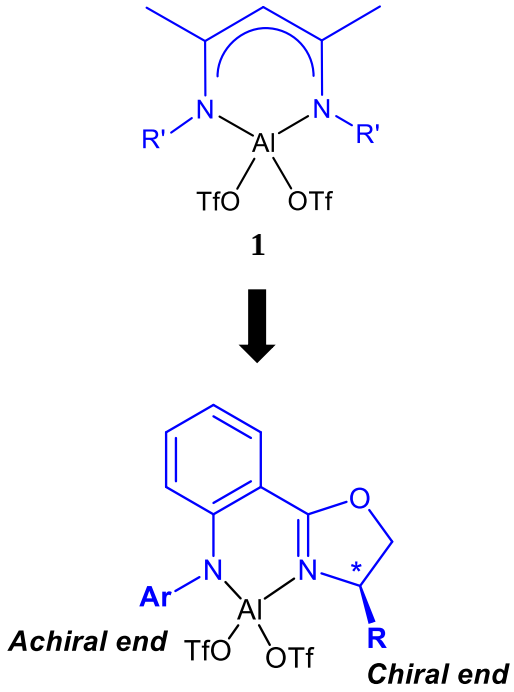

1a $^{Dip}LAl(OTf)_2$: R'= 2,6-*i*-Pr_2-C_6H_3

1b $^{Xyl}LAl(OTf)_2$: R' = 2,6-,Me_2-C_6H_3

1c $^{Ph}LAl(OTf)_2$: R' = C_6H_5

	R	Ar
2	Ph	2,6-$Me_2C_6H_3$
3a	*i*-Pr	2,6-$Me_2C_6H_3$
3b	*i*-Pr	Ph
3c	*i*-Pr	2,6-*i*-$Pr_2C_6H_3$
3d	*i*-Pr	2,4,6-$(CH_3)_3C_6H_2$
3e	*i*-Pr	4-CH_3-2,6-$(CH(Ph)_2)_2C_6H_2$
3f	*i*-Pr	4-*t*-Bu, 2,6-$(CH(Ph)_2)_2C_6H_2$
4a	*t*-Bu	2,6-*i*-$Pr_2C_6H_3$
4b	*t*-Bu	4-CH_3-2,6-$(CH(Ph)_2)_2C_6H_2$
5a	$PhCH_2$-	2,6-*i*-$Pr_2C_6H_3$
5b	$PhCH_2$-	4-CH_3-2,6-$(CH(Ph)_2)_2C_6H_2$
6a	Ph_2CH-	2,6-*i*-$Pr_2C_6H_3$
6b	Ph_2CH-	4-CH_3-2,6-$(CH(Ph)_2)_2C_6H_2$

Figure 1.14: Basic Structure of the reported achiral complex **1** and introducing Chirality at β-diketiminate supporting ligand, basic structures of proposed chiral Al complexes

A carefully chosen collection of different structures with a broad steric variety will be used at the two "*ends*" of these target ligands (Figure 1.14) to create a diverse range of aluminium complexes. The proposed synthetic route (introduced in Chapter 2) for the ligand synthesis explains how these structural varieties at two ends can be easily achieved simply by introducing different starting materials at two different steps involved in the overall ligand synthesis. It is also worth noting that although some of these proposed ligand structures are already reported, most of them are introduced for the first time.[64]

Main targeted application for these complexes will be asymmetric DA reactions of less reactive dienes and dienophiles as described in the reports published by Oestreich and co-workers.[71–74] Their study involves catalytic enantioselective DA reactions of less reactive species 1,3-cyclohexadiene and chalcones using chiral silicon-based compounds,[71–74] achieving enantiomeric excess of low to average enantioselectivities. As some of these DA adducts were prepared in relatively low enantiopurities, it is our understanding that producing enantiopure DA products of these significantly less reactive dienes and dienophiles in good yields will be a challenging task which is yet to be achieved.

Another under-explored area involving aluminium based catalysis is (a)symmetric hydrosilylation reactions of carbonyls and imines and these transformations will be also investigated. Given that a limited amount of studies was carried out describing the ability of aluminium based complexes to catalyse hydrosilylation reactions of carbonyl compounds and imines, we believe that exploring this particular research area, using our aluminium complexes, is worthwhile. We will particularly target to perform these reactions using challenging, yet industrially viable silane Et_3SiH. In addition, as no Al based catalysts have been reported of catalysing asymmetric hydrosilylation reactions of prochiral ketones, we aim to employ our collection of chiral Al based complexes in order to investigate the ability of enantioinduction towards this particular reaction.

Thus, Chapter 2 of this thesis will explore the effects of steric properties of these catalysts at the achiral end (**Ar**) via the synthesis of several chiral ligands and aluminium complexes and examining their reactivity towards asymmetric Diels Alder reactions of electronically unsupported less reactive dienes and dienophiles.

Chapter 3 of this thesis will explore the effects of different structural features of these catalysts at the chiral end (**R**) by synthesising several chiral ligands and aluminium complexes and

exploring their reactivity towards asymmetric Diels Alder reactions between 1,3-cyclohexadiene and chalcones.

Chapter 4 of this thesis focuses on symmetric hydrosilylation reactions of aldehydes, ketones and imines in the presence of Et_3SiH using our achiral catalytic system. It also explores the ability of the chiral catalytic systems to drive asymmetric hydrosilylation reactions of the prochiral ketone, acetophenone.

We believe that the proposed chiral aluminium complexes are the first ever to contain chiral β-diketiminate type ligand(s) and to be utilised in enantioselective catalytic transformations of difficult DA substrates (i.e. between 1,3-cyclohexadiene and chalcones) or asymmetric hydrosilylation reaction of acetophenone, or in any asymmetric small molecule synthesis.

References

1 D. Rodrigues Silva, L. de Azevedo Santos, M. P. Freitas, C. Fonseca Guerra and T. A. Hamlin, *Chem. - An Asian J.*, 2020, **15**, 4043–4054.

2 H. Yamamoto, *Lewis acid reagents - A practical approach - Introduction.*, Oxford University Press, 1999.

3 C. Hertweck, *J. für Prakt. Chemie*, 2005, **342**, 316–321.

4 H. Yamamoto, *Lewis Acids in Organic Synthesis*, Wiley-VCH, 1st edition, 2000.

5 S. I. Murahashi, H. Takaya and T. Naota, *Pure Appl. Chem.*, 2002, **74**, 19–24.

6 C. Moberg, *Lewis Acid-Lewis Base Catalysis*, Wiley Blackwell, 2015.

7 A. Corma and H. García, *Chem. Rev.*, 2003, **103**, 4307–4365.

8 Encyclopædia Britannica, *Encycl. Br.*, 2020.

9 G. I. Nikonov, *ACS Catal.*, 2017, 7, 7257–7266.

10 J. Wisniak, *Educ. Química*, 2009, **20**, 447–455.

11 D. Vidović, in *Reference Module in Chemistry, Molecular Sciences and Chemical Engineering*, Elsevier, 2021.

12 D. B. G. Williams, S. B. Simelane, M. Lawton and H. H. Kinfe, *Tetrahedron*, 2010, **66**, 4573–4576.

13 T. Arai, H. Sasai, K. Aoe, K. Okamura, T. Date and M. Shibasaki, *Angew. Chemie Int. Ed. English*, 1996, **35**, 104–106.

14 M. Zhu, J. Liu, J. Yu, L. Chen, C. Zhang and L. Wang, *Org. Lett.*, 2014, **16**, 1856–1859.

15 Z. Yang, M. Zhong, X. Ma, S. De, C. Anusha, P. Parameswaran and H. W. Roesky, *Angew. Chemie - Int. Ed.*, 2015, **54**, 10225–10229.

16 V. K. Jakhar, M. K. Barman and S. Nembenna, *Org. Lett.*, 2016, **18**, 4710–4713.

17 Z. Yang, Y. Yi, M. Zhong, S. De, T. Mondal, D. Koley, X. Ma, D. Zhang and H. W. Roesky, *Chem. - A Eur. J.*, 2016, **22**, 6932–6938.

18 S. M. Raders and J. G. Verkade, *Tetrahedron Lett.*, 2009, **50**, 5317–5321.

19 W. Su, Y. Kim, A. Ellern, I. A. Guzei and J. G. Verkade, *J. Am. Chem. Soc.*, 2006, **128**, 13727–13735.

20 J. Koller and R. G. Bergman, *Organometallics*, 2012, **31**, 2530–2533.

21 R. Kannan, R. Chambenahalli, S. Kumar, A. Krishna, A. P. Andrews, E. D. Jemmis and A. Venugopal, *Chem. Commun.*, 2019, **55**, 14629–14632.

22 N. Sarkar, R. K. Sahoo, S. Mukhopadhyay and S. Nembenna, *Eur. J. Inorg. Chem.*, 2022, **2022**, e202101030.

23 X. Zhou, X. Liu, X. Yang, D. Shang, J. Xin and X. Feng, *Angew. Chemie - Int. Ed.*, 2008, **47**, 392–394.

24 V. A. Pollard, A. Young, R. McLellan, A. R. Kennedy, T. Tuttle and R. E. Mulvey, *Angew. Chemie - Int. Ed.*, 2019, 58, 12291–12296.

25 J. Koller and R. G. Bergman, *Chem. Commun.*, 2010, **46**, 4577–4579.

26 C. R. Graves, B. S. Zeng and S. B. T. Nguyen, *J. Am. Chem. Soc.*, 2006, **128**, 12596–12597.

27 Z. Liu, R. Ganguly and D. Vidović, *Dalt. Trans.*, 2017, **46**, 753–759.

28 T. T. Dang, F. Boeck and L. Hintermann, *J. Org. Chem.*, 2011, **76**, 9353–9361.

29 I. Šolić, H. X. Lin and R. W. Bates, *Tetrahedron Lett.*, 2018, **59**, 4434–4436.

30 E. T. Sletten, Y. J. Tu, H. B. Schlegel and H. M. Nguyen, *ACS Catal.*, 2019, **9**, 2110–2123.

31 Z. Liu, J. H. Q. Lee, R. Ganguly and D. Vidović, *Chem. - A Eur. J.*, 2015, **21**, 11344–11348.

32 P. N. Liu, Z. Y. Zhou and C. P. Lau, *Chem. - A Eur. J.*, 2007, **13**, 8610–8619.

33 F. Fringuelli, R. Girotti, F. Pizzo and L. Vaccaro, *Org. Lett.*, 2006, **8**, 2487–2489.

34 Z. Liu and D. Vidović, *J. Org. Chem.*, 2018, **83**, 5295–5300.

35 S. Zhai, C. Forsyth, Z. Liu and D. Vidović, *Organometallics*, 2022, **41**, 2562–2571.

36 D. Dissanayake, A. Draper, Z. Liu, J. J. Haven, C. Forsyth, T. Junkers and D. Vidović, *manuscript under revision.*

37 A. Guijarro and M. Yus, *The Origin of Chirality in the Molecules of Life*, Royal Society of Chemistry, 2008.

38 S. K. Bhasin and R. Gupta, *Pharmaceutical Organic Chemistry*, Elsevier Health Sciences APAC, 2011.

39 G. W. Mellin and M. Katzenstein, *N. Engl. J. Med.*, 1962, **267**, 1184–1193.

40 P. J. Walsh and M. C. Kozlowski, *Fundamentals of asymmetric catalysis*, 2008.

41 K. Mikami, *Chiral Lewis Acids*, Springer International Publishing, Cham, 2018, vol. 62.

42 P. Peltier, R. Euzen, R. Daniellou, C. Nugier-Chauvin and V. Ferrières, *Carbohydr. Res.*, 2008, **343**, 1897-1923

43 R. J. Phipps, G. L. Hamilton and F. D. Toste, *Nat. Chem.*, 2012, **4**, 603–614.

44 J. Mlynarski, *Chiral Lewis Acids in Organic Synthesis*, 2017.

45 G. Li, T. Liang, L. Wojtas and J. C. Antilla, *Angew. Chemie - Int. Ed.*, 2013, **52**, 4628–4632.

46 B. Zhao and T. P. Loh, *Org. Lett.*, 2013, **15**, 2914–2917.

47 J. F. Zhao, B. H. Tan, M. K. Zhu, T. B. W. Tjan and T. P. Loh, *Adv. Synth. Catal.*, 2010, **352**, 2085–2088.

48 S.-L. Shi, M. Kanai and M. Shibasaki, *Angew. Chemie*, 2012, **124**, 3998–4001.

49 Y. Suzuki, T. Nemoto, K. Kakugawa, A. Hamajima and Y. Hamada, *Org. Lett.*, 2012, **14**, 2350–2353.

50 W. von E Doering and R. W. Young, *J. Am. Chem. Socie*, 1950, **72**, 631.

51 M. Shimizu, M. Kawamoto, Y. Yamamoto and T. Fujisawa, *Synlett*, 1997, 501–502.

52 K. Maruoka, H. Banno and H. Yamamoto, *J. Am. Chem. Soc.*, 1990, **112**, 7791–7793.

53 H. Suga, K. Ikai and T. Ibata, *Tetrahedron Lett.*, 1998, **39**, 869–872.

54 I. Iovel, Y. Popelis, M. Fleisher and E. Lukevics, *Tetrahedron Asymmetry*, 1997, **8**, 1279–1285.

55 H. Takahashi, M. Yoshioka, M. Ohno and S. Kobayashi, *Tetrahedron Lett.*, 1992, **33**, 2575–2578.

56 L. C. Dorman, *Tetrahedron Lett.*, 1966, **7**, 459–464.

57 W. J. Barry, I. L. Finar and E. F. Mooney, *A comparison of the structures of some dianils with those of analogous diazepines*, Pergamon Press Ltd, 1965.

58 P. B. Hitchcock, M. F. Lappert and D.-S. Liu, *J. Chem. Soc. Chem. Commun.*, 1994, 2637.

59 P. B. Hitchcock, M. F. Lappert and D.-S. Liu, *J. Chem. Soc. Chem. Commun.*, 1994, **1994**, 1699–1700.

60 P. O. Oguadinma and F. Schaper, *Organometallics*, 2009, **28**, 4089–4097.

61 R. L. Webster, *Dalt. Trans.*, 2017, 46, 4483–4498.

62 I. El-Zoghbi, S. Latreche and F. Schaper, *Organometallics*, 2010, **29**, 1551–1559.

63 F. Drouin, P. O. Oguadinma, T. J. J. Whitehorne, R. E. Prudhomme and F. Schaper, *Organometallics*, 2010, **29**, 2139–2147.

64 P. I. Binda, S. Abbina and G. Du, *Synthesis (Stuttg).*, 2011, **2011**, 2609–2618.

65 Z. Lu, S. Abbina, J. R. Sabin, V. N. Nemykin and G. Du, *Inorg. Chem.*, 2013, **52**, 1454–1465.

66 S. Bian, S. Abbina, Z. Lu, E. Kolodka and G. Du, *Organometallics*, 2014, **33**, 2489–

2495.

67 S. Abbina and G. Du, *Organometallics*, 2012, **31**, 7394–7403.

68 D. Kong, Y. Peng, D. Li, Y. Li, P. Chen and J. Qu, *Inorg. Chem. Commun.*, 2012, **22**, 158–161.

69 C. N. de Bruin-Dickason, C. A. Rosengarten, G. B. Deacon and C. Jones, *Chem. Commun.*, 2021, **57**, 1599–1602.

70 Z. Xu, S. Zhang and W. Ren, *Inorganica Chim. Acta*, 2019, **495**, 118970.

71 V. H. G. Rohde, M. F. Müller and M. Oestreich, *Organometallics*, 2015, **34**, 3358–3373.

72 P. Shaykhutdinova and M. Oestreich, *Organometallics*, 2016, **35**, 2768–2771.

73 P. Shaykhutdinova and M. Oestreich, *Org. Lett.*, 2018, **20**, 7029–7033.

74 P. Shaykhutdinova, S. Kemper and M. Oestreich, *European J. Org. Chem.*, 2018, **2018**, 2896–2901.

Chapter 2

2. Synthesis, Characterisation, and Reactivity studies of Chiral β-Diketiminate Supported Aluminium Lewis Acid Complexes Towards Difficult Diels Alder Cycloadditions-*Effects of Structural Modifications at the Achiral end*

2.1 Introduction

This chapter mainly discusses details of synthesis, characterisation and reactivity of a collection of chiral β-diketiminate supporting aluminium Lewis acid complexes, with a focus on how the systematic structural changes at the achiral end would affect the product enantioselectivity values when these complexes are used as catalysts for a "difficult" Diels Alder reaction.

2.1.1 Asymmetric Diels Alder reactions

Diels Alder (DA) reaction is considered as a beneficial synthetic route to produce six membered ring structures. In this single step reaction, a diene and a dienophile react together, forming a stereospecific product (Figure 2.1) and this pericyclic reaction is also known as [4+2] cycloaddition. The reaction was first discovered in 1928, by Otto Paul Hermann Diels and his student Kurt Alder, after whom the reaction was named.[1] The discovery brought duo the Nobel prize in 1950.[2]

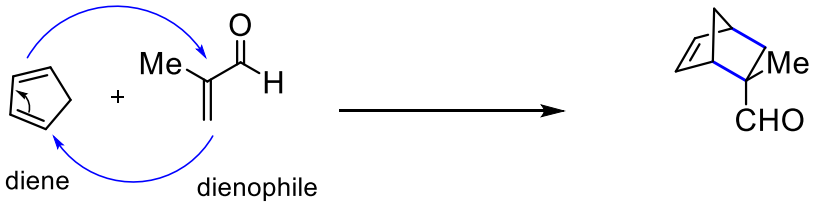

Figure 2.1: Basic Diels Alder reaction

The reaction is stereo- and regio-selective, leading to two stereoisomers arising from the alignment of the diene and the dienophile (Figure 2.2 a, b). These two stereoisomers are known as the *endo* and *exo* products. The *endo* product is the most stable isomer and its stability was initially believed to be due to inductive/charge-transfer interactions, but the secondary orbital overlap of the transition state, as proposed by Hoffmann and Woodward,[3] might be the reason most agreed upon (Figure 2.2 b).[4]

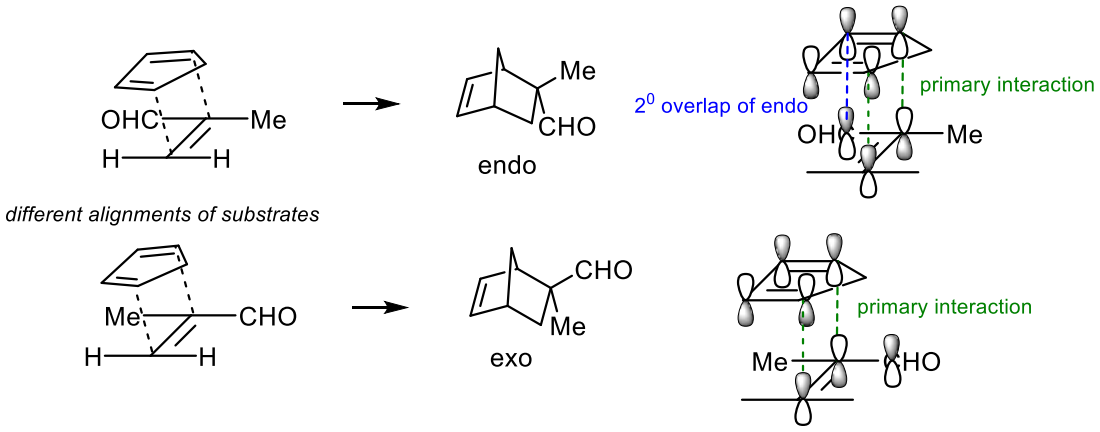

a) formation of endo and exo isomers

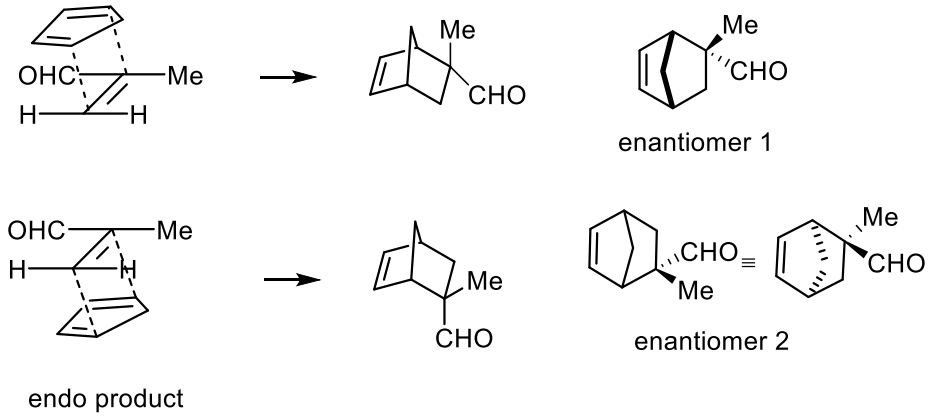

b) formation of enantiomers of endo isomer

**exo isomer will also produce another two enantiomers*

Figure 2.2: stereo- and enantio-specificity of DA reactions

In addition, for specific combinations of dienes and dienophiles (e.g. cyclopentadiene and methacrylaldehyde, in Figure 2.2 a), two enantiomers could be produced, depending on the initial spatial interaction of these two substrates (see Figure 2.2 b). Thus, as there are two stereoisomers (*endo* and *exo*), this particular transformation is capable of generating four isomers in total (Figure 2.2).

DA reaction has been identified as one of the most important reactions in organic synthesis and has notable industrial applications (for e.g. synthesis of ethylidene norbornene using cyclopentadiene and butadiene in commercial synthesis of synthetic rubber)[5] as well as applications in total synthesis of pharmaceutical molecules such as cortisone and (−)-taxol.[6–8] The mechanism and substrate scopes of these reactions are considered as almost fully investigated by numerous different studies dedicated to the field ever since the discovery.[2] However, possibly due to the fact that it can generate four isomers each containing a chiral centre, tremendous research efforts are still being dedicated to these transformations i.e. specific reaction conditions capable of inducing enantioselectivity.[9–12]

As this whole reaction happens via electron density transfer from one molecule to the other, the reactivity usually depends on the energy difference/match between the HOMO of the diene and the LUMO of the dienophile. Therefore, lowering the LUMO of the dienophile normally improves the feasibility of the reaction, which is usually achieved by attaching electron withdrawing substituent(s) to this particular substrate. Alternatively, electron deficient Lewis acids could bind to the dienophile promoting this same effect, which is arguably the main reason why Lewis acids are well-known species capable of catalysing DA reactions.[2,13] Hence, as early as in 1960, the ability of Lewis acids to catalyse DA reactions under mild conditions has been reported.[14] Not too long after that, in 1979, Koga and co-workers reported an asymmetric Diels Alder catalysed by an Al based chiral Lewis acid.[15] This was then followed by a number of reports describing asymmetric Diels Alder transformations catalysed by compounds based on B, Al, Cu, Mg, Zn, Ti, Cr, Co, Fe, Ru and rare earth metals.[2,15] For example, compound **W** (Figure 2.3), was reported to catalyse the DA reaction between cyclopentadiene and 2-bromoacolein with enantiomeric excess (*ee*) of 99%, while compound **X** (Figure 2.3) generated 98% *ee* for the reaction between cyclopentadiene and 2-methacrolein, and up to 99% *ee* values were obtained with the use of compound **Y** (Figure 2.3) towards the

cycloaddition of acryloyl-2-oxazolidinones and cyclopentadiene. Additionally, *in situ* addition of $Zn(SbF_6)_2$ and $MgOTf_2$ to the same PYBOX ligand (in **Y**) formed *ee* values of 92% and 95% respectively towards the same substrates, and chiral ruthenium complex **Z** showed 91% *ee* towards the DA reaction between methacrolein and cyclopentadiene.

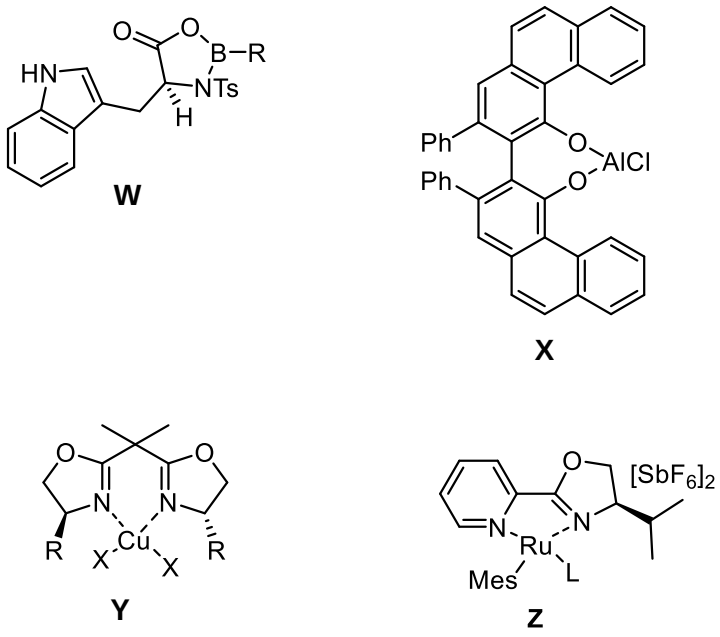

Figure 2.3: Examples for asymmetric catalysts for DA cycloadditions

However, as previously indicated, most of these reports were based on either favourably substituted dienophiles and/or dienes which are considered to be very reactive.[2,15] DA reactions of less reactive dienophiles such as simple α, β-unsaturated ketones, containing no additional electron withdrawing groups, have been considered as challenging with only a few studies being dedicated to these substrates. Works by MacMillan and co-workers, Deng and co-workers and Oestreich and co-workers (see below) can be named as examples for such less-reactive dienes.[12,16,17] In addition, asymmetric DA reactions involving less reactive dienes such

as 1,3-cyclohexadiene are equally underrepresented compared to substrates such as cyclopentadiene which is considered to be 500 times more reactive than the former diene.[18,19] Therefore, asymmetric DA reactions engaging these less reactive substrates are still considered to be underdeveloped and worth exploring. It should be mentioned that a majority of the reports involving asymmetric DA catalysis also lacked sufficient evidence that these specific transformations were indeed catalysed by "true", HBA-free (Hidden Brønsted Acid) Lewis acid compounds as was the case for reported symmetric DA reactions (as discussed in Chapter 1).

As briefly mentioned in Chapter 1, the only reports describing asymmetric DA reactions between electronically unsupported chalcones and 1,3-cyclohexadiene (and a several other dienes) were published by M. Oestreich and co-workers.[17,19–22] Spanned over five reports, a collection of well-defined, S stabilised, Si-based cationic Lewis acid complexes and the attempts to reach an adequate value for *ee*% have been described. As demonstrated, the *ee* values obtained for the examined DA reactions between 1,3-cyclohexadiene and chalcone were ranging from 11-67% (Figure 2.4).[17,19–22] Thus, we carried out our study hoping to improve these enantioselectivity values.

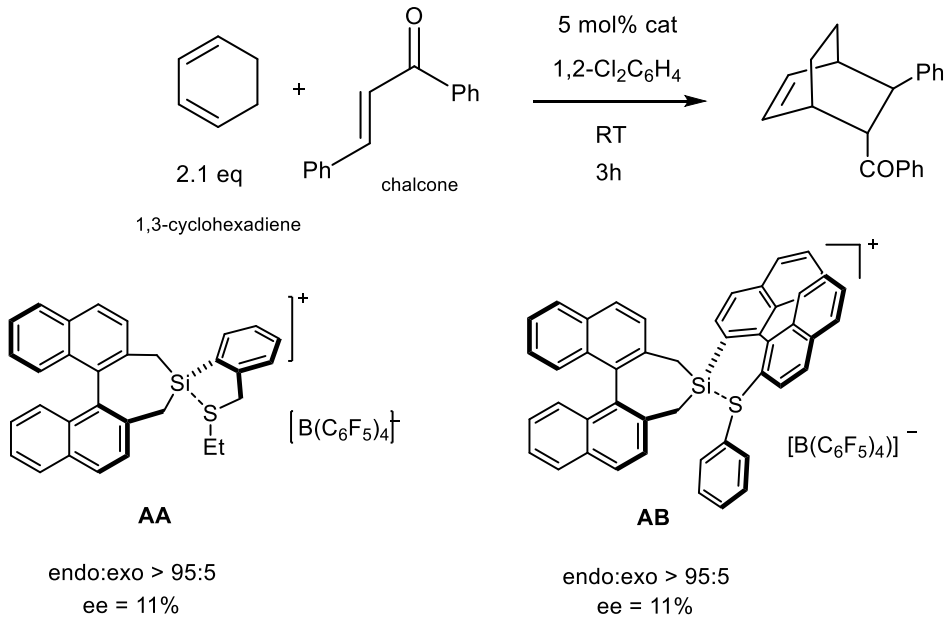

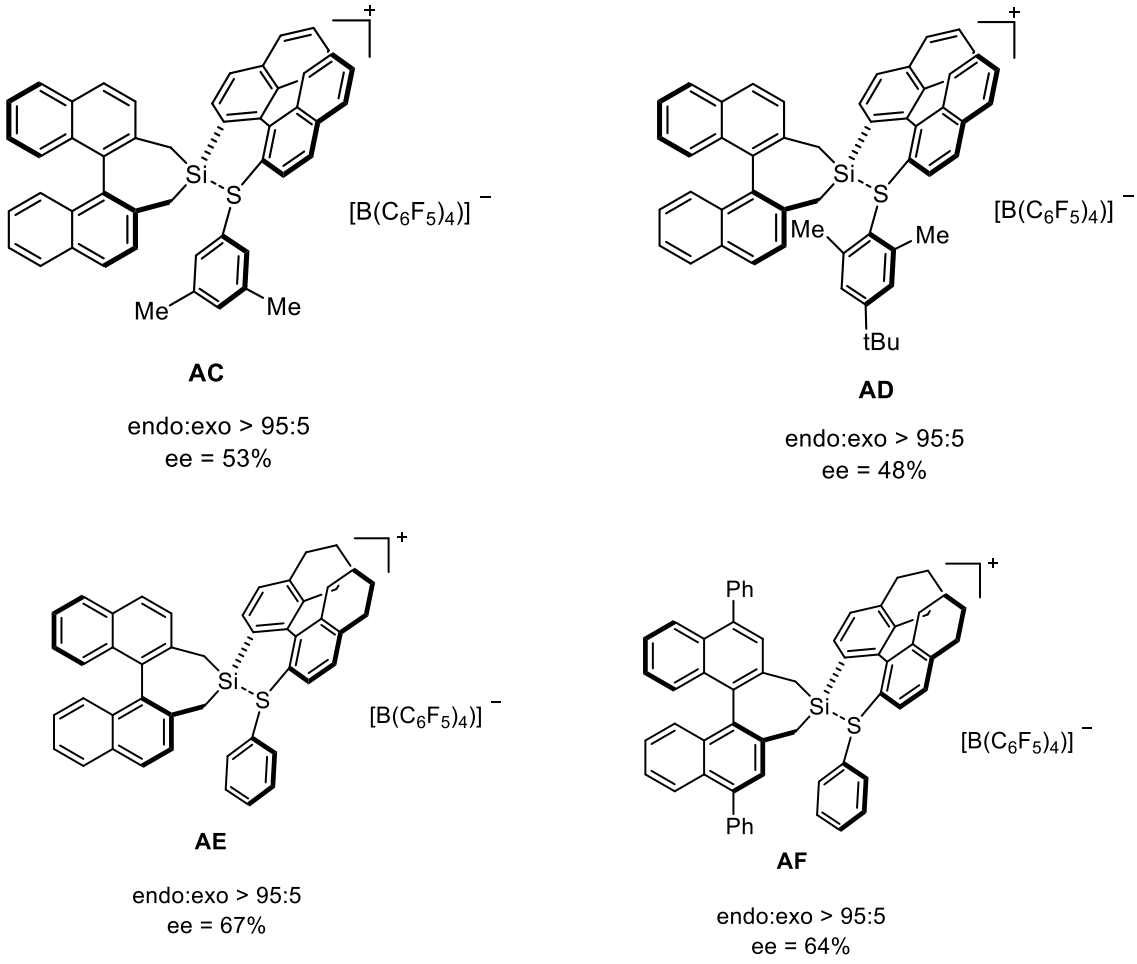

Figure 2.4: Reported *ee*% values for the reaction of interest[17, 19-22]

2.1.2 Systematic changes to the steric bulk at the achiral end

As proposed in Chapter 1, the achiral β-diketiminate supporting ligand in our already published Al bistriflate complex (**1,** Figure 2.5)[18,23] is replaced by a chiral ligand having a similar structure (Figure 2.6). This is achieved by the synthesis of several chiral ligands similar to the ones published by G. Du and co-workers[24] and complexing them with an aluminium fragment. These ligands contain several different groups at the achiral end of the complex introducing different amounts of steric congestion around the central aluminium atom. We initially planned to start with arguably the most cost-effective group at the chiral end i.e. a phenyl group by using (*R*)-

(−)-2-phenylglycinol (see below), followed by inserting different substituents at the achiral end. This would allow us to examine the influence of the steric effects at the achiral end on the *ee* values of the asymmetric DA transformation.

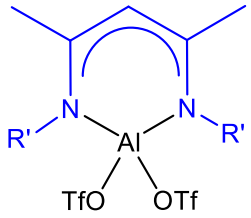

1

1a ^{Dip}LAl(OTf)$_2$: R'= 2,6-iPr$_2$-C$_6$H$_3$

1b ^{Xyl}LAl(OTf)$_2$: R' = 2,6-,Me$_2$-C$_6$H$_3$

1c ^{Ph}LAl(OTf)$_2$: R' = C$_6$H$_5$

Figure 2.5: Basic Structure of the reported achiral complex

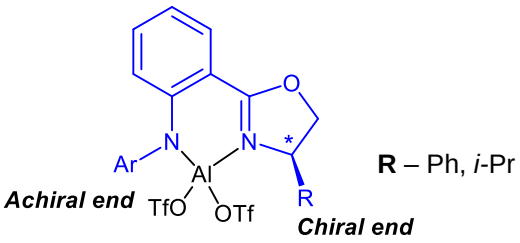

Ar
2,6-Me$_2$C$_6$H$_3$
Ph
2,6-*i*-Pr$_2$C$_6$H$_3$
2,4,6-(CH$_3$)$_3$C$_6$H$_2$
4-CH$_3$-2,6-(CH(Ph)$_2$)$_2$C$_6$H$_2$
4-*t*-Bu, 2,6-(CH(Ph)$_2$)$_2$C$_6$H$_2$

Figure 2.6: Introducing Chirality at β-diketiminate supporting ligand, basic structures of proposed chiral Al complexes

2.1.3 Proposed Synthetic route for chiral β-diketiminate-like supporting ligands

After careful selection, a route for the synthesis of the ligands was adopted from published methods[24,25] with minor modifications (Scheme 2.1). The proposed synthetic method contained two-steps and the first step involved the synthesis of chiral oxazolines by reacting suitable commercially available, enantiomerically pure amino alcohols with 2-bromobenzaldehyde. As depicted in Scheme 2.1, the resulting purified, isolated chiral oxazolines were then subjected (step 2) to a palladium catalysed Buchwald-Hartwig amination reaction for the coupling of the chiral oxazoline with a suitable amine via the attached bromo-group on the benzene ring of the oxazoline.

This two-step method allowed for a facile modification of the whole structure at the two ends. Using a different enantiopure amino alcohol, which are usually commercially available, in the first step of Scheme 2.1, structural modifications at the chiral end could be introduced (**R**). Then, by replacing the Ar-NH_2 (simply by using different aromatic amines) in step 2 of Scheme 2.1, additional structural modifications could be introduced at the achiral end (**Ar**).

Scheme 2.1: Synthetic route for chiral β-diketiminato type ligands

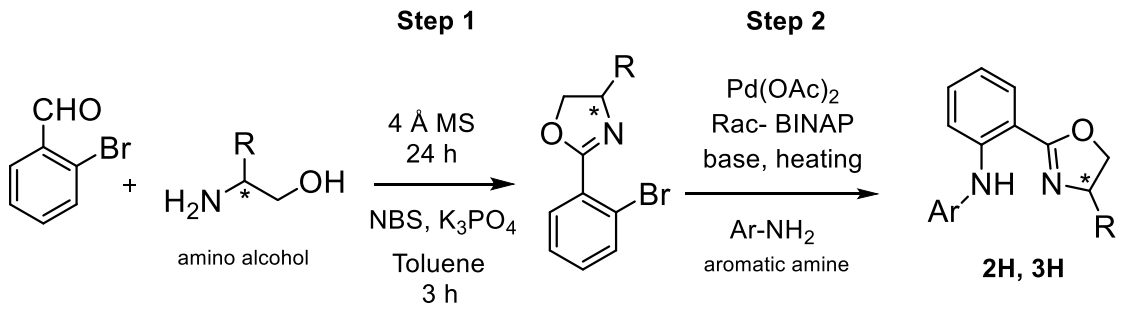

2.2 Results and discussion

2.2.1 Synthesis and characterisation of ligands

Changing the achiral end of these complexes using different commercial and synthesised anilines was identified as the most economically feasible approach to initiate the project.

Table 2.1: Starting materials and yields obtained of ligand synthesis

Entry	**Cat.**	**R**	**Ar-NH_2**	**Yield (%)**		**Physical appearance**
				Step 1	**Step 2**	
1	**2H**	Ph	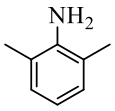	35	20	yellow solid
2	**3aH**	*i*-Pr	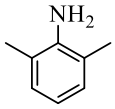	42	30	yellow oil
3	**3bH**	*i*-Pr	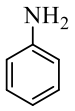	42	44	orange oil
4	**3cH**	*i*-Pr	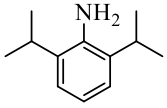	42	37	white solid
5	**3dH**	*i*-Pr	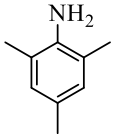	42	50	brown oil
6	**3eH**	*i*-Pr	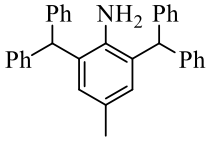	42	23	white solid
7	**3fH**	*i*-Pr	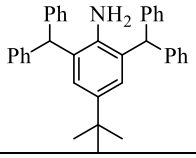	42	20	yellow solid

As briefly indicated above, we started the project with the cost-effective and widely available amino alcohol, (*R*)-(−)-2-phenylglycinol, in order to examine and optimise the influence of steric bulk at the achiral end, with the subsequent intention of using that information to optimise the achiral end by using different amino alcohols (entry 1, Table 2.1).

However, the ligand (i.e. **2H**, Table 2.1) prepared from this particular amino alcohol underwent racemisation (for details see section 2.2.2 below) once the ligand was complexed with aluminium (i.e. after preparing **2AlCl$_2$**), prompting us to change to the isopropyl (*i*-Pr) analogue, which was synthesised by using L-valinol in step 1 (entries 2-7, Table 2.1). Therefore, multiple ligand entities were synthesised by keeping the *i*-Pr group at the chiral end/**R**, while varying the nature of the aromatic fragment at the achiral end/**Ar.**

Synthesis of all proposed ligands in Table 2.1 were achieved by following the two-step method described in Scheme 2.1 producing the anticipated compounds with low to average yields (~ 35-40%). It should be mentioned that the products obtained after step 1 contained impurities according to multinuclear NMR spectroscopy, which was believed to be due to the presence of possible oxazoline intermediate(s) and/or unreacted 2-bromobenzaldehyde. These undesired additional signals in the multinuclear NMR spectra could be reduced by repeating purification step using column chromatography. However, the multinuclear NMR spectroscopic data for final ligand products, after completing both steps, showed the presence of very pure species even when less purified starting materials from initial step 1 were used.

Ligands **2H** and **3aH-3cH** were already reported in literature and ^{1}H and ^{13}C NMR spectroscopic data collected for these ligands were in accordance with the literature values confirming that the expected products were obtained.[24,26–28] In addition, ligand **2H** could easily be recrystallised in hexane, producing yellow needle like crystals, which were further characterised using single crystal X-ray analysis. The crystal structure supported that this

particular ligand was chiral, belonging to $P2_12_12_1$ space group (Figure 2.7). However, as **3aH** and **3bH** were isolated as oils these ligands could not be characterised by single crystal X-ray crystallography, while numerous attempts to crystallise **3cH** were not successful. Nevertheless, as all these structures were extensively studied in reports published by Du and co-workers and matching multinuclear NMR spectroscopic data were considered to be sufficient for establishing their respective identities.[24,26–28]

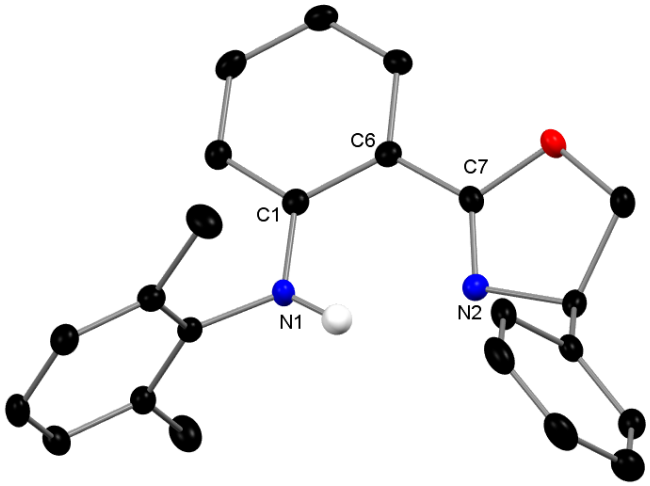

Figure 2.7: Single crystal X ray structure of **2H** as drawn at the 30% probability level. All hydrogen atoms, apart from N-H, as well as residual solvent molecules are omitted for clarity. Selected bond distances (Å); N1-C1 1.282(4), C1-C6 1.455(3), C6-C7 1.429(3), N2-C7 1.369(4)

Moreover, in order to investigate the effects of even more sterically demanding structural elements, more bulkier anilines were introduced in step 2 of Scheme 2.1, forming three novel ligands (**3dH**, **3eH** and **3fH** in Table 2.1). In order to achieve this, two anilines, 2,6-bis(diphenylmethyl)-4-methylaniline (for **3eH**) and 2,6-bis(diphenylmethyl)-4-*tert*-butylaniline (for **3fH**), had to be synthesised using published methods (entries 6 and 7 Table 2.1)[29] and were reacted with the chiral bromo oxazoline obtained in step 1 under the same

conditions described in Scheme 2.1. It was found that these bulky ligands were less stable and were, hence, stored under inert conditions after purification. Initial characterisation of these new ligands was attempted using multinuclear NMR spectroscopy. However, due to the very bulky nature of the ligands, and consequent restricted rotation around the ^{Ar}N-C bond, the ^{1}H NMR signals were not well-defined and some of the expected signals, such as the one assigned to the N-H fragment, were barely visible. In order to resolve this matter, multinuclear NMR spectra were obtained at high temperatures (i.e. at 55°C) which proved to be sufficient to overcome the restricted rotation around the ^{Ar}N-C bond as more defined multinuclear NMR signals were observed. Additionally, a crop of crystals for ligands **3eH** and **3fH** were obtained, which were, then, successfully characterised using single crystal X-ray analysis (Figure 2.8 and Figure 2.9). For **3eH** (Figure 2.8), two unique molecules were present in the asymmetric unit that differed only in the relative orientations of the substituent phenyl rings. The X-ray structure also supported the chirality of the ligand as it was solved in the enantiomorphic I_2 space group (Table 2.2). Similarly, the structure of **3fH** was solved in the non-centrosymmetric space group P1, with two full molecules in the asymmetric unit (Figure 2.9 and Table 2.2). Furthermore, the values for N1-C1 (average 1.368 Å) and N2-C7 (average 1.273 Å) bond distances clearly indicated electron localisation for the central N_2C_3 fragment, which were, albeit at a significantly smaller extent, observed for achiral β-diketiminato ligands.[30]

Unfortunately, **3dH** could not be crystallised as it was an oil in nature, but the structure could sufficiently be characterised using multinuclear NMR spectroscopy. In addition, most of the structures were further confirmed using high-resolution mass spectrometry (HRMS) as well elemental analyses (see appendix for relevant data).

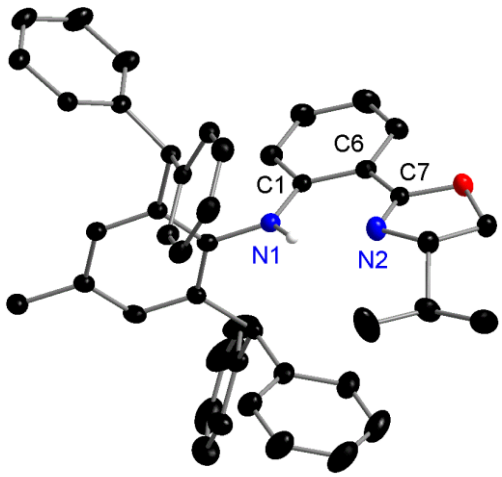

Figure 2.8: Solid state structures for **3eH** as drawn at the 30% probability level. All hydrogen atoms, apart from N-Hs, as well as residual solvent molecules are omitted for clarity. Selected bond distances (Å); N1-C1 1.368(4), C1-C6 1.405(5), C6-C7 1.462(5), N2-C7 1.275(5)

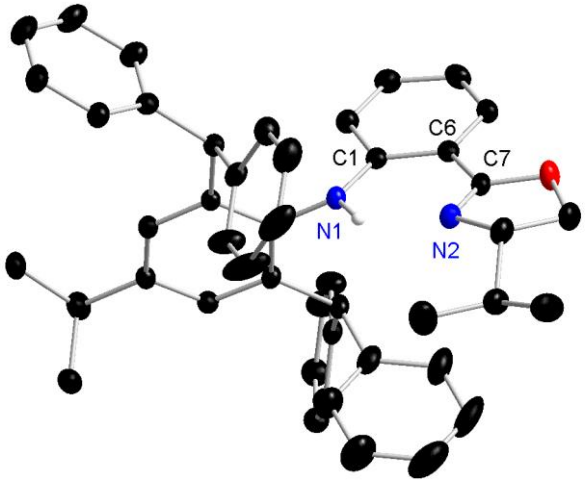

Figure 2.9: Solid state structures for **3fH** as drawn at the 30% probability level. All hydrogen atoms, apart from N-Hs, as well as residual solvent molecules are omitted for clarity. Selected bond distances (Å); N1-C1 1.368(4), C1-C6 1.421(5), C6-C7 1.461(5), N2-C7 1.271(5)

Table 2.2: Summary of the crystallographic data for ligand synthesis

	2H	**3eH**	**3fH**
Formula	$C_{23}H_{22}N_2O$	$C_{91}H_{85}Cl_3N_4O_2$	$C_{48}H_{48}N_2O$
Formula weight	342	1372.97	668.88
Crystal system	Orthorhombic	Monoclinic	Triclinic
Space group	$P2_12_12_1$	I_2	P1
a /Å	10.7263(5)	25.8439(2)	10.4019(3)
b/Å	10.8731(5)	10.5505(1)	13.7970(3)
c/Å	15.7407(9)	28.3697(2)	15.2529(4)
α /deg	90	90	66.674(2)
β /deg	90	101.6780(10)	77.295(2)
γ /deg	90	90	77.259(2)
V / Å^3	1835.81(16)	7575.33(11)	1939.00(9)
Z	4	4	2
Dc/ g cm^{-3}	1.239	1.204	1.146
F(000)	728.0	2904	716.0
Crystal size/ mm	0.18 x 0.159 x 0.08	0.15 x 0.08 x 0.05	0.15 × 0.08 × 0.05
θ range/°	7.436 to 52.04	4.223 to 77.497	7.056 to 155.478
Reflections collected / unique	7192/3368 [R_{int} = 0.0446]	61556/15643 [R_{int} = 0.0337]	26609/10453 [R_{int} = 0.0568]
R_1 [I >2σ (I)]	R_1 = 0.0421, wR_2 = 0.0948	R_1 = 0.0513, wR_2 = 0.1285	R_1 = 0.0580, wR_2 = 0.1528
wR_2 (all data)	R_1 = 0.0527, wR_2 = 0.1007	R_1 = 0.0529, wR_2 = 0.1295	R_1 = 0.0654, wR_2 = 0.1656
Peak and hole/e Å^{-3}	0.15 and − 0.15	0.820 and − 0.422	0.32 and − 0.26
Flack Parameter	− 3.5(10)	0.045(10)	0.0(4)

2.2.2 Synthesis and characterisation of Al complexes

The synthesis of the target aluminium bistriflate complexes was adopted from our previous reported method with minor modifications.[18] Firstly, the ligands were lithiated at low temperature, and quenched with aluminium trichloride, obtaining ligand-aluminium dichloride complexes. The final targeted aluminium bistriflate complexes were synthesised by ligand exchange using silver triflate (AgOTf) as elaborated in Scheme 2.2.

As we mentioned previously, our initial plan was to use the ligand(s) prepared from (*R*)-(−)-2-phenylglycinol i.e. the ligands what would have a phenyl group connected to the chiral end while the nature of the groups at the achiral end would be modified. Indeed, we used the above-mentioned synthetic procedure (Scheme 2.2) to prepare **2AlCl$_2$** with a yield of 62%. The

Scheme 2.1: suggested synthetic route for chiral β-diketiminato type ligand supported Al bis triflate complexes

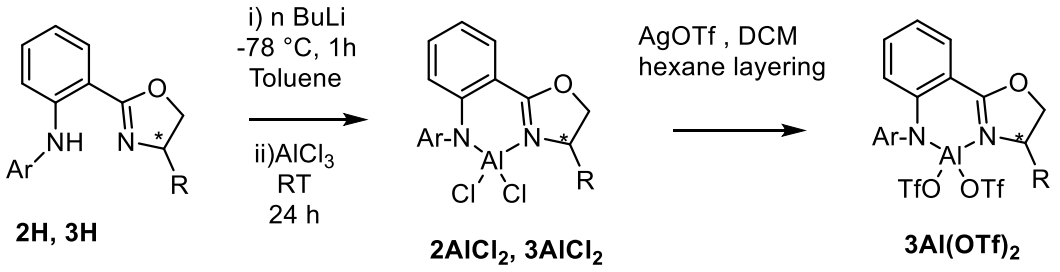

multinuclear NMR spectroscopic data suggested that the structure was as expected. In addition, a crop of crystals afforded from hexane were subjected to single crystal X-ray crystallography for further investigation of the structure and chirality.

Although the ligand was chiral, and the basic structure of the aluminium dichloride complex contained a chiral C atom, the crystal system was found to be centrosymmetric and, thus, achiral. The X-ray structure depicted the presence of a pair of enantiomers with either S or R configuration (at 1:1 ratio) and showed a 100% fit for the achiral space group I 2/a. This aligns with a previous study by Bian, et al.[28] which described the same scenario during the synthesis of an $AlMe_2$ complex using the same chiral ligand. Similar to our finding, the reported crystal structure showed both (*S*) and (*R*) conformers in the centrosymmetric space group P-1. We postulated that this racemisation could be the result of the propensity of the phenyl ring at the chiral end to form an extended conjugate system with the central six-membered ring via shuffling of the H atom found at C17, (Figure 2.10) converting it to a sp^2 carbon instead. Thus, this momentary conversion might be responsible for the loss of the enantiospecificity of the complex leading to the racemic mixture.

In order to further support this hypothesis, we replaced the phenyl group with an isopropyl group, which was unlikely to contribute to extended conjugation with the N_2C_3 fragment.

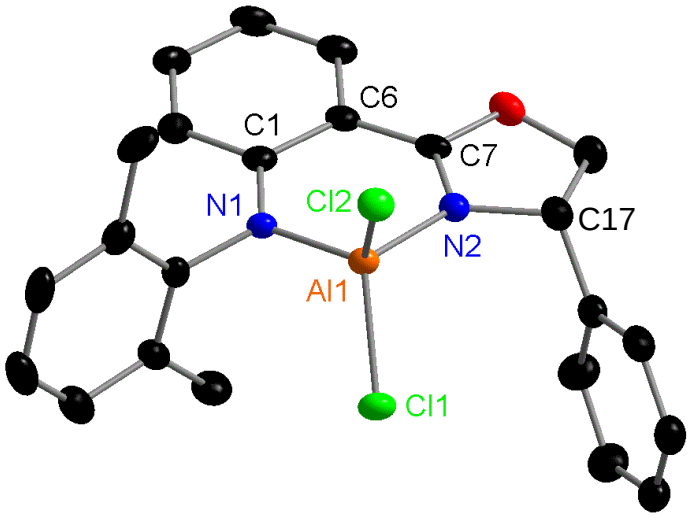

Figure 2.10: Single crystal X ray structure of **2AlCl$_2$** as drawn at the 30% probability level. All hydrogen atoms are omitted for clarity. Selected bond distances (Å) and angles (˚); Al1-N1 1.823(3), Al1-N2 1.867(4), Al1-Cl1 2.107(2), Al1-Cl2 2.139(2), N1-C1 1.377(6), C1-C6 1.426(6), C6-C7 1.434(4), N2-C7 1.312(5) N1-Al1-N2 97.7(2), Cl1-Al1-Cl2 106.91(7).

Therefore, **3aH** ligand was subjected to the reaction with $AlCl_3$, after the lithiation step, to obtain **3aAlCl$_2$**. Initially, the structure of **3aAlCl$_2$** was confirmed by comparison of the ^{1}H NMR spectrum with that of the ligand, **3aH**. Absence of the N-H signal observed at δ_H 9.96 ppm suggested that the deprotonation had occurred and that the binding of the N atoms to aluminium had happened. Furthermore, major changes in δ_H signal patterns were also observed for the oxazoline ring area as it was directly affected by the aluminium binding. All three proton signals assigned to the oxazoline ring were shifted downfield by *ca*. δ_H 0.4 ppm, supporting the presence i.e. coordination of an aluminium atom. In addition, the proton signal for C*H*$(CH_3)_2$ of the adjacent *i*-Pr group also shifted downfield from δ_H 1.82 to 2.71 ppm further confirming that aluminium binding had occurred. On the other hand, the ^{1}H NMR spectroscopic signals assigned to the aromatic region of both N^{Ar} and ligand backbone, including various substituents bound to it N^{Ar}, appeared to be almost identical as the analogous ones observed for the free ligand. Further, the ^{13}C NMR spectroscopic signal assigned to the C=N fragment, which

appeared at δ_C 163.8 ppm in the free ligand, shifted downfield to δ_C 171.7 ppm providing more evidence for aluminium binding. In addition, all other δ_C signals with a close proximity to the coordinating N atoms also appeared to be slightly shifted. The other most significant evidence of aluminium binding was the appearance of a clear singlet observed at δ_{Al} ~ 104 ppm. Since multinuclear NMR spectroscopy is not capable of confirming whether the chirality of the ligand is being preserved after the binding had occurred, optical activity of the aluminium dichloro complex, **3aAlCl$_2$** was also tested. An $[\alpha]_D$ value of – 46.0 (*c* = 1.0 g/100 mL, $CHCl_3$) was obtained confirming that the complex was chiral. Unfortunately, all the attempts taken to crystallise this solid were unsuccessful.

Encouraged by these findings, other ligands containing the same *i*-Pr functional group at chiral C were reacted with $AlCl_3$ after the lithiation step (entries 2-7, Table 2.1). All these dichloro Al complexes, **3bAlCl$_2$-3fAlCl$_2$** were collected as solids in good yields (63-95%) after evaporating the residual toluene and washing with dry hexane. Initial characterisation by ^{1}H NMR spectroscopy revealed, similar to the analysis for **3aAlCl$_2$**, that the most obvious and notable change was the loss of the N-H proton (δ_H 9 -10 ppm). This change provided significant evidence that the ligands were successfully binding with the aluminium centre creating the target complexes. Although only very minute changes were seen (if any) for most of the δ_H signals found in the aromatic regions (both N^{Ar} and ligand backbone), major changes were observed for the δ_H signals belonging to the oxazoline ring, presumably due to its direct interaction with the metal. For example, all three δ_H signals for the oxazoline ring shifted downfield by about 0.3-1.0 ppm. In addition, the δ_H signals belonging to the C*H*$(CH_3)_2$ of the adjacent *i*-Pr group at the chiral end also shifted downfield from δ_H *ca.*1.7 to *ca.* 2.6 ppm. Moreover, the ^{13}C NMR spectroscopic signal assigned to the C=N fragment, which appeared at around δ_C 160 ppm in the free ligand, shifted downfield to around δ_C 170 ppm providing more evidence for aluminium biding to the N atom. Additionally, other ^{13}C NMR spectroscopic

signals which were adjacent to the binding core were also observed to shift downfield but only slightly. Notably, the ^{27}Al NMR spectra of almost all these complexes showed a signal at around δ_{Al} 102 ppm confirming that aluminium was bound to the ligands as expected.

Fortunately, three of these complexes, **3bAlCl$_2$** **3eAlCl$_2$** and **3fAlCl$_2$** were crystallised in mixtures of dichloromethane or 1,2-difluorobenzene and hexane, and were subjected to single crystal X-ray analysis. To our delight, all structures showed the expected structural geometries and chirality. Two unique molecules were found in the crystal structure of **3bAlCl$_2$** (Figure 2.11) differing only in the orientation of the phenyl ring. The chirality was supported as the data were solved in a triclinic crystal system belonged to the chiral space group P1 (Table 2.3).

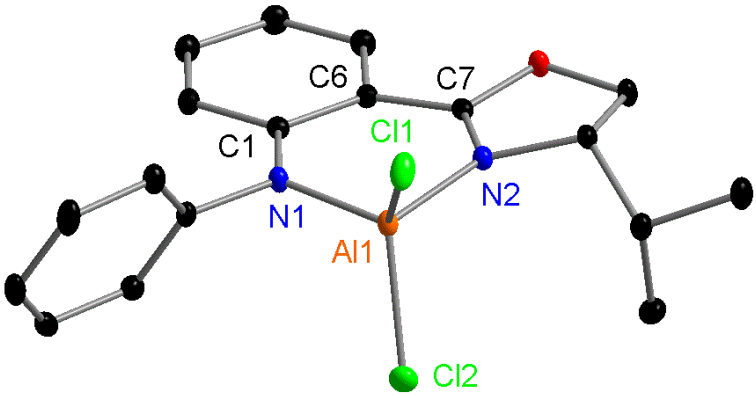

Figure 2.11: Single crystal X ray structure of **3bAlCl$_2$** as drawn at the 30% probability level. All hydrogen atoms and any solvent molecules are omitted for clarity. Unit cells consisted of two unique molecules only one of them is shown. Selected bond distances (Å) and angles (˚); Al1-N1 1.835(2), Al1-N2 1.8689(2), Al1-Cl1 2.130(1), Al1-Cl2 2.1237(7), N1-C1 1.377(3), C1-C6 1.428(2), C6-C7 1.445(2), N2-C7 1.306(3) N1-Al1-N2 97.56(8), Cl1-Al1-Cl2 109.61(3).

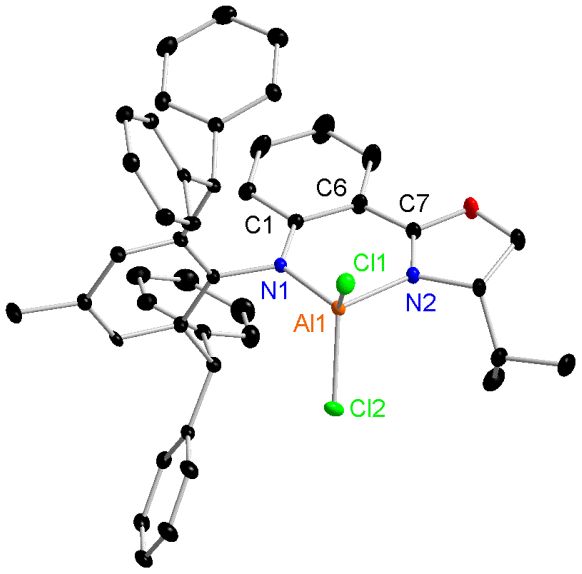

Figure 2.12: Single crystal X ray structure of **3eAlCl$_2$** as drawn at the 30% probability level. All hydrogen atoms and any solvent molecules are omitted for clarity. Unit cells consisted of two unique molecules only one of them is shown. Selected bond distances (Å) and angles (˚); Al1-N1 1.835(1), Al1-N2 1.871(1), Al1-Cl1 2.1377(6), Al1-Cl2 2.1190(7), N1-C1 1.383(2), C1-C6 1.427(2), C6-C7 1.439(3), C7-N2 1.301(2), N1-Al1-N2 98.48(6), Cl1-Al1-Cl2 107.50(3).

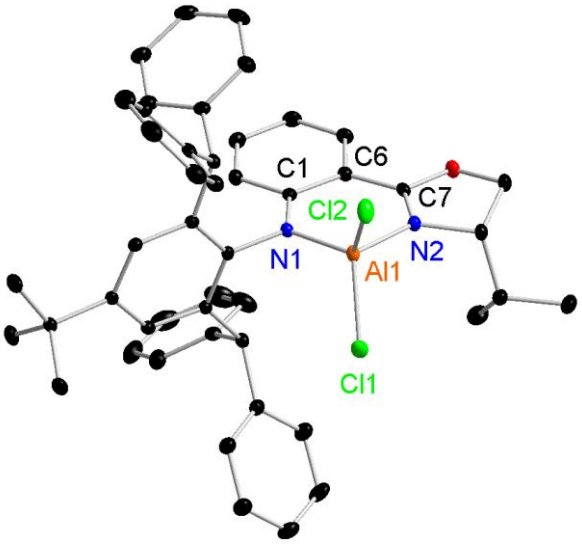

Figure 2.13: Single crystal X ray structure of **3fAlCl$_2$** as drawn at the 30% probability level. All hydrogen atoms and any solvent molecules are omitted for clarity. Unit cells consisted of two unique molecules only one of them is shown. Selected bond distances (Å) and angles (˚); Al1-N1 1.847(3), Al1-N2 1.873(2), Al1-Cl1 2.122(1), Al1-Cl2 2.134(1), N1-C1 1.385(3), C1-C6 1.421(2), C6-C7 1.440(4), N2-C7 1.308(4) N1-Al1-N2 98.19(9), Cl1-Al1-Cl2 108.53(3).

Table 2.3: Summary of the crystallographic data for Al-dichloro complexes

	3aAlCl$_2$	**3bAlCl$_2$**	**3eAlCl$_2$**	**3fAlCl$_2$**
Formula	$C_{23}H_{21}AlCl_2N_2O$	$C_{18}H_{19}AlCl_2N_2O$	$C_{45}H_{41}AlCl_2N_2O$	$C_{54}H_{51}AlCl_2F_2N_2O$
Formula weight	439.30	377.23	723.68	879.85
Crystal system	Monoclinic	Triclinic	Monoclinic	triclinic
Space group	I2/a	P1	I_2	P1
a /Å	16.0600(14)	8.05680(10)	12.7756(2)	10.05910(10)
b/Å	15.5021(11)	9.7524(2)	9.9253(2)	10.2551(2)
c/Å	18.4978(17)	12.7427	30.1239(5)	12.5367(2)
α /deg	90	73.1720(10)	90	113.677(2)
β /deg	112.814(11)	75.0700(10)	98.056(2)	95.1890(10)
γ /deg	90	72.673(2)	90	102.2070(10)
V / Å^3	4245.0(7)	898.63(3)	3782.07(12)	1135.18(3)
Z	8	2	4	1
Dc/ g cm^{-3}	1.375	1.394	1.271	1.287
F(000)	1824	392	1520	462
Crystal size/ mm	0.112 x 0.088 x 0.018	0.173 x 0.129 x 0.097	0.287 x 0.260 x 0.161	0.6 × 0.1 × 0.1
θ range/°	3.392 to 26.021	3.401 to 31.961	3.221 to 32.037	7.852 to 159.894
Reflections collected/ unique	21472/4172	34610/10032	49969 / 11268	45509/ 9189
R_{int}	0.0992	0.0307	0.0352	0.0388
R_1 [$I > 2\sigma(I)$]	R_1 = 0.0688, wR_2 = 0.1394	R_1 = 0.0277, wR_2 = 0.0631	R_1 = 0.0318, wR_2 = 0.0778	R_1 = 0.0299, wR_2 = 0.0793
wR_2 (all data)	R_1 = 0.1066, wR_2 = 0.1549	R_1 = 0.0304, wR_2 = 0.0643	R_1 = 0.0360, wR_2 = 0.0796	R_1 = 0.0306, wR_2 = 0.0799
Peak and hole/e Å^{-3}	0.460 and − 0.420	0.242 and − 0.219	0.234 and − 0.218	0.26 and − 0.24
Flack parameter	− 3.5(10)	− 0.005(16)	− 0.032(14)	− 0.014(5)

Comparably, the crystal structures for **3eAlCl$_2$**, and **3fAlCl$_2$** were also chiral, belonging to the non-centrosymmetric space groups monoclinic I2 and triclinic P1, respectively (Figure 2.11, Figure 2.12, Table 2.3). The average bond distances for Al1-N1 (*ca.* 1.84 Å), Al-N2 (*ca.* 1.87 Å), N1-C1 (*ca.* 1.38 Å) and N2-C7 (ca. 1.30 Å) exhibited a great degree of localisation of electron density in the central AlN_2C_3 ring. This was expected considering the fact that ligands' carbon backbones contained a phenyl ring whose presence was probably responsible for the overall electron localisation. It was also noticeable that the N1-Al1-N2 bite angles increased while Cl1-Al1-Cl2 angles decreased as the steric bulk increased from **3bAlCl$_2$** to **3eAlCl$_2$** and **3fAlCl$_2$** (Figure 2.11, Figure 2.12, Figure 2.13). With this collection of structural information and in-depth analysis via multinuclear NMR spectroscopy together with CHN elemental

analysis and HRMS data, it was concluded that expected dichloro aluminium complexes were successfully synthesised.

We then proceeded to investigate the ligand exchange to obtain the final proposed bistriflate complexes (Scheme 2.2). We initiated the process by synthesising **3aAl(OTf)$_2$**, which was obtained as a dark brown solid, and characterised by multinuclear NMR spectroscopy and polarimetry as no crystals could be obtained after numerous attempts. Evidently, the most notable change was the shift of the ^{27}Al NMR spectroscopic signal which was observed at δ_{Al} – 22 ppm (as compared to the values of δ_{Al} 102 ppm for the dichloro precursors), showing that the environment surrounding the central aluminium atom changed. In addition, the ^{19}F NMR spectrum showed a signal around δ_F – 77.7 ppm indicating that the triflate groups were bound, as the free/unbound group is usually observed at δ_F – 79 ppm. The ^{1}H NMR spectrum for **3aAl(OTf)$_2$** contained only slightly shifted signals in comparison to that of **3aAlCl$_2$**, showing that the ligand protons were intact after the dichloro to bistriflate transition. These slight shifts were mostly observed in the protons representing the oxazoline ring area. Further, the ^{13}C NMR spectroscopic signal assigned to the C=N fragment shifted to δ_C 171.7 ppm (from δ_C 174.1) indicating the possible change of the coordination environment around the aluminium centre. In addition, the other δ_C signals surrounding the binding region also appeared to be slightly shifted. An $[\alpha]_D$ value of – 26.0 (*c* = 0.05 g/100 mL, $CHCl_3$) confirmed that the complex was chiral.

These results/observations confirmed that the proposed synthetic route could be successfully adopted for the synthesis of the suggested chiral bistriflate complexes. Therefore, all other obtained Al dichloro complexes were reacted with AgOTf and the resulting products were primarily analysed with the aid of multinuclear NMR spectroscopy. However, when bulkier dichloro complexes, **3eAlCl$_2$**, and **3fAlCl$_2$** were reacted with AgOTf, the presence of unidentified side products was also evident in the overall product mixtures. This was

circumvented by replacing dichloromethane with 1,2-difluorobenzene as the solvent medium because the latter was considered as a more inert and non-coordinating solvent than the former.[31,32] All ^{1}H NMR spectra of these bistriflate complexes were similar to that of the respective Al dichloro complexes with minor shifts and slight differences in peak patterns. This confirmed that the coordination environment around the aluminium centre has changed but the structure of the ligand was intact as expected. For almost all the complexes, observed changes were similar to that of **3aAl(OTf)$_2$**. Further, the ^{13}C NMR signal belonging to the C=N fragment, observed at around δ_C 171 ppm in the dichloro precursors, shifted upfield to around δ_C 173 ppm. It was evident that all these changes in proton signals were occurring at a close proximity to the two N atoms, confirming that the binding core around aluminium was structurally modified. Furthermore, the ^{19}F NMR spectra showed a signal around δ_F – 77 ppm representing a bound triflate group. In some instances, this signal was either broadened or split, which we attributed to the restricted rotation of the bulky aryl substituents of these asymmetric complexes. Additionally, the ^{27}Al NMR spectroscopic signals were seen at around δ_{Al} – 22 ppm (instead of around δ_{Al} 102 ppm) for almost all the bistriflate complexes suggesting that the coordination environment around Al had changed. Unfortunately, numerous attempts to crystallise these bistriflate complexes were not successful.

2.2.3 Catalysis of asymmetric Diels Alder reactions

In order to make an assessment regarding the catalytic activity of these complexes, including possible enantioinduction, **3aAl(OTf)$_2$** was initially used as the catalyst for asymmetric DA reactions. Similar to the published achiral catalytic system by our group, a 1:1 mixture of **3aAl(OTf)$_2$** and Na[BAr$^{Cl}_4$] (Ar^{Cl} = 3,5-Cl$_2$-C$_6$H$_3$) was used as the catalytic system.[18,33–35] We selected a few dienes and dienophiles, including a few that are considered to be relatively less reactive and less explored. We chose different combinations of these dienes and dienophiles (Figure 2.14), which were known to show different reactivities towards DA cycloaddition, in

order to gain a general idea of how active our synthesised complexes were. We also used simple means of optical rotation to make initial qualitative measurements of enantiospecificity of the products.

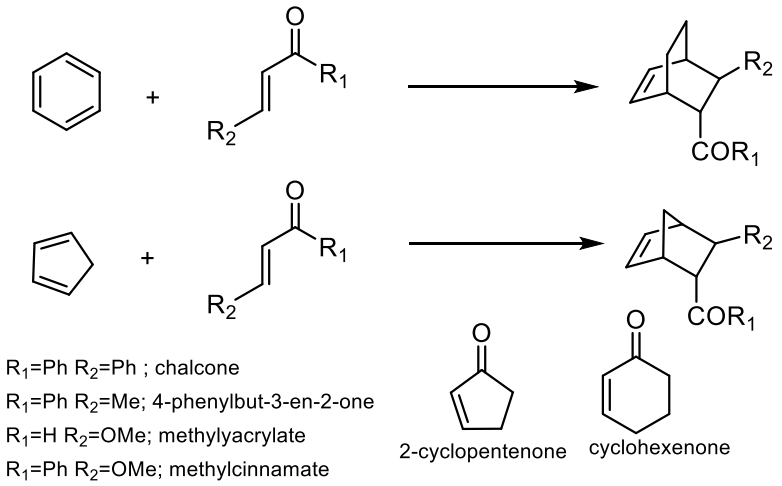

Figure 2.14: less reactive DA substrates selected for initial screening

When methylacrylate was reacted with cyclopentadiene, which was regarded as a reactive diene, we observed excellent reactivity (entry 1, Table 2.4). Encouraged by this, we moved on to test the other two dienophiles, chalcone (entry 2, Table 2.4) and 4-phenylbut-3-en-2-one (entry 3, Table 2.4) with the same diene. Both these dienophile substrates are considered to have a relatively low reactivities towards DA reactions, as they have electron donating substituents at the carbonyl carbon and β-carbon atoms. Observing substrate conversion above 99% within 2-3 hours at room temperature for both reactions indicated that the catalyst was active towards anticipated reactions with cyclopentadiene. Two cyclic dienophiles were also reacted with cyclopentadiene to obtain good conversion percentages (entries 5,6 Table 2.4). However, low reactivity was observed towards the least reactive dienophile we tested, i.e. methyl-cinnamate, showing only 85% conversion in 5 days. Nevertheless, this reactivity towards cyclopentadiene encouraged us to move forward with the much less reactive diene i.e. 1,3- cyclohexadiene.

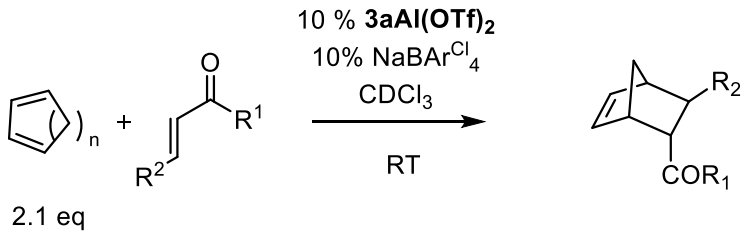

Table 2.4: Initial screening of catalytic efficiency and enantioselectivity towards selected DA reactions using **3aAl(OTf)$_2$**

entry	n	dienophile	adduct	time (h)	*endo*:*exo* [a]	conv. (%)[b]	yield (%)[c]	$[\alpha]_D$ [e]	ee (%)[d]
1	1	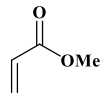	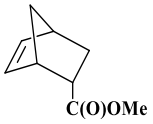	1.5	(96:4)	>99	80	+15	N/A
2	1	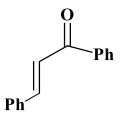	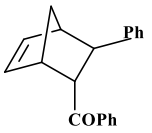	2	(80:20)	> 99	88	+53	N/A
3	1	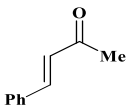	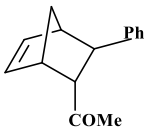	3	(76:24)	> 99	90	+16	N/A
4	1	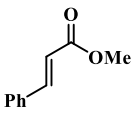	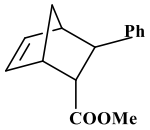	120	(80:20)	>85	70	+14	24
5	1	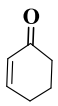	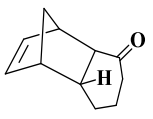	18	(87:13)	95	59	+17	N/A

6	1		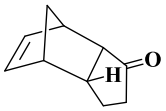	3	(86:14)	>95	50	+15	N/A
7	2	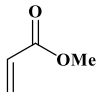	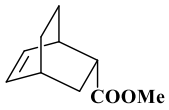	12	(99:1)	> 95	65	+15	N/A
8	2	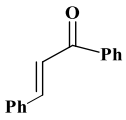	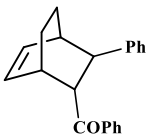	24	(98:2)	> 98	60	+19	12
9	2	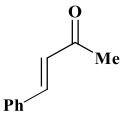	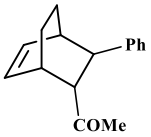	60	(99:1)	>80	45	+51	N/A
10	2	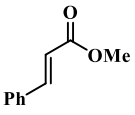	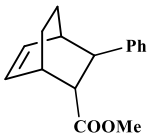	336	-	<10	-	-	-
11	2	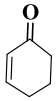	polymerised	12	-	-	-	-	-
12	2		polymerised	12	-	-	-	-	-

[a] Determined by GLC analysis of the reaction mixture prior to purification. [b] Determined by NMR analysis. [c] Analytically pure *endo*-product after column chromatography on silica gel. [d] Determined by HPLC or GLC analysis using suitable chiral stationary phases. [e] c = 1 g/100 mL, solvent; $CHCl_3$

Although the respective reaction times when 1,3-cyclohexadiene was used were significantly longer than in the case of cyclopentadiene, the catalytic system showed respectable activity towards a number of reactions. With more reactive methyl acrylate, adequate conversion was accomplished in 12 h (entry 7, Table 2.4), while with less reactive chalcone and 4-phenylbut-

3-en-2-one the reaction times increased to 24 and 60 h, respectively (entries 8 and 9, Table 2.4). However, a very slow reaction progress was observed with methyl-cinnamate, as even after 2 weeks a small amount of the product formed. When cyclic dienophiles were mixed with cyclohexadiene, self-polymerisation reactions of the dienophiles occurred instead of the DA reaction (entries 11, 12 Table 2.4). This observation has been seen with our previous achiral catalytic systems as well.[34] It should be also noted that excellent *endo*:*exo* ratios were observed for with 1,3-cyclohexadiene, while comparatively lower stereoselectivities were observed for cyclopentadiene reactions. Additionally, all the products were purified via column chromatography to obtain yields ranging from 45 - 90%.

After observing satisfactory reactivity of the catalytic system towards majority of the examined reactions, we also obtained preliminary data for optical rotation. As the values obtained were considerably larger than zero, it was clear that the catalytic system was capable of driving the asymmetric DA reactions favouring one product. It is worth mentioning that these were tested against control reactions carried out with the analogous achiral system **1b** (Figure 2.15) and the optical rotation values obtained for the symmetric reactions were zero or negligible.

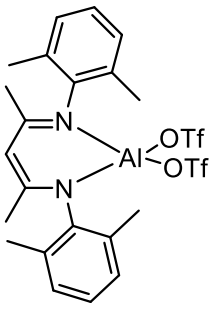

Figure 2.15: Achiral aluminium complex **1b**

We then progressed to analyse the *ee* values of the products using HPLC (High Performance Liquid Chromatography) and GLC (Gas Liquid Chromatography) coupled with chiral columns. The DA adduct between 1,3-cyclohexadiene and chalcone (entry 8, Table 2.4) was successfully separated and an *ee* value of 12% was obtained. In addition, the DA adduct between cyclopentadiene and methyl-cinnamate (entry 4, Table 2.4) was also successfully separated and exhibited an *ee* value of 24%. However, unfortunately, even after a number of attempts and developing many HPLC and GLC methods, others adducts (entries 1-3, 5-7, and 9 Table 2.4) were not successfully separated with the chiral columns available to us, in order to obtain a quantitative value for enantiomeric excesses. As the reaction between cyclopentadiene and methyl-cinnamate has been successfully studied by B. List and co-workers achieving up to 97% *ee* at low temperatures,[36] we decided to mainly focus on developing the activity of our chiral aluminium bistriflate complexes towards the synthesis of the DA adduct between 1,3-cyclohexadiene and chalcone.

Moving towards our major objective of exploring how steric factors at the achiral end of these complexes would affect the enantioselectivity results towards the DA reaction of less reactive dienophile chalcone and 1,3-cyclohexadiene, reactions represented in Table 2.5, were carried out. Complete conversion of chalcone into the DA adduct was observed in about 24 - 48 h, depending on the bulkiness of the complex. Understandably, higher reaction times were observed with the bulkier complexes. This revealed that although the basic structure of these chiral complexes was modified from our already published achiral catalyst,[18] the Lewis acidity was relatively unaffected. The products could be purified and collected in satisfactory yields of ~ 65% for all the reactions. Although a couple of complexes were out of the trend, improved enantiomeric induction was directly correlated with increasing steric demand at the achiral end of the complex.

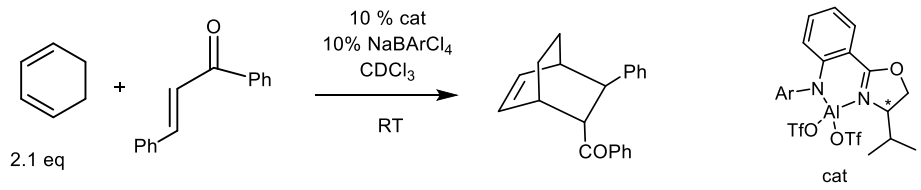

Table 2.5: Testing the effects of steric factors at achiral end of the catalyst on the DA reaction

entry	cat 	time (h)	*endo*:*exo* [a]	conv. (%)[b]	yield (%)[c]	ee (%)[d]
1	**3aAl(OTf)$_2$** 	24	98:2	> 98	60	12
2	**3aAlCl$_2$**	36	98:2	> 97	59	16
3	**3bAl(OTf)$_2$** 	24	98:2	> 98[e]	60	24
4	**3bAlCl$_2$**	36	98:2	> 98	57	8
5	**3cAl(OTf)$_2$** 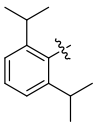	24	99:1	> 98[f]	70	35
6	**3cAlCl$_2$**	36	99:1	> 98	68	23
7	**3dAl(OTf)$_2$** 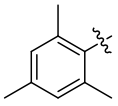	48	99:1	> 98[e]	67	19
8	**3dAlCl$_2$**	72	99:1	> 97	70	11

9	**3eAl(OTf)$_2$**		48	98:2	> 98[f]	73	42
10	**3eAlCl$_2$**	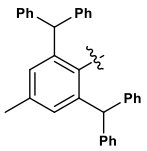	72	98:2	> 96	70	31
11	**3fAl(OTf)$_2$**		48	98:2	> 98[f]	55	41
12	**3fAlCl$_2$**	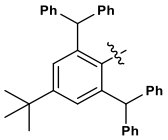	72	98:2	> 96	58	28

[a] Determined by GLC analysis of the reaction mixture prior to purification. [b] Determined by NMR analysis. [c] Analytically pure *endo*-product after flash column chromatography on silica gel. [d] Determined by HPLC analysis using a chiral OD-H column 98:2 (hexane: *i*-PrOH) 0.65 mL/min, λ = 254 nm, t_R = 10.0 min t_R = 12.0 min. [e] completion of reaction ~ 24 h. [f] completion took ~ 48 h.

It was postulated that the increased steric properties at the achiral end would guide the dienophile binding at the Al centre in the direction of the chiral end and, thus, it would increase the chance of enantioinduction. This was reflected in the almost doubled enantiomeric excess value generated by **3eAl(OTf)$_2$** in comparison to **3bAl(OTf)$_2$** (entries 1-4, Table 2.5). Further, we believe that the phenyl rings of the bulky -CHPh$_2$ groups at the *ortho* positions of the N^{Ar} fragment, could also interact with the dienophile, increasing the possibility of "guided" substrate orientation for a more enantioselective interaction with the incoming diene molecule. However, comparing entries 3/4 with entries 7/8 and entries 9/10 with entries 11/12 (Table 2.5), it could be observed that the added bulky groups at the para position of the phenyl ring has little to no effect on the enantioselectivity values. When we investigated the ability of the aluminium dichloro complexes to catalyse the reaction (entries 2, 4, 6, 8, 10 and12, Table 2.5),

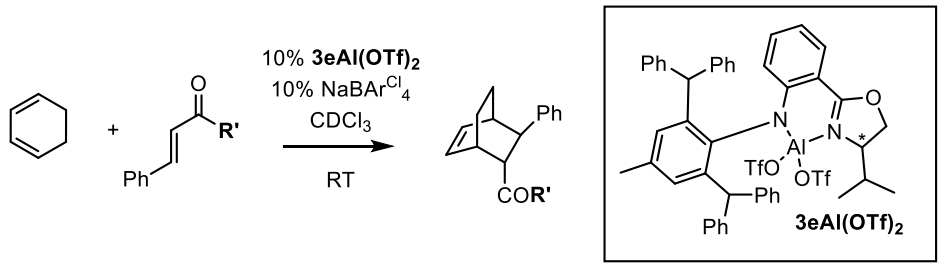

Table 2.6: Enantioselective Diels−Alder reactions of 1,3- cyclohexadiene and different chalcones catalysed by **3eAl(OTf)$_2$**

entry	R'	Adduct	time (h)	endo:exo[a]	conv. (%)[b]	yield (%)[c]	ee (%)[d]
1		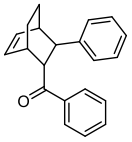	48	(98:2)	> 95	73	42
2	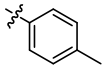	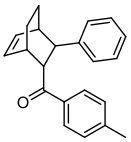	48	(97:3)	> 90	73	17
3		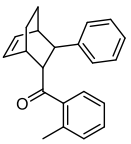	48	(97:3)	>95	76	33
4	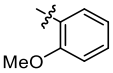	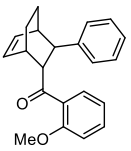	48	(98:2)	> 95	81	25
5	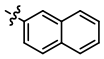	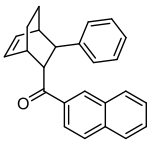	48	(98:2)	>98	78	40

[a] Determined by GLC analysis of the reaction mixture prior to purification. [b] Determined by NMR analysis. [c] Analytically pure product after flash column chromatography on silica gel. [d] Determined by HPLC analysis using a chiral OD-H column 98:2 (hexane: *i*-PrOH) 0.65 mL/min, λ = 254 nm.

it was revealed that the reaction completion time was increased by ~ 12 h, and, thus, the efficiency of the catalyst decreased. The other observation with respective dichloro complexes was that the *ee* values were lessened, possibly due to the lower steric demand by the chloro compared to triflate groups (Table 2.5). Encouraged by these results, we wanted to potentially expand the versatility of this catalytic system. Therefore, we attempted the DA cyclisation reaction between a few more different chalcones and 1,3-cyclohexadiene using **3eAl(OTf)$_2$** complex, which generated the highest *ee* values towards the DA reaction between 1,3-cyclohexadiene and "naked" chalcone (Table 2.6). With our small substrate sample, the *ee* values ranging from 17-42% were observed. It was noticed that the efficiency of the catalysed reaction was not changed as all the reactions were completed in 48 h, i.e. with a similar rate compared to the "naked" chalcone. However, reduced enantioselectivity was observed when the **R'** group was changed from phenyl to any substituted phenyl (entries 2,3 and 4 in Table 2.6). The presence of *ortho*-substituted phenyl groups at **R'** generated higher *ee* values (25% and 33%, entries 3, 4 Table 2.6) compared to the *para*-methyl substituted analogue (17%, entry 2, Table 2.6). When **R'** was changed to -naphthyl group similar enantioselectivity as to the naked chalcone was observed (entry 5, Table 2.6).

It should be mentioned that unfortunately, our initial goal of obtaining improved enantioselectivity values compared to the published records were not met, as almost all our complexes generated lesser or similar (%*ee* for conversion of *ortho*-methylphenyl was 33% in entry 3, Table 2.6 vs 31% reported) %*ee* values compared to the published data by Oestreich and co-workers.[17,19-22] However, it is noteworthy to mention that, the reaction of 1,3-cyclohexadiene together with *o*-methoxy substituted chalcone (entry 4, Table 2.6) formed the respective DA adduct with a much improved enantiomeric excess of 25% in comparison to reported 7%, which, to the best of our knowledge, was the highest generated *ee* value by a chiral Lewis acid catalyst so far for this particular set of substrates.

2.3 Summary

We were able to successfully synthesise a series of chiral analogues of our published achiral aluminium bistriflate complex.[18] These complexes composed of two ends, chiral and achiral, both of which could hold different functional groups.

A total of seven different chiral ligands (**2H, 3aH-3fH**) were successfully synthesised, containing different substituents at the chiral and achiral ends. However, after complexation with aluminium to form **2AlCl$_2$**, the ligand that contained a phenyl group at the chiral end was found to have produced a racemic mixture of the complex. After replacing the phenyl group with an *i*-Pr group at the chiral end, six different chiral aluminium based bistriflate complexes, **3aAl(OTf)$_2$-3fAl(OTf)$_2$**, which contained varying steric bulks at the achiral end, were successfully synthesised. The synthesised chiral analogues were able to display comparable efficiency and stereoselectivity (*endo*:*exo*) towards the target DA reactions between less reactive substrates such as 1,3-cyclohexadiene and simple α, β-unsaturated chalcones as our achiral system.

In addition, chiral aluminium based complexes **3aAl(OTf)$_2$-3fAl(OTf)$_2$** showed the ability of driving the asymmetric DA cycloaddition reaction between 1,3-cyclohexadiene and chalcone favouring one enantiomer exhibiting %*ee* values ranged from 12 - 42%. A general trend of improved enantioselectivity with increased steric hindrance at the achiral end was demonstrated. The highest %*ee* value obtained was 42% by **3eAl(OTf)$_2$**. A small substrate scope of different chalcones containing several substituted phenyl groups at the carbonyl carbon showed *ee* values ranging from 17 - 40 %. In addition, the cycloadduct between 1,3-cyclohexadiene together with *o*-methoxy substituted chalcone displayed the best reported %*ee* values so far. Our next aim is to attempt to improve these values by modifying the chiral end of the complex.

References

1 J. G. Martin and R. K. Hill, *Chem. Rev.*, 1961, **61**, 537–562.

2 H. Du, K. Ding and S. Ma, *Asymmetric Catalysis of Diels–Alder Reaction*, 2009, vol. 1.

3 I. Fernández and F. M. Bickelhaupt, *J. Comput. Chem.*, 2014, **35**, 371–376.

4 R. Woodward and R. B. Hoffmann, *J. Am. Chem. Soc.*, 1965, **87**, 4388–4389.

5 A. Behr, in *Ullmann's Encyclopedia of Industrial Chemistry*, 2000, p. 19.

6 J. D. Winkler, *Chem. Rev.*, 1996, **96**, 167–176.

7 R. L. Funk and K. J. Yost, *J. Org. Chem.*, 1996, **61**, 2598–2599.

8 E. G. Mackay and M. S. Sherburn, *Synth.*, 2015, **47**, 1–21.

9 D. A. Evans, K. T. Chapman and J. Bisaha, *J. Am. Chem. Soc.*, 1988, **110**, 1238–1256.

10 E. J. Corey, T. Shibata and T. W. Lee, *J. Am. Chem. Soc.*, 2002, **124**, 3808–3809.

11 S. Otto, G. Boccaletti and J. B. F. N. Engberts, *J. Am. Chem. Soc.*, 1998, **120**, 4238–4239.

12 A. B. Northrup and D. W. C. MacMillan, *J. Am. Chem. Soc.*, 2002, **124**, 2458–2460.

13 P. Vermeeren, T. A. Hamlin, I. Fernández and F. M. Bickelhaupt, *Angew. Chemie - Int. Ed.*, 2020, **59**, 6201–6206.

14 P. Yates and P. Eaton, *J. Am. Chem. Soc.*, 1960, 82, 4436–4437.

15 H. Yamamoto, *Lewis Acids in Organic Synthesis*, Wiley-VCH, 1st editio., 2000.

16 R. P. Singh, K. Bartelson, Y. Wang, H. Su, X. Lu and L. Deng, *J. Am. Chem. Soc.*, 2008, **130**, 2422–2423.

17 V. H. G. Rohde, M. F. Müller and M. Oestreich, *Organometallics*, 2015, **34**, 3358–3373.

18 Z. Liu, J. H. Q. Lee, R. Ganguly and D. Vidović, *Chem. - A Eur. J.*, 2015, **21**, 11344–11348.

19 P. Shaykhutdinova and M. Oestreich, *Org. Lett.*, 2018, **20**, 7029–7033.

20 P. Shaykhutdinova and M. Oestreich, *Organometallics*, 2016, **35**, 2768–2771.

21 P. Shaykhutdinova and M. Oestreich, *Synthesis (Stuttg).*, 2019, **51**, 2221–2229.

22 P. Shaykhutdinova, S. Kemper and M. Oestreich, *European J. Org. Chem.*, 2018, **2018**, 2896–2901.

23 Z. Liu and D. Vidović, *J. Org. Chem.*, 2018, **83**, 5295–5300.

24 P. I. Binda, S. Abbina and G. Du, *Synthesis (Stuttg).*, 2011, **2011**, 2609–2618.

25 K. Schwekendiek and F. Glorius, *Synthesis (Stuttg).*, 2006, **18**, 2996–3002.

26 S. Abbina and G. Du, *Organometallics*, 2012, **31**, 7394–7403.

27 Z. Lu, S. Abbina, J. R. Sabin, V. N. Nemykin and G. Du, *Inorg. Chem.*, 2013, **52**, 1454–1465.

28 S. Bian, S. Abbina, Z. Lu, E. Kolodka and G. Du, *Organometallics*, 2014, **33**, 2489–2495.

29 S. Dai, S. Zhou, W. Zhang and C. Chen, *Macromolecules*, 2016, **49**, 8855–8862.

30 M. Stender, R. J. Wright, B. E. Eichler, J. Prust, M. M. Olmstead, H. W. Roesky and P. P. Power, *J. Chem. Soc. Dalt. Trans.*, 2001, 3465–3469.

31 I. I. Levina, O. N. Klimovich, D. S. Vinogradov, T. A. Podrugina, D. S. Bormotov, A. S. Kononikhin, O. V. Dement'eva, I. N. Senchikhin, E. N. Nikolaev, V. A. Kuzmin and T. D. Nekipelova, *J. Phys. Org. Chem.*, 2018, **31**, e3844.

32 T. R. O. Toole, J. N. Younathan, B. P. Sullivan and T. J. Meyer, *Inorg. Chem.*, 1989, **28**, 3923–3926.

33 Z. Liu and D. Vidović, *J. Org. Chem.*, 2018, **83**, 5295–5300.

34 D. Dissanayake, A. Draper, Z. Liu, J. J. Haven, C. Forsyth, T. Junkers and D. Vidović, *manuscript under revision.*

35 S. Zhai, C. Forsyth, Z. Liu and D. Vidović, *Organometallics*., 2022, **41**, 2562-2571.

36 T. Gatzenmeier, M. Turberg, D. Yepes, Y. Xie, F. Neese, G. Bistoni and B. List, *J. Am. Chem. Soc.*, 2018, **140**, 12671–12676.

Chapter 3

3. Synthesis, Characterisation, and Reactivity studies of Chiral β-Diketiminate Supported Aluminium Lewis Acid Complexes Towards Difficult Diels Alder Cycloadditions-*Effects of Structural Modifications of the Chiral End*

3.1 Introduction

This chapter discusses details of the synthesis, characterisation and reactivity of a collection of chiral β-diketiminate supporting aluminium Lewis acid complexes, with a focus on structural changes at the chiral end of the supporting ligand. This chapter evolves from the knowledge that we acquired from Chapter 2. Thus, this part of work assesses how systematic structural changes at the chiral end of the supporting ligand could be used to improve the enantioselectivity values generated by the target aluminium complexes with respect to several Diels Alder (DA) reactions.

3.1.1 Systematic changes to the steric bulk at the chiral end

This chapter initially discusses introduction of various different chiral structural features into the aluminium complexes via structural modifications at the β-diketiminate supporting ligand. Next, the study progresses to highlight how these systematic structural changes at the chiral end affected the enantioselectivity values generated by these complexes towards several DA reactions. As introduced in Chapter 1 and investigated in Chapter 2, this is approached by replacing the achiral β-diketiminate supporting ligand of the original achiral complex **1** by a chiral ligand having a similar structure (Figure 3.1 and Figure 3.2).[1–4] Chiral β diketiminato type ligands published by G. Du and co-workers[5] have been chosen as suitable ligands for the task. These ligands are then complexed to aluminium to obtain the target Lewis acid compounds. Finally, details of these complexes' abilities to catalyse difficult DA cycloadditions between less reactive 1,3-cyclohexadiene and chalcones favouring one enantiomer are discussed.

In Chapter 2, systematic modifications of the achiral end/**Ar** of the complexes have been achieved by synthesising several aluminium based complexes. More importantly, after testing their ability, as catalysts, to discriminate between the enantiomers for DA reactions, optimal

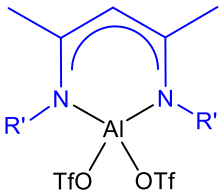

1

1a ^{Dip}LAl(OTf)$_2$: R'= 2,6-i-Pr$_2$-C$_6$H$_3$

1b ^{Xyl}LAl(OTf)$_2$: R' = 2,6-,Me$_2$-C$_6$H$_3$

1c ^{Ph}LAl(OTf)$_2$: R' = C$_6$H$_5$

Figure 3.1: Basic Structure of the reported achiral complex

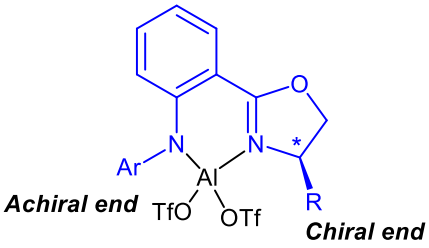

		R	Ar
Synthesised in Ch.2	**2**	Ph	2,6-Me$_2$C$_6$H$_3$
	3a	*i*-Pr	2,6-Me$_2$C$_6$H$_3$
	3b	*i*-Pr	Ph
	3c	*i*-Pr	2,6-*i*-Pr$_2$C$_6$H$_3$
	3d	*i*-Pr	2,4,6-(CH$_3$)$_3$C$_6$H$_2$
	3f	*i*-Pr	4-CH$_3$-2,6-(CH(Ph)$_2$)$_2$C$_6$H$_2$
In this Ch.3	**4a**	*t*-Bu	2,6-*i*-Pr$_2$C$_6$H$_3$
	4b	*t*-Bu	4-CH$_3$-2,6-(CH(Ph)$_2$)$_2$C$_6$H$_2$
	5a	PhCH$_2$-	2,6-*i*-Pr$_2$C$_6$H$_3$
	5b	PhCH$_2$-	4-CH$_3$-2,6-(CH(Ph)$_2$)$_2$C$_6$H$_2$
	6a	Ph$_2$CH-	2,6-*i*-Pr$_2$C$_6$H$_3$
	6b	Ph$_2$CH-	4-CH$_3$-2,6-(CH(Ph)$_2$)$_2$C$_6$H$_2$

Figure 3.2: Introducing Chirality at β-diketiminate supporting ligand, basic structures of proposed chiral Al complexes

structural features at the achiral were realised. In general, the observed trend was that higher the steric hindrance at the achiral end, better the complexes' ability to drive the DA reaction enantioselectively. As this trend was observed when the steric congestion increased at a site

rather away from the chiral centre, it was expected that by systematically improving the steric hindrance at a site much closer to the chiral centre would result in even better influence at the ability of enantioinduction. Therefore, together with the optimal steric properties at the achiral end, structural features at the chiral end were systematically changed by introducing several different groups at the chiral end. Then, the effects of these varying steric elements on the ability of the target aluminium compounds to induce enantioselectivity of generated DA adducts were investigated. Initially, it was planned to synthesise several complexes with having the "best" bulky achiral end, 4-CH_3-2,6-$(CH(Ph)_2)_2C_6H_2$), while varying the nature of the chiral ends (Figure 3.2). Nevertheless, for comparison reasons, it was also decided to prepare a few more complexes containing Dip/2,6-*i*-$Pr_2C_6H_3$ (second best) at the achiral end while, again, varying the nature of the chiral end. (Figure 3.2).

As the key chiral element of these complexes is introduced during the formation of a five-membered 2-oxazoline ring structure (with a chiral C atom), the synthesis of these structural motives with high enantiopurity and stereospecificity is of critical importance.

3.1.2 Synthesis of chiral 2-oxazolines

Oxazoline is a five membered heterocycle that contains a nitrogen and an oxygen atom in its ring structure. A double bond is also a part of the ring and depending on its position, these heterocyclic compounds can adopt three different sub classes/isomers, namely 2-, 3-, or 4-oxazolines (Figure 3.3).[6] When dissimilar substituents are at the lone sp^3 carbon atom/s within the ring for each isomer, these compounds are classified as chiral.

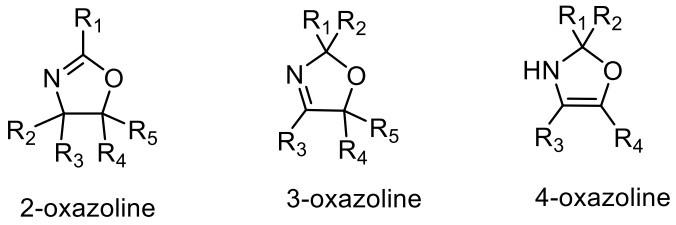

Figure 3.3: Different types of oxazolines

Among the three types, 2-oxazolines can be identified as the most common type. In fact, as these compounds have been utilised as starting materials in polymerisation reactions,[7] chiral auxiliaries,[8] key elements in chiral ligand synthesis,[9] and protection groups of both carbonyl and hydroxyl groups of carboxylic acids,[10] 2-oxazolines were identified as a versatile class of organic compounds ever since their discovery in the 19th century.[11] This particular interest has led to the development of multiple synthetic routes for the synthesis of these species. Therefore, many pathways have been examined for the preparation of 2-oxazolines and the ones which started with amino alcohols or low-cost carboxylic acids were of industrial interest while some other preparation methods that initiated the synthesis with amides, aziridines and epoxides have also been explored at the laboratory scale.[6]

A few of these methods are summarised in Figure 3.4. The oxidative synthesis of 2-oxazolines demonstrated in method **A** (Figure 3.4) was described as a very versatile method to prepare enantioselective and stereoselective 2-oxazoline products.[5,11] This method involves the reaction of an aromatic aldehyde with an amino alcohol, followed by oxidation with/without the presence of a base. With a substantial substrate scope and a mild synthetic route this method was capable of producing comparatively high yields of 2-oxazolines.[5] However, it was reported that the oxidizing agent of choice (N-bromosuccinimide) was critical for the stereoselectivity of the product, as inadvertent formation of 3-oxazolines could be present. In addition, for electron poor-aromatic substrates, an additional base was required due to the increased acid sensitivity. In one-pot method **B** (Figure 3.4), an amino alcohol was coupled with a nitrile in the presence of a Lewis acid catalyst at elevated temperature.[5, 12] Method **C** (Figure 3.4), consisting of 3 steps, was reported to produce good yields while proceeding via the formation of an amido alcohol, followed by dehydroxylation and cyclisation upon addition of a base.[13] Although both **B** and **C** are considered to be relatively more efficient, both of them required harsh reaction conditions such as high reaction temperatures. Method **D** requires significantly

mild conditions for the reaction between carboxylic acids and amino alcohols, however, it requires undesirable purification steps.[14] In method **E**, nitrile is converted to iminium salt and reacted with amino alcohol, which involves multiple steps and the intermediate salt synthesis is required.[15] As described in Chapter 2, following the same method used by G. Du co-workers,[5] we have chosen method **A** for the synthesis of 2-oxazolines for this thesis project, as it was one of the most efficient and facile among the reported methods.

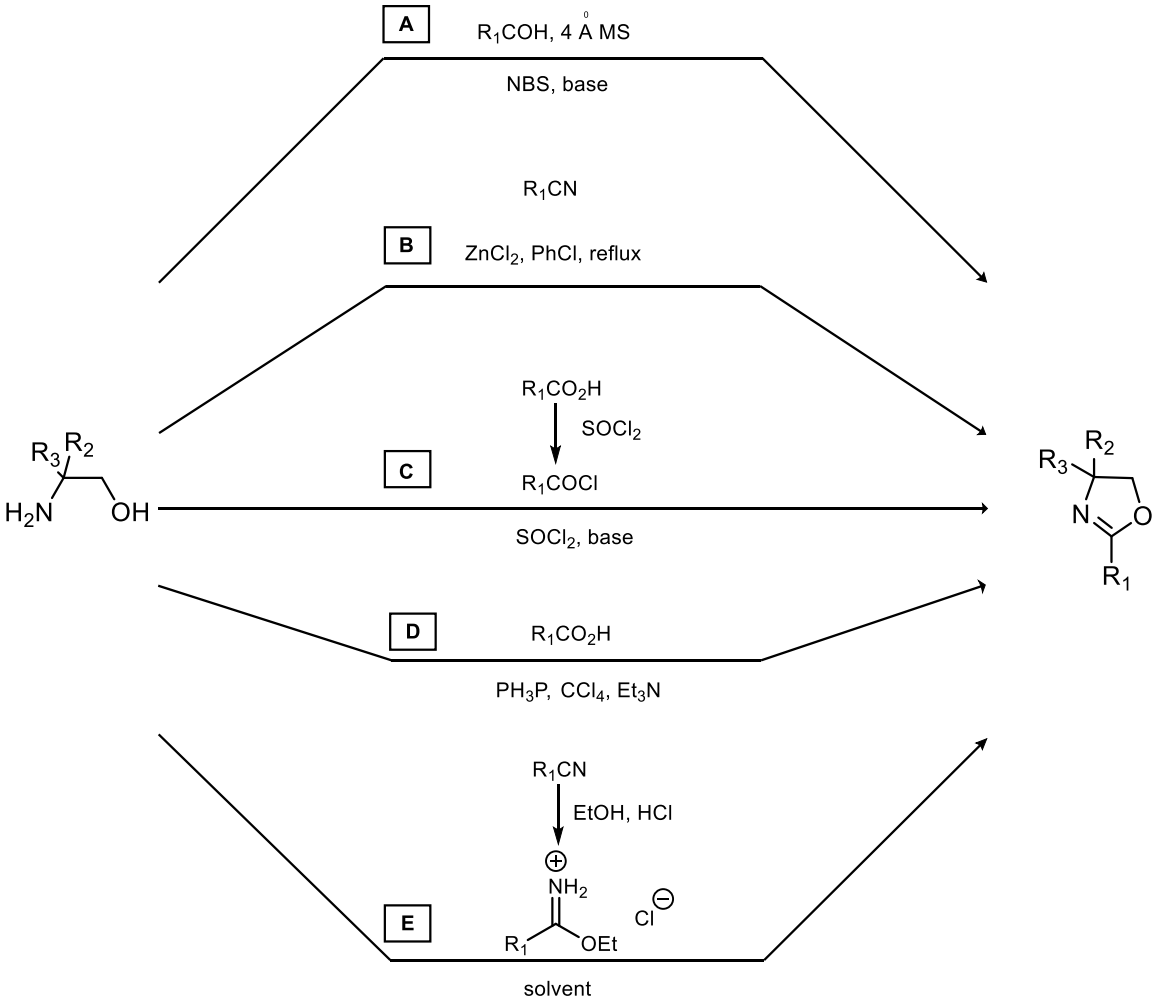

Figure 3.4: Common synthetic routes for 2-oxazolines

3.2 Results and Discussion

3.2.1 Synthesis and characterisation of ligands

For the synthesis of ligands with varying the nature of the chiral end, several different enantiopure amino alcohols would be required (Figure 3.5). Due to the higher cost and lesser commercial availability, it was more cost-effective to synthesise these amino alcohols by reducing the corresponding enantiopure amino acids. Reduction of amino acids to amino alcohols was achieved using $LiAlH_4$ as the reducing agent generating good product yields. (Scheme 3.1).[16]

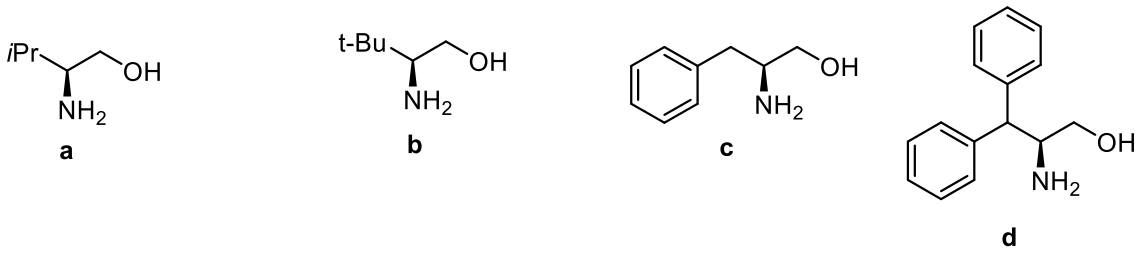

Figure 3.5: Structures of chiral amino alcohols used in the synthesis of 2-oxazolines. **a**) L-valinol, **b**) L-tert-leucinol, **c**) L-phenlyalaninol, **d**) 3,3-diphenyl-L-alaninol

Scheme 3.1: Synthesis of ligands

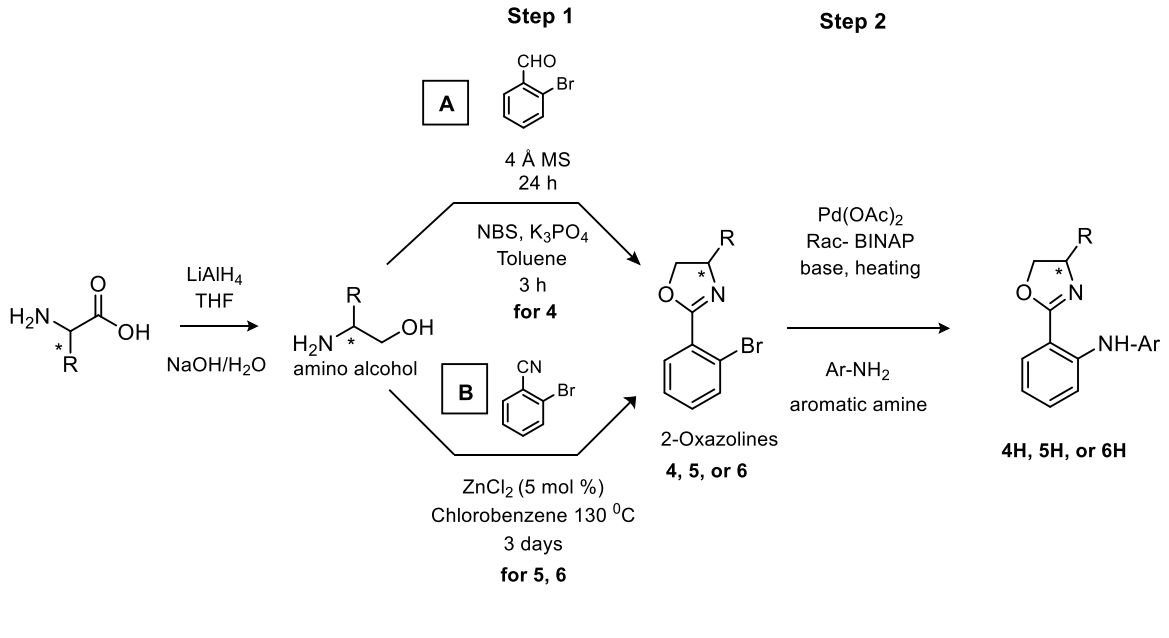

After reducing the amino acid L-tert-leucine, the amino alcohol L-tert-leucinol (**b** in Figure 3.5, *tert*-butyl group at chiral end, Scheme 3.1) was obtained, which was then reacted with 2-bromobenzaldehyde to produce the corresponding 2-oxazoline, in good yields **(**Table 3.1**)** via the same reaction conditions as used for the preparation of the ligands with the *i*-Pr group connected to the chiral end (**a** in Figure 3.5, *iso*-propyl at the chiral end, following step 1, method **A** in Scheme 3.1). The resulting 2-oxazoline was then coupled with the relevant aromatic amines to obtain the final ligands **4aH** and **4bH** (step 2, Scheme 3.1, Table 3.1).

Table 3.1: Starting materials and yields obtained of ligand synthesis

	R	**Ar-NH_2**	**Yield (%)**		**Physical appearance**
			Step 1	**Step 2**	
4aH	*t*-Bu	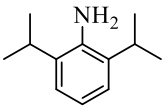	50	55	yellow solid
4bH		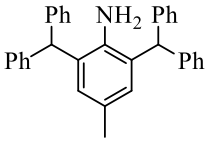	50	43	orange oil
5aH	$PhCH_2$-	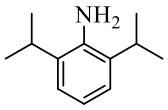	32	58	white solid
5bH		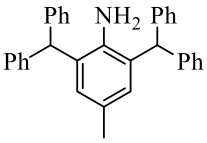	32	37	brown oil
6aH	Ph_2CH-	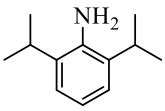	33	60	white solid
6bH		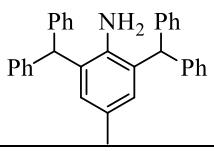	33	50	yellow solid

However, when L-phenylalaninol (**c** in Figure 3.5, $PhCH_2$ at the chiral end) or 3,3-diphenyl-L-alaninol (**d** in Figure 3.5, Ph_2CH at the chiral end) was used, stereospecificity of the reaction was lost and an additional isomeric 3-oxazoline product (Figure 3.6) was also observed in the ^1H NMR spectra of the reaction mixture after the first step of the synthesis (Figure 3.7). As the chiral carbon is at the 4th position of the heterocycle, this double bond formation between N(3)=C(4) caused a temporary loss of the chirality, which ultimately led to racemisation of the final ligand product.

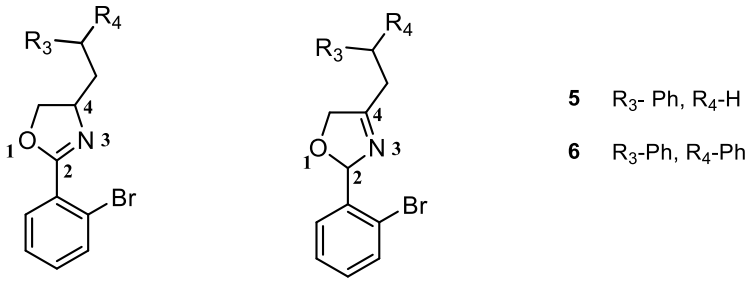

Figure 3.6: Desired 2-oxazoline product (left) and the counter 3-oxazoline product (right) for **6** and **7**

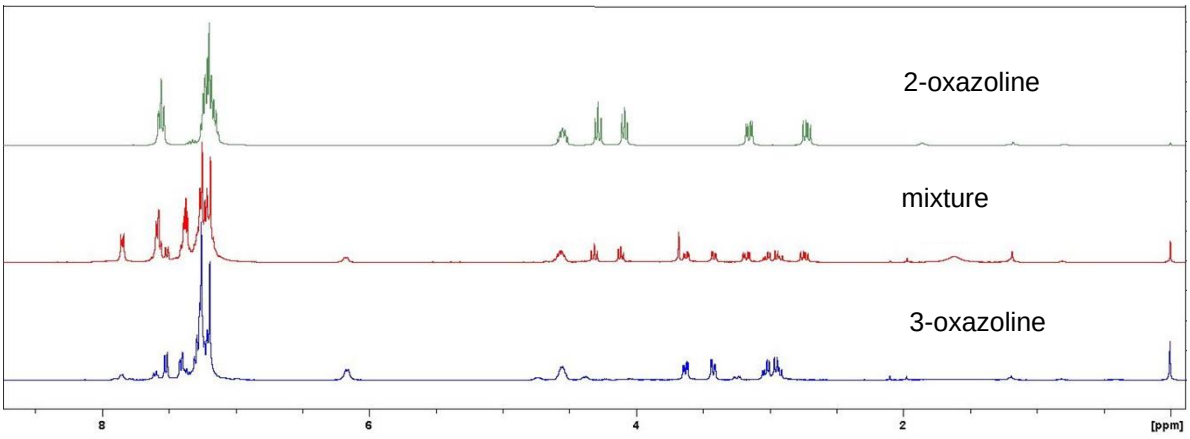

Figure 3.7: ^1H NMR spectra observed for top; 2-oxazoline, middle; mixture of products, bottom; 3-oxazoline

We believe that with the presence of bulky phenyl substituents at the 3-position of the oxazoline ring, 3-oxazoline and 2-oxazoline products become almost equally favourable during this synthesis. In order to find out the driving forces behind this loss of stereospecificity, we attempted to influence the reaction so that it formed only the desired 2-oxazoline product by experimenting with the reaction times and the amount of base added in the step 1, but without a successful resolution. Nevertheless, these experiments led to the understanding that the amount of base was playing a part in the formation of 3-oxazoline. We further confirmed this by studying the mechanism for the synthesis of these 2-oxazolines (Scheme 3.2).

The initial synthetic step involved coupling of the 2-bromobenzaldehyde with the amino alcohol in the presence of molecular sieves. This coupling would form the basic oxazolidine ring structure with elimination of water. It was understood that as removal of water facilitates the formation of oxazolidine ring motif, which was in equilibrium with the ring open form, therefore, molecular sieves were added. The next step involved oxidation with the use of NBS (N-bromosuccinimide) and deprotonation of the resulting oxazoline hydrobromide salt. According to Glorius and co-workers, elimination of HBr could be achieved without a base for

Scheme 3.2: Published mechanism for Oxidative 2-oxazoline formation by Glorius and co-workers.

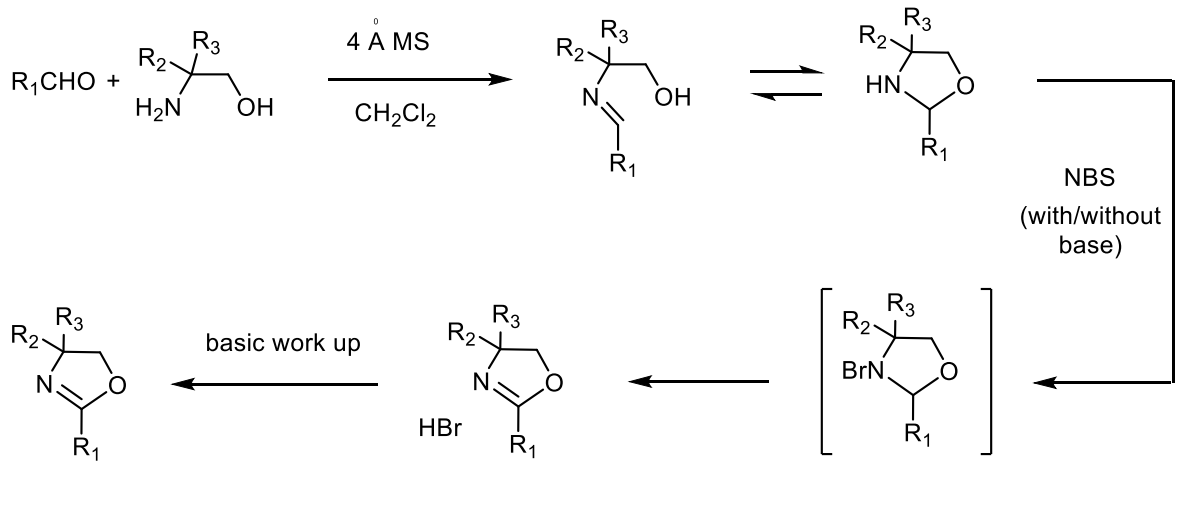

most of the substrates, but due to increased acid sensitivity of electron-poor aromatic substrates at R_1, a base was required. [11] Therefore, with our 2-bromobenzyl substituent at R_1, we needed to add a base in order to eliminate HBr (Scheme 3.2). With this information and our observation of the increased formation the 3-oxazoline isomer with the increased amounts of the base, we came to an understanding that the presence of the base was playing a role in the loss of stereospecificity of the reaction.

Compelled by this, other possible methods for the preparation of these bulky 2-oxazolines were sought out. Methods **C** and **D** (Figure 3.4) were considered inappropriate because of the involvement of bases in the reaction and method **D** required multiple synthesis and purification steps. Thus, method **B**, which involved Lewis acid catalysis under high temperatures, offered the best chance of obtaining the desired synthesis.

To our delight, the target 2-oxazolines compounds could be obtained in fairly high yields by reacting 2-bromobenzonitrile with relevant amino alcohols, even at higher temperatures (130 °C in chlorobenzene) and for prolonged reaction times of about 72 h (Scheme 3.1). The ^{1}H NMR spectroscopic data confirmed that this method produced solely 2-oxazoline products i.e. in the absence of any amounts of the 3-oxazoline isomers (Figure 3.7, top). These 2-oxazoline products could then be reacted with the relevant anilines in order to synthesise proposed ligands (step 2 in Scheme 3.1, Table 3.1).

All ligands could be obtained in moderate yields following the appropriate two step method, **A** or **B** (Scheme 3.1, Table 3.1). These synthesised ligands were initially characterised using multinuclear NMR spectroscopy. All ^{1}H NMR spectra displayed a characteristic, broad singlet for a single proton around δ_H 9-10 ppm, indicating the presence of an N-H fragment. Further, another three multiplets were observed for all the ligands around δ_H 3-5 ppm which were indicative of the three protons in the oxazoline ring area. The ^{13}C NMR spectra also confirmed

the existence of the expected ligand structures and the O-*C*=N carbon signal was observed around δ_C163 ppm. In addition, we obtained crystalline material for **5aH** suitable for single crystal X-ray analysis. To our delight, the crystal structure depicted expected geometry and the data was solved in enantiomorphic trigonal $P3_121$ space group, supporting the chiral nature of the ligand (Figure 3.8, Table 3.2). We also obtained the crystals suitable for analysis of **7aH**, which displayed the expected geometry and belonged to the chiral space group monoclinic $P2_1$, supporting the chiral nature of the structure (Figure 3.9, Table 3.2). In addition, the bond distances for the N_2C_3 fragment i.e. bond distances for N1-C1 (average 1.363 Å) and N2-C7 (average 1.273 Å) indicated similar electron localisation as observed for **2H** and **3aH-3fH** in Chapter 2. Furthermore, we also attempted to characterise all these ligands using HRMS and CHN elemental analysis data (see appendix).

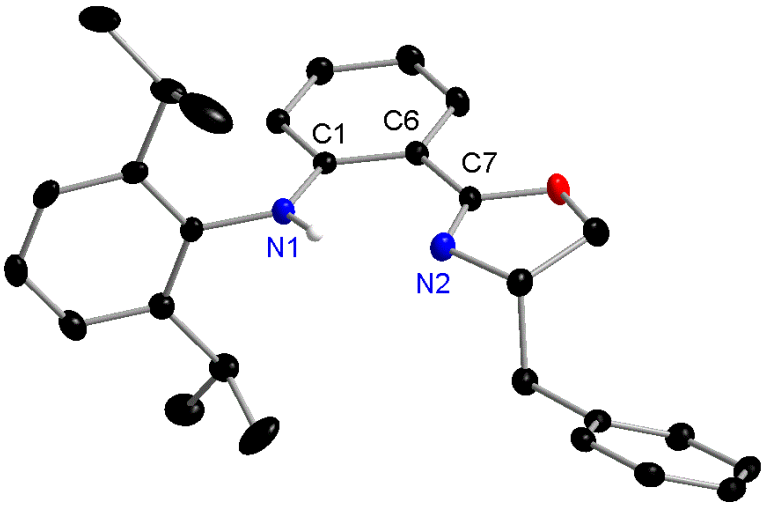

Figure 3.8: Solid state structure for **5aH** as drawn at the 30% probability level. All hydrogen atoms, apart from N-Hs, as well as residual solvent molecules are omitted for clarity. Selected bond distances (Å); N1-C1 1.365(2), C1-C6 1.419(2), C6-C7 1.467(2), N2-C7 1.277(2)

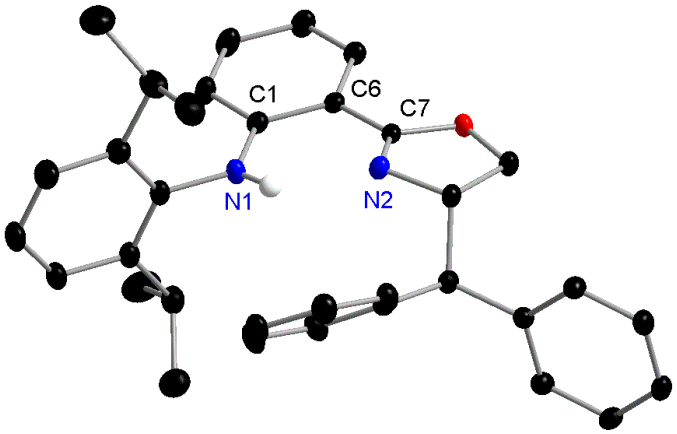

Figure 3.9: Solid state structures for **7aH** as drawn at the 30% probability level. All hydrogen atoms, apart from N-Hs, as well as residual solvent molecules are omitted for clarity. Selected bond distances (Å); N1-C1 1.361(4), C1-C6 1.428(3), C6-C7 1.463(4), N2-C7 1.269(4)

Table 3.2: Summary of the crystallographic data for ligand synthesis

	5aH	**7aH**
Formula	C_{28} $H3_2$ N_2 O	C_{68} $H_{72}N_4O_2$
Formula weight	412.55	977.29
Crystal system	trigonal	Monoclinic
Space group	$P3_121$	$P2_1$
a /Å	10.56220(10)	15.9991(2)
b/Å	10.56220(10)	10.05330(10)
c/Å	37.6815(3)	19.1215(2)
α /deg	90	90
β /deg	90	112.015(2)
γ /deg	120	90
V / Å^3	3640.55(7)	2851.32(7)
Z	6	2
Dc/ g cm^{-3}	1.129	1.138
F(000)	1332.0	1048
Crystal size/ mm	0.7 x 0.1 x 0.1	0.5 x 0.2 x 0.1
θ range/°	7.038 to 159.536	9.096 to 160.014
Reflections collected / unique	50580/5263 [R_{int} = 0.0338]	59697/12188 [R_{int} = 0.0690]
R_1 [I >2σ (I)]	R_1= 0.0340, wR_2 = 0.0894	R_1 = 0.0498, wR_2 = 0.1340
wR_2 (all data)	R_1 = 0.0347, wR_2= 0.0900	R_1 = 0.0529, wR_2 = 0.1368
Peak and hole/e Å^{-3}	0.28 and − 0.20	0.46 and − 0.29
Flack Parameter	0.00(6)	-0.07(10)

3.2.2 Synthesis and characterisation of Al complexes.

After ligand synthesis and satisfactory characterisation, we moved forward with the synthesis of the aluminium complexes. The same method that was used in Chapter 2 was implemented in this case, which involved ligand deprotonation with ^{n}BuLi at low temperatures followed by quenching with $AlCl_3$ and potential ligand exchange with AgOTf (Scheme 3.3).

Scheme 3.3: suggested synthetic route for chiral β-diketiminato type ligand supported Al bis triflate complexes

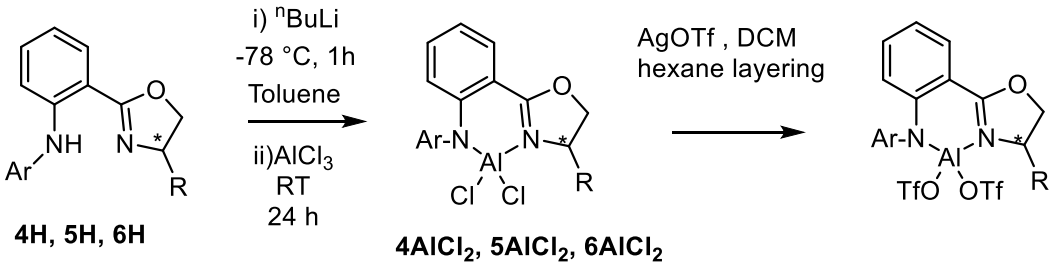

4H, 5H, 6H

$4AlCl_2$, $5AlCl_2$, $6AlCl_2$

All synthesised aluminium dichloro complexes were initially characterised using multinuclear NMR spectroscopy. The most obvious and notable change observed in the ^{1}H NMR spectra was the loss of the broad singlet, characteristic of the N-H proton of the ligand which appeared around δ_H 9-10 ppm. This confirmed that the deprotonation was successful and that the ligand could coordinate to the Al metal centre. For all the other δ_H signals for the synthesised dichloride complexes, similar overall signal patterns to that of the free ligands were observed. Nevertheless, noticeable signal shifts (downfield by about 0.2 ppm) for almost all the proton signals in the δ_H 3-5 ppm region assigned to the oxazoline ring fragment were observed. Similarly, the δ_H signals assigned to the protons of any group (e.g. *t*-butyl, $PhCH_2$- or Ph_2CH-) attached to the stereogenic centre or any substituent at the 2 and 6 positions of the phenyl group of the achiral end (e.g. $(CH_3)_2CH$-, Ph_2CH-) were also experiencing notable shifts ranging from 0.2 to 0.5 ppm. On the other hand, protons belonging the aromatic regions,

including the ligand backbone and N^{Ar}, exhibited only slight signal shifts. It should be noted that although changes were expected for the aromatic signals of the ligand backbone after aluminium binding, we were unable to identify these changes due to the presence of multiple N^{Ar} signals. In addition, the ^{13}C NMR spectra of these complexes also exhibited a similar trend as for a majority of the signals only minor shifts were observed. However, the ^{13}C NMR spectroscopic signals assigned to the C=N fragment, which was observed at around δ_C 160 ppm for the free ligands, was shifted downfield to around δ_C 170 ppm. This observation provided more evidence for coordination of this particular N atom to the electrophilic aluminium centre as electron density was donated from the N atom to the metal. The other most significant evidence of Al binding was a clear singlet observed for almost all the aluminium dichloro complexes at around δ_{Al} 104 ppm in the ^{27}Al NMR spectra.

Fortunately, after a few attempts we were also successful in obtaining a crop of crystals for **4bAlCl$_2$**, in a mixture of 1,2-difluorobenzene and hexane, suitable for single crystal X-ray crystallography. To our delight, the X-ray structure depicted the expected structural geometry and it belonged to the chiral space group (monoclinic) $P2_1$, supporting the chiral nature of the complex (Figure 3.10, Table 3.3). Similar to many solved crystal structures in the Chapter 2, two unique molecules were found in the asymmetric unit of **4bAlCl$_2$**, with a notable difference only in the orientation of the phenyl ring. In addition, the bond distances for Al1-N1 (*ca.* 1.83 Å), Al-N2 (*ca.* 1.88 Å), N1-C7(*ca.* 1.31 Å) and N2-C1 *(ca*. 1.39 Å) exhibited a similar degree of localisation of electron density in the central AlN_2C_3 ring as observed for the structures in Chapter 2 (i.e. Al1-N1 (*ca.* 1.84 Å), Al-N2 (*ca.* 1.87 Å), N1-C1 (*ca.* 1.38 Å) and N2-C7 (*ca.* 1.30 Å)). This was, again, expected due to the phenyl group in the ligands' carbon backbone (Figure 3.10). It was also noticeable that the N1-Al1-N2 bite angle (*ca.* 99.7˚) increased, while Cl1-Al1-Cl2 angle (*ca.* 108.6˚) decreased as the steric bulk increased when compared to **3eAlCl$_2$** (showed best enantiospecificity (see below); *ca.* 98.5˚ and 107.5˚ respectively) in

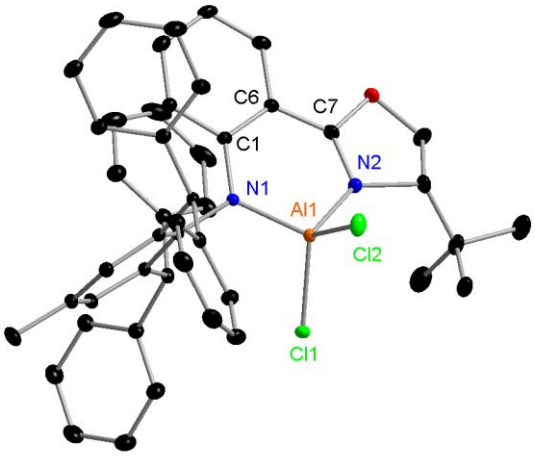

Figure 3.10: Single crystal X ray structures of **4bAlCl$_2$** as drawn at the 30% probability level. All hydrogen atoms and any solvent molecules are omitted for clarity. For unit cells consisted of two unique molecules only one of them is shown. Selected bond distances (Å) and angles (˚); Al1-N2 1.830(2), Al1–N2 1.879(2), Al1-Cl1 2.116(1), Al1-Cl2 2.143(1), N1-C1 1.387(3), C1-C6 1.422(3), C6-C7 1.444(3), N2-C7 1.311(3) N1-Al1-N2 99.67(9), Cl1-Al1-Cl2 108.57(3).

Table 3.3: Summary of the crystallographic data for Al-dichloro complex, **4bAlCl$_2$**

	4bAlCl$_2$
Formula	$C_{46}H_{43}AlCl_2N_2O$
Formula weight	737.70
Crystal system	Monoclinic
Space group	$P2_1$
a /Å	15.2370(2)
b/Å	17.2186(2)
c/Å	15.4659(2)
α /deg	90
β /deg	105.529(2)
γ /deg	90
V / Å^3	3909.51(9)
Z	4
Dc/ g cm^{-3}	1.253
F(000)	1552.0
Crystal size/ mm	0.8 x 0.1 x 0.1
θ range/°	6.668 to 62.026
Reflections collected/ unique	80470/20379
R_{int}	0.0328
R_1 [$I > 2\sigma(I)$]	R_1 = 0.0344, wR_2 = 0.0873
wR_2 (all data)	R_1 = 0.0404, wR_2 = 0.0897
Peak and hole/e Å^{-3}	0.58 and − 0.28
Flack parameter	− 0.010(16)

Chapter 2. With the crystal structures and in-depth analysis of multinuclear NMR spectroscopic data, together with some CHN elemental analysis and HRMS data (see appendix), it was concluded that expected dichloro complexes were successfully synthesised, thus we progressed to obtain the respective Al bistriflate complexes.

We initially followed the same procedure in Chapter 2 for the target synthesis and attempted to convert the aluminium dichloro complexes into their bistriflate analogues using ligand substitution with AgOTf (Scheme 3.3). Unfortunately, multiple preparatory attempts at this required ligand exchange (e.g. synthesis of target **4aAl(OTf)$_2$** from **4aAlCl$_2$** and AgOTf) were unsuccessful as the ^{1}H NMR spectra of these reaction mixtures did not exhibit any evidence of the target bistriflate complexes. In fact, green solutions or solids were observed after the dichloro complexes were reacted with AgOTf, which might have signalled the formation of radical or highly unstable species. Recalling that the syntheses of the complexes with different groups at the achiral end (Chapter 2), changing the solvent from dichloromethane to 1,2-difluorobenzene for the bulkier analogues was necessary, we believed that, as the steric bulk at the chiral end increased, these complexes become increasingly unstable. In addition, another published, pincer ligand containing Al triflate complex by our group also showed high instability and increased air and moisture sensitivity leading to the use of its dichloro precoursors in the catalytic activity investigations.[17] It should be also mentioned that according to our previous experiments with different groups at the achiral end, it was observed that the capability of enantioinduction towards DA reactions was better with the bistriflate complexes in comparison to the corresponding dichloro complexes. However, as we were unable to synthesise the preferred bistriflate complexes, we decided to use the prepared aluminium dichloro complexes and investigate their ability of enantioinduction towards asymmetric DA reactions.

3.2.3 Catalysis of asymmetric Diels Alder reactions

With the objective of investigating the increasing steric effects of the chiral end (**R**) on enantioinduction towards DA reactions of the less reactive 1,3-cyclohexadiene and chalcone, all synthesised Al dichloro complexes were used as catalysts and the enantiomeric excess (*ee*) values were determined in a similar approach to Chapter 2. It was observed that all complexes, **4aAlCl$_2$** – **6bAlCl$_2$** were capable of driving the reaction between less reactive 1,3-cyclohexadiene and chalcone (Table 3.4). The catalytic reaction efficiency of **4AlCl$_2$** and **5AlCl$_2$** complexes were similar to that of previous complexes (i.e. **3cAl(OTf)$_2$**, **3eAl(OTf)$_2$**, and **3fAl(OTf)$_2$**), but using **6AlCl$_2$** the reaction rate decreased, probably due to the bulky nature of two phenyl groups. Similar stereospecificity towards the *endo* product was also observed (> 98%). All products could be successfully purified obtaining yields ranging from 62-80%.

Enantiomeric excess values ranging from 6-68% were observed for the DA product using the prepared aluminium dichloro complexes. Although we expected a better enantioinduction by **5AlCl$_2$** and **6AlCl$_2$** due a potential interaction between the dienophile Ph groups and their counterpart(s) at the chiral end, to our dismay, the introduction of $PhCH_2$ and Ph_2CH groups connected to the chiral C atom did not increase the enantioselectivity values generated by the respective aluminium complexes (entries 3-6, Table 3.4). However, **4AlCl$_2$** having a *t*-Bu group at the chiral end generated improved enantioselectivity towards the reaction in comparison to our previous observations from Chapter 2 (entries1 and 2, Table 3.4). Moreover, the use of **4aAlCl$_2$** as catalyst produced an *ee* value of 40%, while the *i*-Pr analogue **3cAlCl$_2$** displayed 35% *ee*. In addition, **4bAlCl$_2$** generated the best *ee* value thus far (of 68 %) while the *i*-Pr analogue **3eAlCl$_2$** of only 42% *ee*. Therefore, it was apparent that having the *t*-Bu group at the chiral end produced the optimum steric effect as this complex was the only one in which a quaternary C atom was located adjacent to the chiral C atom instead of secondary ($PhCH_2$) or

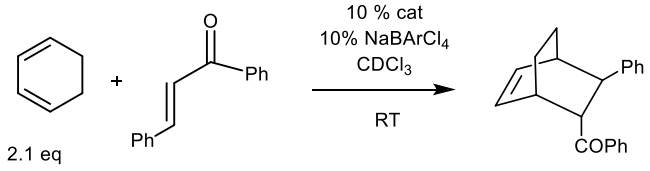

Table 3.4: Testing the effects of steric factors at achiral end of the catalyst on the DA reaction

entry	cat	*endo*:*exo* [a]	conv. (%)[b]	yield (%)[c]	ee (%)[d]
1	**4aAlCl$_2$**	(99:1)	> 98[e]	62	40
2	**4bAlCl$_2$**	(99:1)	> 98[e]	80	68
3	**5aAlCl$_2$**	(98:2)	> 98[e]	65	18
4	**5bAlCl$_2$**	(98:2)	> 98[e]	82	17
5	**6aAlCl$_2$**	(99:1)	> 98[f]	65	11
6	**6bAlCl$_2$**	(98:2)	>98[f]	70	6

[a] Determined by GLC analysis of the reaction mixture prior to purification. [b] Determined by NMR analysis. [c] Analytically pure *endo*-product after flash column chromatography on silica gel. [d] Determined by HPLC analysis using a chiral OD-H column 98:2 (hexane: *i*-PrOH) 0.65 mL/min, λ = 254 nm, t_R = 10.0 min t_R = 12.0 min. [e] completion of reaction ~ 48 h. [f] completion took ~ 60 h

tertiary [$(CH_3)_2CH$), Ph_2CH] C atoms. Hence, it was then appropriate to conclude that the most significant steric effect was induced not by having large group(s) connected to the C atom adjacent to the chiral end (e.g. Ph_2CH) but by making this C atom quaternary (i.e. using *t*-Bu). This supposedly generated a larger steric crowding around the aluminium centre; a similar observation was previously made by our group during the synthesis of various borenium cations.[18]

Next, as an attempt to establish the versatility of catalyst **4bAlCl$_2$**, a substrate scope containing several different variations of chalcone as dienophiles has been expanded. Unfortunately, as chalcone was replaced with substituted chalcones (Table 3.5), the efficiency of the reaction

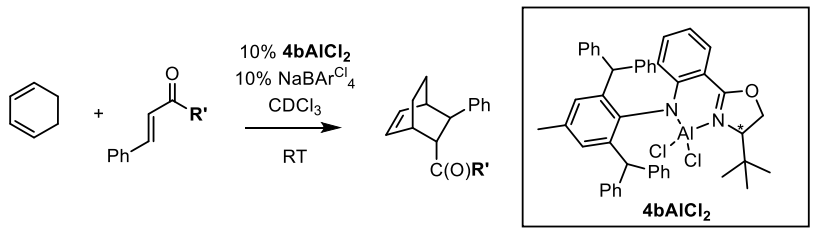

Table 3.5: Enantioselective Diels−Alder reactions of 1,3-cyclohexadiene and different chalcones catalysed by **4bAlCl$_2$**

entry	R'	time (h)	endo:exo[a]	conv. (%)[b]	yield (%)[c]	ee (%)[d]	ee (%)[e]	ee (%) (reported)
1		48	(99:1)	> 98	80	68	42	67[f]
2	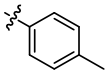	60	(98:2)	> 85	60	53	17	40[g]
3		60	(98:2)	>98	74	40	-	-
4		60	(98:2)	>98	76	24	33	31[g]
5	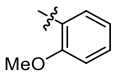	60	(98:2)	> 95	68	39	25	7[g]
6	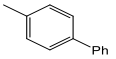	60	(98:2)	>90	63	40	-	81[f]
7	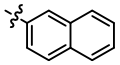	48	(98:2)	>98	78	25	40	65[h]

[a] Determined by GLC analysis of the reaction mixture prior to purification. [b] Determined by NMR analysis. [c] Analytically pure product after flash column chromatography on silica gel. [d] Determined by HPLC analysis using a chiral OD-H column 98:2 (hexane: *i*-PrOH) 0.65 mL/min, λ = 254 nm. [e] obtained using **3eAl(OTf)$_2$** as the catalyst [f] Catalysed by **AE**. [g] Catalysed by **AB**. [h] Catalysed by **AC**.

decreased for most of the tested substrates. In other words, the reaction times increased from 48 to 60 h for complete substrate conversions or until a reasonable amount of the DA adducts was produces. These extended reaction times could be attributed to a potentially decreased

interaction between the aluminium centre and the more sterically demanding substrates as compared to chalcone. Nevertheless, all DA adducts exhibited excellent stereospecificity towards the *endo* product (≥ 98%). In addition, all products could be separated and purified to produce average to good yields (60-80%). Lesser %*ee* values were observed for all substituted chalcones, irrespective of their positions (*ortho*, *para* and *meta*) with **4bAlCl$_2$** compared to the use of "naked" chalcone.

When comparing the *ee* values generated by the conversion of the tested substrates with the available literature data for the same transformations, [19–21] (Figure 3.11) it can be observed that, for conversion of certain substrates, the *ee* values generated by **4bAlCl$_2$** were actually higher or at least quite similar. Firstly, according to entry 1, Table 3.5, the best *ee* value of 68% that we have obtained when complex **4bAlCl$_2$** was used as the catalyst and "naked" chalcone as the substrate, was more or less similar to what has already been published (67% by **AE** in Figure 3.11). Secondly, even though the chiral silicon-based compounds, as reported by Oestreich and co-workers (Figure 3.11),[20–22] were in general, superior to our aluminium complexes with regard to catalyst loadings and reaction rates, for the examined catalytic transformations, the conversion of the *para*-methyl and *ortho*-methoxy chalcone substrates (entries 2 and 5, Table 3.5) by our catalytic system, **4bAlCl$_2$** produced noticeably better *ee* values (53 vs 40% and 39 vs 7% by **AB**, respectively).

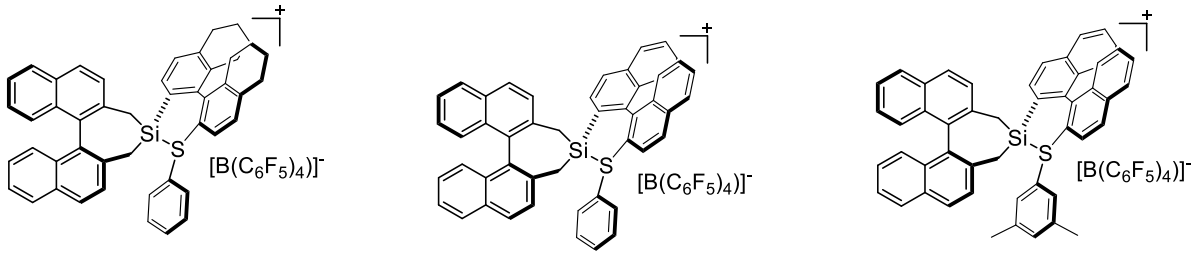

AE **AB** **AC**

Figure 3.11: selected silicon-sulphur Lewis acid catalysts by Oestreich and co-workers

Lastly, it should be also worth mentioning that, to the best of our knowledge, the conversion of the *meta*-methyl substituted chalcone, obtaining the *ee* value of 40% (entry 3, Table 3.5), has not been reported previously in the literature including the works by Oestreich and co-workers.[20–22]

3.3 Summary

This chapter highlights the synthesis of several different aluminium complexes with varying steric congestion at the chiral end together with the most optimal groups at the achiral end from Chapter 2. Synthesised complexes were successfully used as suitable catalysts for difficult DA reactions between 1,3-cycloaddition and chalcones and they all exhibited ability to drive these reactions favouring the formation of one enantiomer of the DA adducts.

The ligand syntheses were carried out via first obtaining the corresponding 2-oxazoline precursors. However, the usual synthetic method used in Chapter 2 was found to be inappropriate due to the formation of 3-oxazoline product when bulky phenyl groups were attached to C atom adjacent to the chiral C atom. Thus, another method involving Lewis acid ($ZnCl_2$) catalysis and high temperatures was introduced for this particular synthesis. This ultimately led to the synthesis of desired 2-oxazoline precursors which were then used in the ligand syntheses.

As the preparation of the targeted aluminium bistriflate complexes was not possible due to the unstable nature of the bulky complexes, aluminium dichloro complexes were then examined as the catalysts in the DA transformations. A 10 mol% loading of each of the synthesised dichloro complexes was sufficient to catalyse the DA reaction between 1,3-cyclohexadiene and chalcone effectively within 48-60 hours depending on the steric properties of the complex used. Excellent *endo*:*exo* ratios were observed (≥ 98%) with the *endo* product being favoured. The DA adducts were purified to give good to average yields ranging from 62-82%. Enantiomeric

excess values ranging from 6-68% were observed and **4bAlCl$_2$** showed the best *ee* value of 68% towards the formation of the DA adduct between 1,3-cyclohexadiene and chalcone. As a conclusion, we believe that having a quaternary carbon atom (e.g. a *t*-Bu group) adjacent to the chiral C was crucial for a notable improvement of enantioselectivity towards the chosen DA reactions, while the optimal steric hindrance at the achiral end was provided by 4-CH_3-2,6-$(CH(Ph)_2)_2C_6H_2$ group.

A substrate scope was then expanded to investigate the versatility of the complex **4bAlCl$_2$** towards several different chalcones. Although lower %*ee* values were observed compared to the naked chalcone, our complex was still able to produce *ee values* ranging from 24-53% towards the DA reactions between 1,3-cyclohexane and substituted chalcones. In addition, an *ee* value of 53% observed for *para*-methyl substituent (vs 40% by **AB**, Figure 3.10) and 39% *ee* observed for *ortho*-methoxy (vs 7% by **AB**, Figure 3.10) were significantly better compared to the published values for generated the same transformations.[22] In addition, **4bAlCl$_2$** also generated *ee* of 40% for *meta*-methyl substituent; a substrate which has not been reported in literature so far to the best of our knowledge.

References

1 Z. Liu, J. H. Q. Lee, R. Ganguly and D. Vidović, *Chem. - A Eur. J.*, 2015, **21**, 11344–11348.

2 Z. Liu and D. Vidović, *J. Org. Chem.*, 2018, **83**, 5295–5300.

3 S. Zhai, C. Forsyth, Z. Liu and D. Vidović, *Organometallics*., 2022, **41**, 2562-2571.

4 D. Dissanayake, A. Draper, Z. Liu, J. J. Haven, C. Forsyth, T. Junkers and D. Vidović, *manuscript under revision.*

5 P. I. Binda, S. Abbina and G. Du, *Synthesis (Stuttg).*, 2011, **2011**, 2609–2618.

6 J. A. Frump, *Chem. Rev.*, 1971, **71**, 483–504.

7 H. Huang, R. Hoogenboom, M. A. M. Leenen, P. Guillet, A. M. Jonas, U. S. Schubert and J.-F. F. Gohy, *J. Am. Chem. Soc.*, 2006, **128**, 3784–3788.

8 A. I. Meyers and M. Shipman, *J. Org. Chem.*, 1991, **56**, 7098–7102.

9 G. Helmchen and A. Pfaltz, *Acc. Chem. Res.*, 2000, **33**, 336–345.

10 T. W. Greene and P. G. M. Wuts, *Protective Groups in Organic Synthesis*, John Wiley & Sons, Inc., 1999.

11 K. Schwekendiek and F. Glorius, *Synthesis (Stuttg).*, 2006, **18**, 2996–3002.

12 Z. Qi-Lin and A. Pfaltz, *Tetrahedron*, 1994, **50**, 4467–4478.

13 T. G. Gant and A. I. Meyers, *Tetrahedron*, 1994, **50**, 2297–2360.

14 H. Vorbrüggen and K. Krolikiewicz, *Tetrahedron*, 1993, **49**, 9353–9372.

15 D. Hoppe and U. Schöllkopf, *Angew. Chemie Int. Ed. English*, 1970, **9**, 300–301.

16 S. Nair, J. R. Zeevaart and R. Hunter, *Arkivoc*, 2020, **2020**, 90–102.

17 Z. Liu, R. Ganguly and D. Vidović, *Dalt. Trans.*, 2017, **46**, 753–759.

18 S. Muthaiah, D. C. H. Do, R. Ganguly and D. Vidović, *Organometallics*, 2013, **32**, 6718–6724.

19 P. Shaykhutdinova and M. Oestreich, *Organometallics*, 2016, **35**, 2768–2771.

20 P. Shaykhutdinova and M. Oestreich, *Org. Lett.*, 2018, **20**, 7029–7033.

21 P. Shaykhutdinova, S. Kemper and M. Oestreich, *European J. Org. Chem.*, 2018, **2018**, 2896–2901.

22 P. Shaykhutdinova and M. Oestreich, *Organometallics*, 2016, **35**, 2768–2771.

Chapter 4

4. Catalysis of symmetric and asymmetric hydrosilylation reactions using achiral and chiral β-diketiminate supported aluminium complexes

4.1 Introduction

4.1.1 Hydrosilylation reaction and organosilicon compounds

Addition of a Si-H bond across an unsaturated bond is simply known as hydrosilylation reaction. This usually involves the reaction between a silane or a siloxane and a multiple bond between carbon-heteroatom, carbon-carbon or even, in rare cases, hetero atom-hetero atom, resulting in an organosilicon compound (Figure 4.1).[1–4] Apart from the widespread use in industrial applications such as adhesives, oils, resins, rubbers, coupling reagents, and binders, these organosilicon compounds are also equally popular in academia, in studies of silicon chemistry, bio-active compounds, polymers, and dendrimers (Figure 4.2).[5–8] Organosilicon compounds (e.g. as silylating reagents) and hydrosilylation reactions (i.e. reduction) are of indispensable value especially for organic chemists. In fact, hydrosilylation transformations offer a safer, comparatively facile and milder alternative to, for example, hydrogenation and various other reduction reactions that use different hydrogen/hydride sources such as organo- and metal- hydrides- as reducing reagents while silylating agents are quite popular as protecting groups (for e.g. alcohol group protection).[3,9,10]

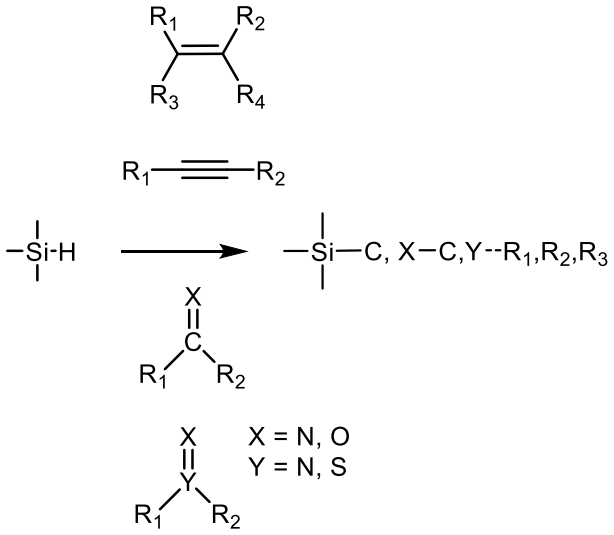

Figure 4.1: Basic hydrosilylation reaction

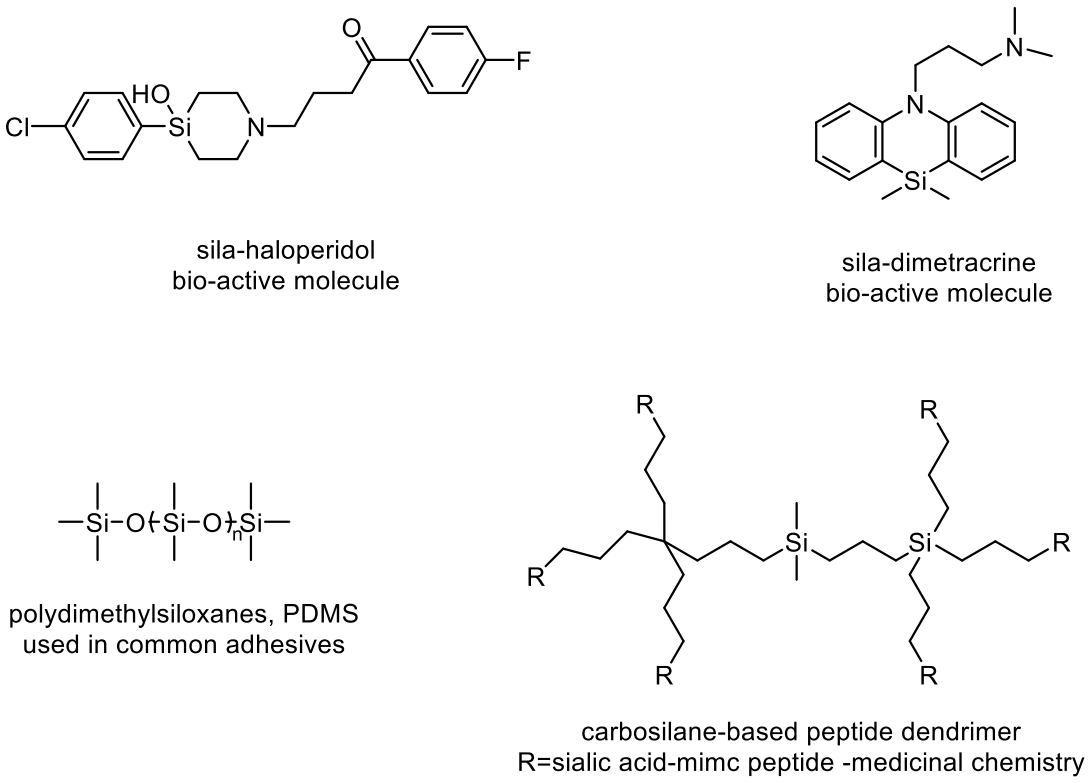

Figure 4.2: Some organosilicon compounds with commercial applications

Catalytic hydrosilylation reactions of alkenes and alkynes (C=C, C≡C) are inarguably the most studied types of the hydrosilylation reactions since they were first discovered as early as 1940s.[1] Numerous catalytic systems based on (i) noble metals (e.g. Pt, Pd, Rh, Ru, and Os[1,2]), (ii) first-row transition metal (e.g. Ni, Co, Fe, Re, Mn, Cu[11]), (iii) lanthanides and actinides,[12,13] and even (iv) radicals have been reported as efficient catalysts for hydrosilylation reaction of unsaturated hydrocarbons.[14] However, the hydrosilylation reactions of carbonyl compounds (C=O) and imines (C=N) were not reported until Moreau and co-workers reported the use of the Wilkinson's catalyst ($RhCl(PPh_3)_3$) in 1973, almost three decades later.[15–17]

Aldehydes, ketones and imines could be clearly identified as the main substrates of hydrosilylation reactions of polarised substrates i.e. of C=X fragments (X = heteroatom). It must be noted that hydrosilylation reactions involving CO_2, C=S, S=O, N=N, and C≡N are also known, but carbonyls and imines are the most popular substrate types.[4] Due to the ability of

facile hydrolysis of silicon-oxygen (Si-O) and silicon-nitrogen (Si-N) bonds to produce alcohols and amines, respectively, hydrosilylation reactions involving carbonyl compounds are not falling significantly behind their much-studied counterparts i.e. hydrosilylation of unsaturated hydrocarbons. In addition, when a ketone or an aldehyde is subjected to hydrosilylation, the respective silyl ether is produced, which itself can appear as a protected silylated alcohol or it can simply be converted in to the alcohol by hydrolysis. Retaining the silyl group as a protective group may appear interesting to organic chemists as protection alcohols using silyl groups is a frequently utilised step in, for example, total syntheses of natural products.[18] On the other hand, hydrosilylation of imines followed by hydrolysis provides a facile and safe alternative method for synthesis of amines, which have a growing demand in fields of pharmaceutical and agricultural industries.[19]

Similar to many catalytic reactions used in organic synthesis, first developed catalysts for these reactions were also based on noble metals such as Rh (Wilkinson's catalyst -$RhCl(PPh_3)_3$, $RhCl_3 \cdot 6H_2O$, $HRh(PPh_3)_4$, Rh(I)DIOP (DIOP = (2,3-O-isopropylidene-2,3-dihydroxy-1,4-bis(diphenylphosphino)butane))), Pt (Speier's catalyst-$H_2PtCl_6 \cdot 2H_2O$) and Ru ($RuCl(PPh_3)_3$), etc. As cheaper and readily available options, numerous first-row transition metal-based complexes have also been well established in this area of catalysis. For example, compounds such as $NiCl_2$, $ZnCl_2$, $ZnBr_2$, $Ni(OAc)_2 \cdot 4H_2O$, etc. as well as complexes such as $Co(CO)_8$, $Cp_2Ti(OC_6H_4Cl_4)_2$ and $(Ph_3P)(CO)_4Mn\text{-}COCH_3$ (see below for more in Figure 4.3) have been reported to act as efficient catalysts for hydrosilylation.[1,2,11] While the catalysts based on the first-row transition metals hold the predominance in the inexpensive category, main group compounds such as $SnCl_4$, $InCl_3$, $GaCl_3$, KF, CsF, have also been reported to catalyse these reduction reactions.[2,11,19,20] A few boron based Lewis acid catalytic systems such as $B(C_6F_5)_3$ have been used for hydrosilylation of aromatic aldehydes and ketones; a process well-known as Pier's hydrosilylation,[20,21] $[Mes\text{-}B\text{-}TMP]^+$ boronium cation (Mes = mesityl, TMP = 2,2,6,6-

tetramethylpiperidine) reported by Chen-Wen Chiu and co-workers,[22] was also capable of performing hydrosilylation but with a very limited control in reactivity resulting in questionable synthetic utility.[23,24] A more recent report emerged in 2021, describing the synthesis of a Si based super Lewis acid and its preliminary applications in aldehyde and ketone hydrosilylation, but unfortunately, the depth of substrates was very low.[25] Nevertheless, one can rationally argue that the development of these main group catalysts have not been as rapid compared to other types of catalysts (specially for imine hydrosilylation).[1,2,11,19,20]

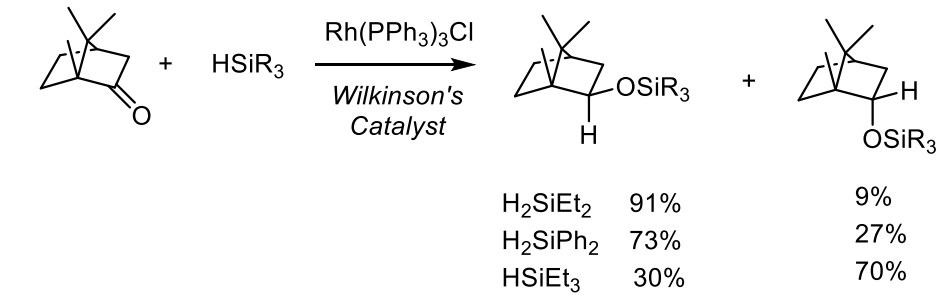

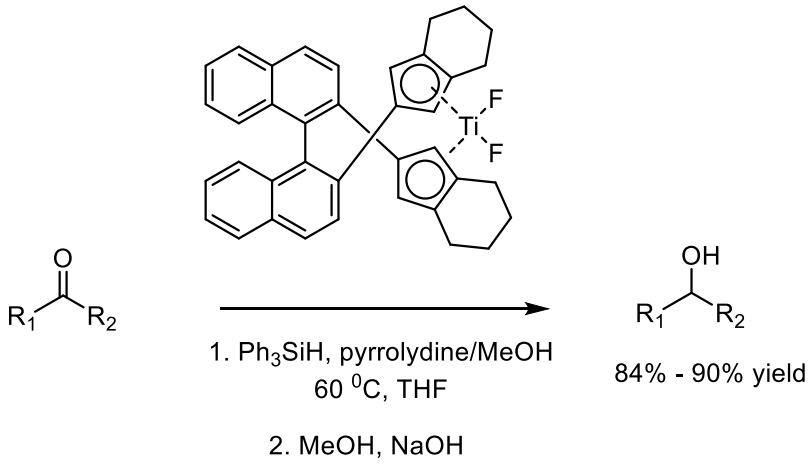

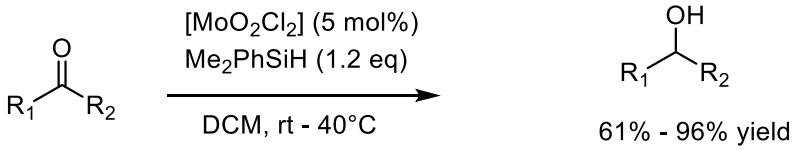

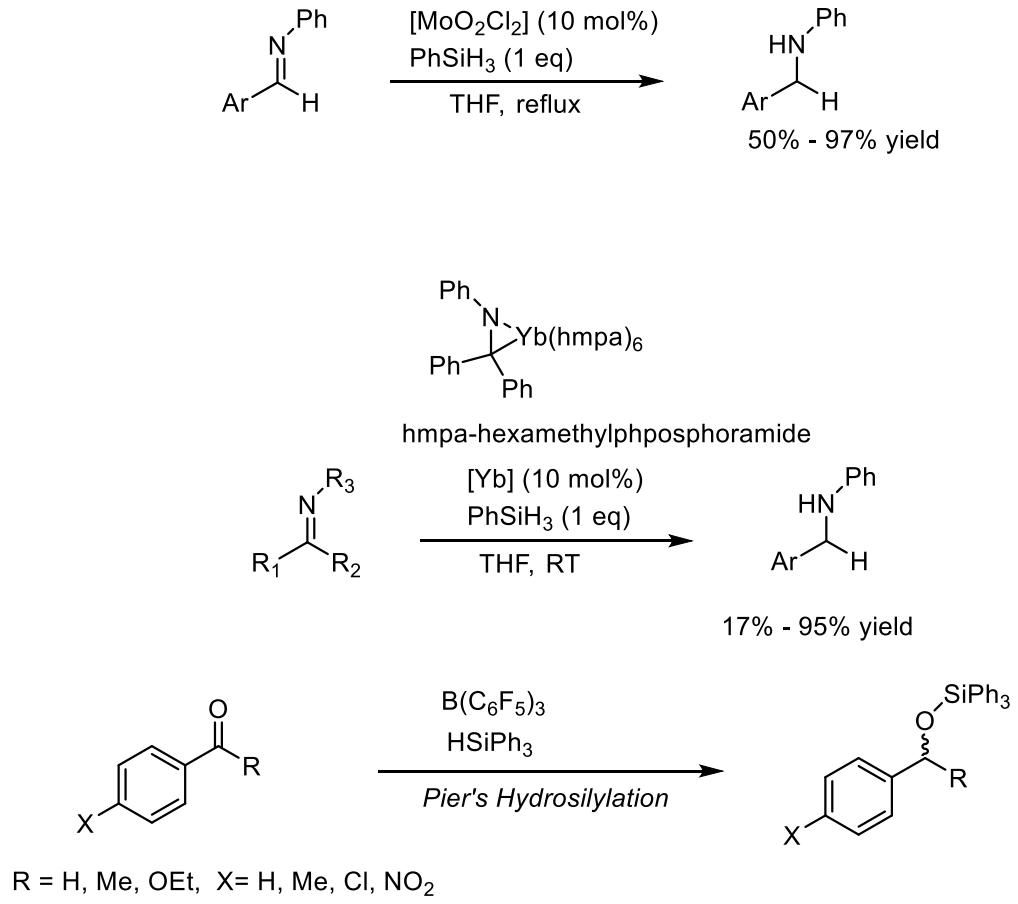

Figure 4.3: Some examples for reported catalytic systems for carbonyl and imine hydrosilylation reactions[2,16,21,26]

4.1.2 Asymmetric hydrosilylation of pro-chiral ketones

Although hydrolysis of silyl ethers generated from aldehydes produces achiral primary alcohols, subsequent hydrolysis of silyl ethers of prochiral ketones forms chiral secondary alcohols, paving the path for asymmetric catalysis. These chiral alcohols are known to be important building blocks for the synthesis of a variety of biologically active compounds, pharmaceuticals, fine chemicals, agrochemicals, artificial flavouring agents and fragrances.[3,4] Perhaps owing to this versatility of applications, first ever reports on catalytic asymmetric hydrosilylation appeared as early as in 1970s.[27,28] Similar to hydrosilylation of its achiral counter-parts, primary catalysts for hydrosilylation of pro-chiral substrates were mainly based

on noble metals but only relatively low enantiomeric excesses were achieved during the initial stages (see Figure 4.4 for examples).[4]

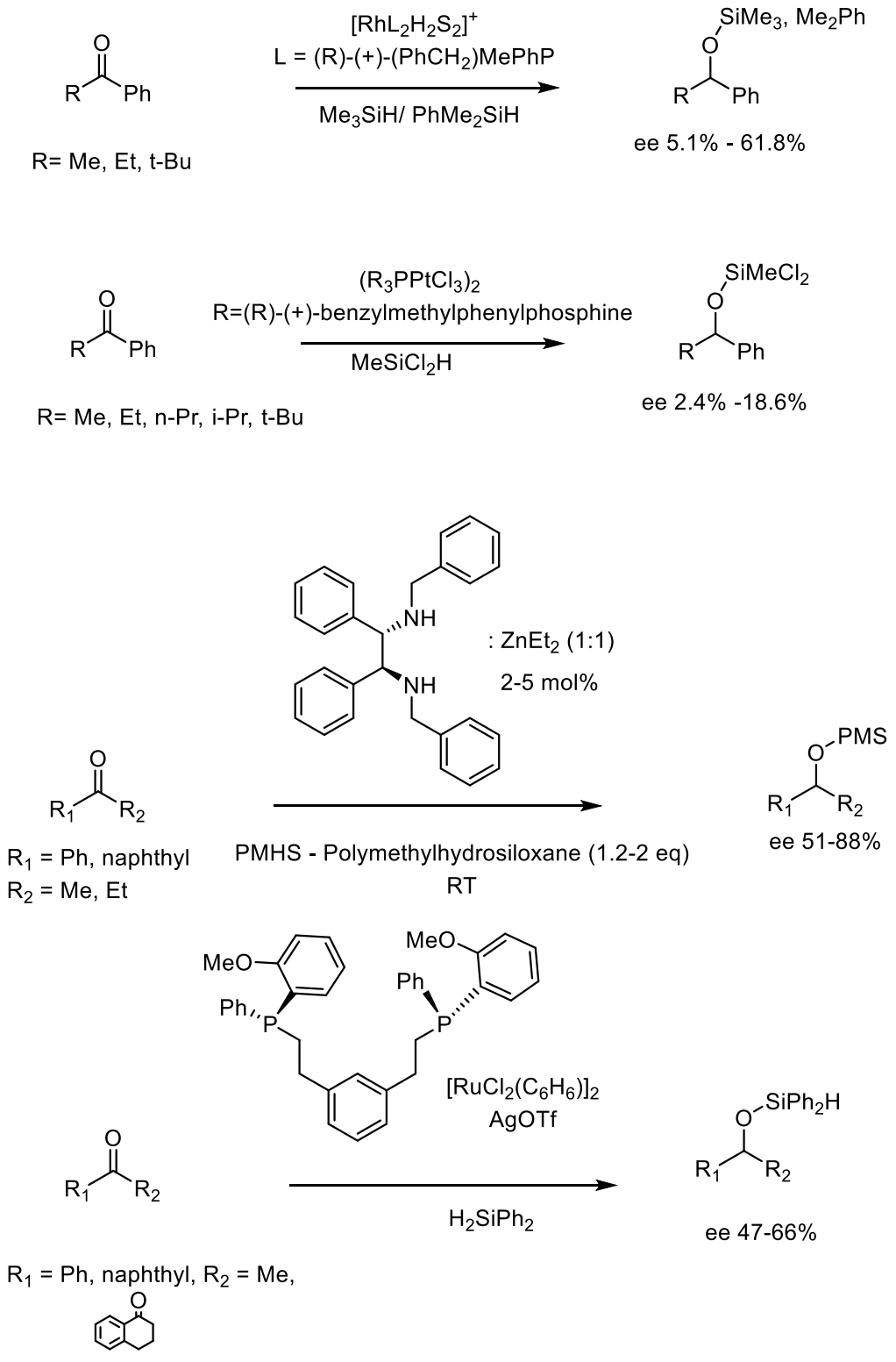

Figure 4.4: Examples for reported noble and first-row transition metal based catalytic systems for asymmetric hydrosilylation reaction of ketones

After Mimoun reported an effective Zn base catalyst reaching an enantiomeric excess of about 88% in 1999, first-row transition metal-based catalysts started slowly taking over the predominance held by the classic noble metal catalysts.[3] In the last decade, a number of studies exploring the activity of almost all the first-row transition metal-based complexes in catalytic hydrosilylation have been reported. Apart from being inexpensive and environmentally benign, these catalysts were able to transform an expanded scope of ketones. However, adding to the scarce number of main group catalysts reported for hydrosilylation reactions, the ones which are focusing on asymmetric catalysis are also shockingly low.[23] Few works were devoted to develop the asymmetric counterpart of Pier's hydrosilylation by replacing one or more of C_6F_5 groups of $B(C_6F_5)_3$ (see Figure 4.5 for examples), producing enantiomeric excesses ranging from 15%-93%.[29] Another report on a chiral oxazaborolidinium ion with highly improved enantiomeric excess of 99% was reported recently in 2017 by Ryu and co-workers (Figure 4.5).[30]

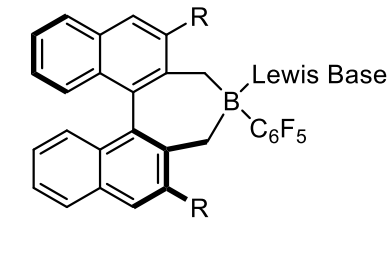

by Oestreich and co-workers

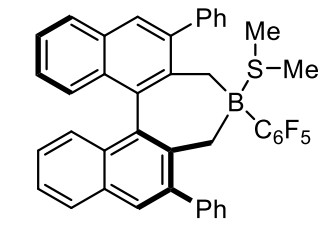

by Oestreich and co-workers

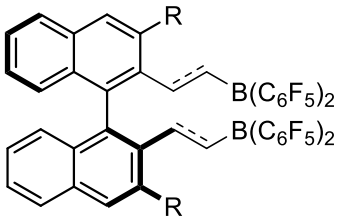

by Du and co-workers

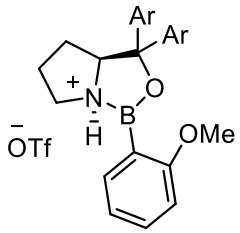

by Ryu and co-workers

Figure 4.5: Boron based catalysts for asymmetric hydrosilylation of ketones (mainly acetophenone)

4.1.3 Aluminium based catalysts for asymmetric and symmetric hydrosilylation reactions of carbonyls and imines

Despite of its Lewis acidic properties, an extremely small number of Al based catalysts were reported for hydrosilylation in general and most of them focus on hydrosilylation reactions of alkynes and cyclic substances.[23] Only a handful of reports discussed hydrosilylation of ketones and none of them described the use of chiral catalysts (i.e. asymmetric catalysis).[23,31–33] Interestingly, we also observed that all these reported catalytic systems involving hydrosilylation reactions were cationic aluminium species. Bergman and Koller s' 2012 report pointed out that the high reactivity of Lewis acids towards these transformations, which typically resulted in multiple products, could be the main reason why such catalysts lagged behind first-row transition and noble metal catalysts.[23] Thus, they attempted to stabilise highly reactive cationic Al species by maintaining a tetrahedral geometry producing the first ever significant study focuses on catalysis of hydrosilylation of ketones using an Al based complex. This report elaborated on the use of different silylating agents and achieved up to 98% conversion at elevated temperatures (75-100℃). In 2015, Roesky and co-workers reported about the possibility of their Al hydride catalyst to catalyse hydrosilylation of aldehydes, but their report only contained preliminary results without any further optimisations.[32] In 2019, Venugopal and co-workers published a report on the activity of their organoaluminium catalyst towards the hydrosilylation reactions of ketones using triethylsilane (Et_3SiH) and phenylsilane ($PhSiH_3$) with excellent yields of 95%-99%, but under elevated temperatures of 60℃ and prolonged times for most of the substrates.[31] A common occurrence for almost all of these catalysts were the ability of utilising milder, industrially viable choice of silylating agent, Et_3SiH. In addition to being less expensive, Et_3SiH also produces a single product, but it was shown to be incompatible with many other catalytic systems except for a few transition metal catalysts.[23,29] Nevertheless, to the best of our knowledge, there aren't any reports about

aluminium based catalysis capable of performing asymmetric hydrosilylation. Thus, it seemed appropriate to focus on developing a chiral Al based complex that would be able to execute efficient asymmetric hydrosilylation of ketones under mild (e.g. at room temperature) reaction conditions.

It is worth mentioning that by the time that we almost finalised our achiral catalysis study for a publication, a similar work by Nembenna and co-workers,[34] reporting a β-diketiminate supported cationic Al based system with similar efficiency and a versatile substrate scope containing aldehydes and ketones, was published and, thus, preventing us from publishing our findings presented in the first part of this chapter (Figure 4.6).

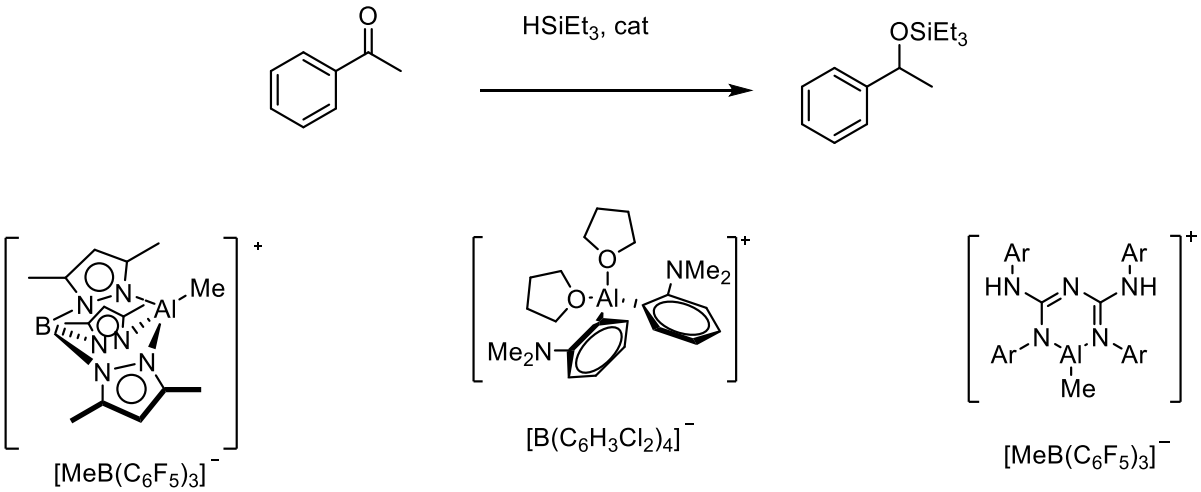

Bergman, 2012
TON=39.2
TOF(h^{-1})=39.2
$CDCl_3$, 100 ^{0}C, 1 h
98%(NMR)

Venugopal, 2019
TON=19.6
TOF(h^{-1})=0.57
C_6D_6, 60 ^{0}C, 34 h
98%(NMR)

Nembenna, 2022
TON=50
TOF(h^{-1})=12.5
neat, rt, 4 h
99%(NMR)

Figure 4.6: Reported work on Al based catalysts for hydrosilylation reactions; comparison on hydrosilylation of ketones

4.2 Catalysis of symmetric hydrosilylation reaction

Initially, the ability of the published achiral catalytic system (section 1.4 Chapter 1) to drive hydrosilylation reactions was investigated. For this, three different aluminium complexes were examined. All three have been previously used in different reactions such as Diels Alder (DA) cycloadditions,[35] Michael additions,[36] hydroboration of imines,[37] and polymerisation reactions[38] with extremely efficient catalytic activity (Figure 4.7).

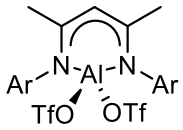

1a $^{Dip}LAl(OTf)_2$: Ar = 2,6-iPr_2-C_6H_3, **1a'** $^{Dip}LAlCl_2$

1b $^{Xyl}LAl(OTf)_2$: Ar = 2,6-,Me_2-C_6H_3

1c $^{Ph}LAl(OTf)_2$: Ar = C_6H_5

Figure 4.7: achiral Al complexes tested for the hydrosilylation reaction

Initially, catalytic hydrosilylation of acetophenone with triethylsilane was tested. To our delight, with addition of 1 equiv. of $NaBar^{Cl}{}_4$ all three systems showed capability of catalysing the hydrosilylation reaction of acetophenone, with our preferred silylating agent, Et_3SiH (Table 4.1).

^1H NMR spectroscopy could be conveniently used to monitor reaction progress and to determine the yield in the presence of 1,3,5-trimethoxybenzene as an internal standard (via the singlet at δ_H 5.96 ppm). Reaction progress was monitored either by the disappearance of a characteristic proton signal for PhCOCH_3 observed at δ_H 2.40 ppm (a singlet), or using the

appearance of the characteristic proton signal for PhC*H*MeOSiEt$_3$ at δ_H 4.75 ppm (a quartet; Figure 4.8).

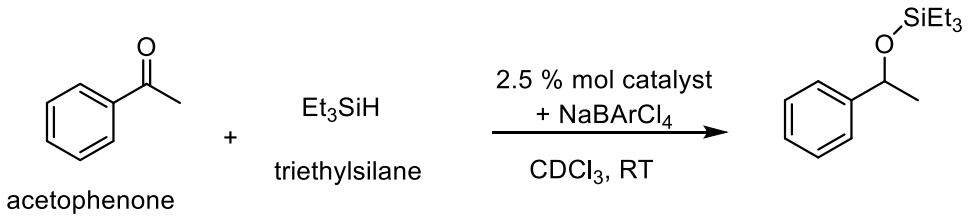

Table 4.1: catalyst screening and loading optimisation for hydrosilylation reaction of acetophenone

Entry	Catalyst	Catalyst loading (% mol)	Time (h)	Yield% (NMR)[a]	TON[b]	TOF (h^{-1})[c]
1	**1a**	2.5	7	98	40	5.7
2	**1a**	1	10	98	100	10
3	**1a**	2	8.5	98	50	5.8
4	**1a**	5	3	98	20	6.7
5	**1a'**	5	5	98	20	4
6	**1b**	2.5	10	98	40	4
7	**1c**	2.5	5	98	40	8

Reaction conditions: acetophenone (1.0 equiv., 1.0 mmol), triethylsilane (1.1 equiv., 1.1 mmol), catalyst (2.5 mol%), $CDCl_3$, at RT under N_2. [a] The yield was determined by ^{1}H NMR spectroscopy based on consumption of starting material and identified newly formed characteristic proton (PhCHMeOSiEt$_3$) signal at (δ) 4.75 ppm against the internal standard 1,3,5-trimethoxybenzene (10 mol%). [b] TON was calculated by dividing the number of moles of the product by the number of moles of catalyst used. [c] TOF was determined to divide TON by time of reaction.

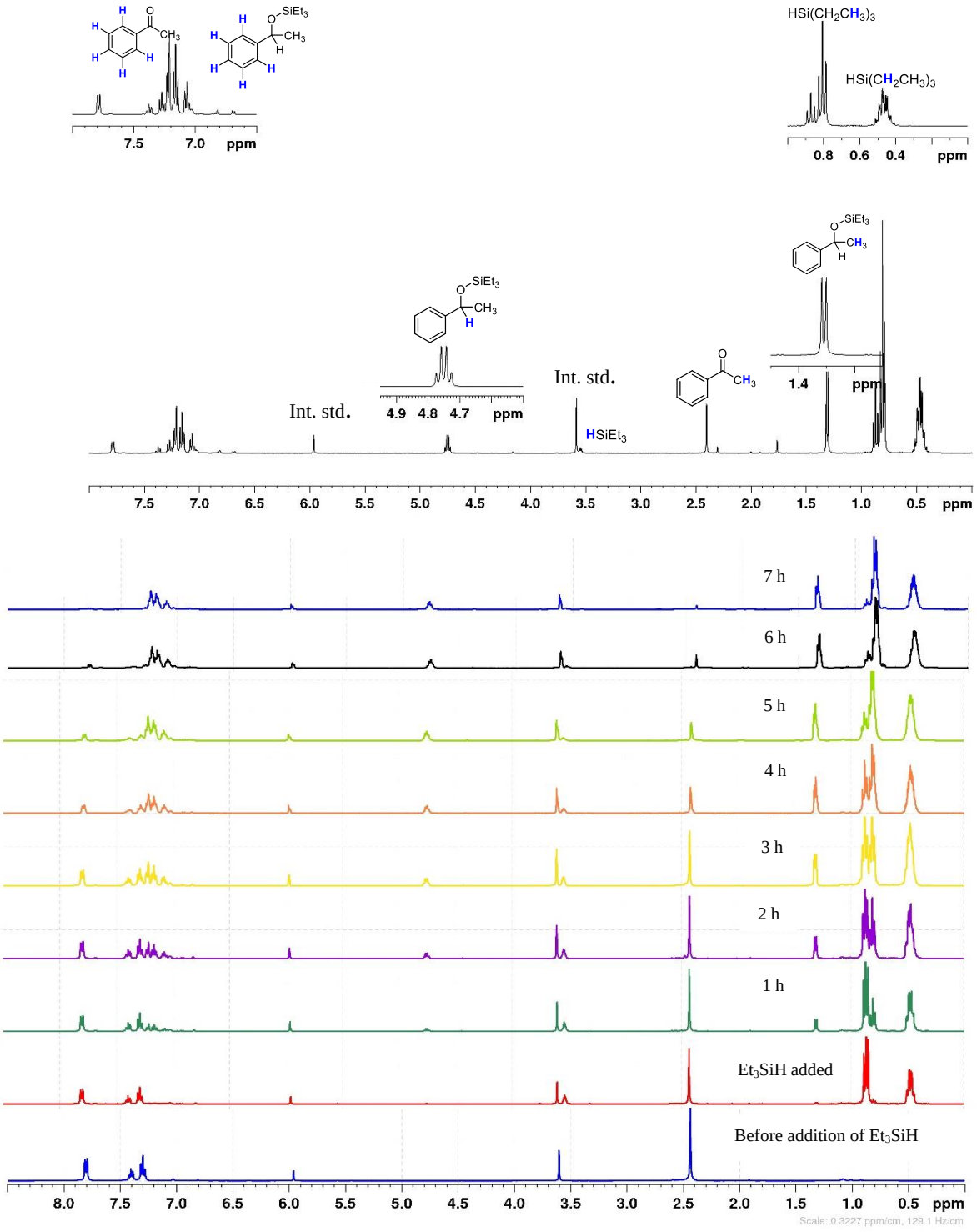

Figure 4.8: An overlay of ^{1}HNMR spectra for the reaction between acetophenone and triethylsilane.

Given its excellent reactivity in Diels Alder cycloadditions,[35] $^{Dip}LAl(OTf)_2$ (**1a**) was initially tested for the catalytic activity (entries 1-4, Table 4.1). To our delight, the catalyst showed excellent activity towards the reaction at room temperature, by reaching completion within 3 hrs at room temperature with 5 mol% catalyst loading (entry 4, Table 4.1). Catalyst loadings were then reduced to 2.5, 2, and 1 mol%, and it was decided that 2.5 mol% as the optimum loading percentage, considering all the reaction's parameters. (entries 1-3, Table 4.1). It should be noted that one reaction was carried out using $^{Dip}LAlCl_2$ (**1a'**) catalyst, (entry 5, Table 4.1) as our previous work in Chapter 3 showed that the chiral, dichloro analogues of the same catalyst were capable of efficiently catalysing Diels Alder cycloadditions. However, it was observed that the efficiency decreased, as the reaction time increased by 2 h. Next, two other catalysts, $^{Xyl}LAl(OTf)_2$ (**1b**) and $^{Ph}LAl(OTf)_2$ (**1c**) were also tested for the same reaction. It was clear that **1c** was the most efficient towards the reaction among the tested aluminium complexes. TON and TOF values for each reaction were also calculated in order to compare the results with already published data. **1c** at room temperature showed comparatively better TON (of 40) and TOF (of 8 h^{-1}) than already reported Al based systems at the time, which were all run at elevated temperatures (Bergmann's catalyst showing TON of 39 and TOF of 39 h^{-1} at 100 ˚C and Venugopal' catalyst showing TON of 19 and TOF of 0.57 h^{-1} at 60 ˚C).[23,31] It should be noted that although 1 mol% loading of **1a** (entry 2 of Table 4.1. TON = 100, TOF = 10 h^{-1}) showed the best TON and TOF values, it was decided to use **1c** (2.5 mol% catalyst loading with TON of 40; TOF of 8 h^{-1}) for further studies simply because using the latter reaction conditions allowed us to shorten the reaction time by a half (i.e. from 10 to 5 h).

With this information in hand, we decided to expand the substrate scope by using **1c** together with 1 equivalent of $NaBAr^{Cl}{}_4$ and a vast range of substrates were tested, including electron rich, poor and sterically hindered ketones, aldehydes, and imines (Table 4.2). All reactions wer-

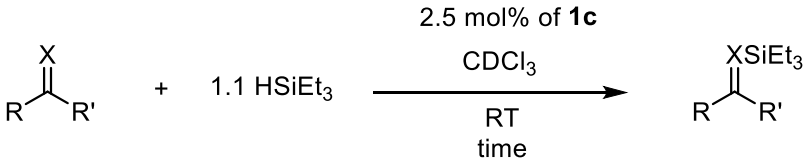

Table 4.2: Substrate scope study of hydrosilylation reaction of aldehydes, ketones and imines

Entry	Substrate	Time (h)	product	Yield% (NMR)
1	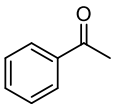	5	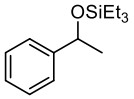	98
2	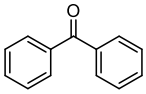	6 days	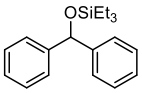	97
3	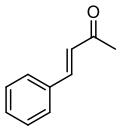	4.5	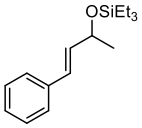	98
4	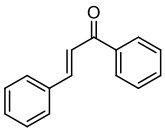	3	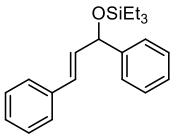	98
5		15	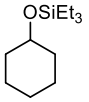	95
6		48		96
7	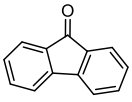	6	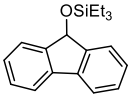	97
8	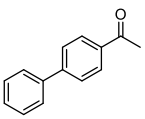	7 days	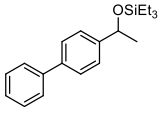	95

9	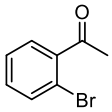	7 days	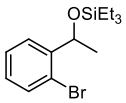	98
10	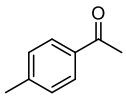	3	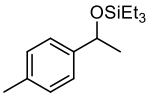	98
11	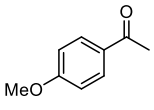	10 days	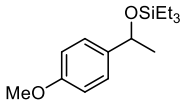	96
12	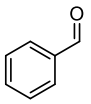	10	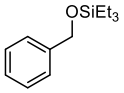	98
13	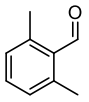	48	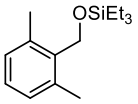	98
14	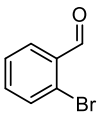	4	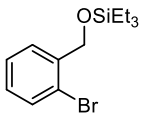	98
15	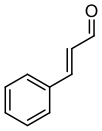	72	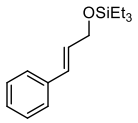	98
16	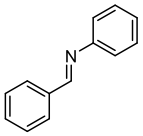	20[a]	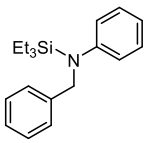	99

Reaction conditions: ketone/aldehyde (1.0 equiv., 1.0 mmol), triethylsilane (1.1 equiv., 1.1 mmol), catalyst (2.5 mol%), $CDCl_3$, at RT under N_2. [a] The yield was determined by ^1H NMR spectroscopy based on consumption of starting material and identified newly formed characteristic proton ($RCHR'OSiEt_3$) against the internal standard 1,3,5-trimethoxybenzene (10 mol%). [a] reaction completed at 100 °C

-e carried out with 1.1 equivalent of triethylsilane, in $CDCl_3$ using 2.5 mol% catalyst loading, at room temperature, except for the imine, *N*-benzylideneaniline, for which the reaction had be carried out at elevated temperatures in order to obtain a reasonable high product yield (entry 16, Table 4.2). All reactions were monitored via ^1H NMR spectroscopy, until at least 95% of a substrate was consumed. All substrates were able to selectively produce the expected silyl ethers without undergoing any side reactions that have been reported with some catalytic systems.[22,23,31] When the methyl group of acetophenone was replaced with phenyl substituent, (benzophenone, entry 2, Table 4.2) expected silyl ether product was still observed, although efficiency of the reaction dropped significantly, similar to most reported data when other Lewis acid complexes were used as the catalysts.[29,34] Nevertheless, this confirmed that the catalytic system based on **1c** was well capable of converting sterically demanding substrates. For conjugated α, β-unsaturated substrates, which are considered as challenging as only a few catalytic systems being able to produce the silyl enol ether, we observed increased efficiency, with good yields (entries 3,4, Table 4.2).[23] Reduction of three different cyclic substrates (entries 5-7, Table 4.2) to their respective silyl ethers was also successful, proving the versatility of our catalytic system. Several different acetophenone-based substrates possessing fragments/groups of varying electronic demand at the phenyl ring were also tested (entries 8-11, Table 4.2). While all the tested substrates were successfully converted to the respective silyl ethers, decreased efficiencies without any rational trend, were observed, except for *p*-methyl acetophenone (entry 10) whose conversion showed a much-improved reaction rate during hydrosilylation. Unsurprisingly, aldehydes were also equally viable substrates. However, contrary to other reported cationic aluminium based systems, reduced catalytic activity towards aldehyde in comparison to ketone hydrosilylation was observed. Similar observations were reported by Chiu and co-workers involving cationic boronium Lewis acid catalyst, and the authors suggested competition between carbonyl-borane and Si-H activation at the active site as the

main reason for the lower conversions.[22] Nevertheless, a considerable range of different aldehydes were successfully reduced to their respective silyl ethers with fair yields (entries 12-15, Table 4.2). As mentioned previously, even though elevated temperatures were required, the imine, *N*-benzylideneaniline, was also reduced to the respective silylamine, representing the most efficient hydrosilylation of this particular substrate by an aluminium catalyst.[23] After successfully confirming the versatility of the achiral catalytic system, our next step was to investigate the chiral catalytic system for asymmetric hydrosilylation reaction.

4.3 Catalysis of asymmetric hydrosilylation reaction of ketones

Driven by the discovery of the catalytic activity of our achiral system towards hydrosilylation reactions and the ability of enantioinduction of its chiral counterpart towards DA cycloadditions, we were keen to explore whether our collection of chiral complexes (Figure 4.9) could be active, with a high level of enantioselectivity, in asymmetric hydrosilylation of

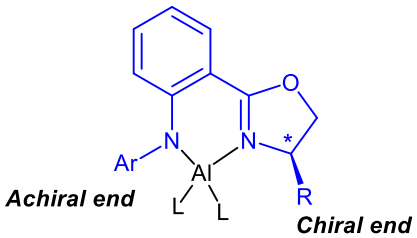

	R	Ar	L
3a	*i*-Pr	2,6-$Me_2C_6H_3$	OTf
3b	*i*-Pr	Ph	OTf
3c	*i*-Pr	2,6-*i*-$Pr_2C_6H_3$	OTf
3d	*i*-Pr	2,4,6-$(CH_3)_3C_6H_2$	OTf
3e	*i*-Pr	4-CH_3-2,6-$(CH(Ph)_2)_2C_6H_2$	OTf
3f	*i*-Pr	4-*t*-Bu-2,6-$(CH(Ph)_2)_2C_6H_2$	OTf
4a	*t*-Bu	2,6-*i*-$Pr_2C_6H_3$	Cl
4b	*t*-Bu	4-CH_3-2,6-$(CH(Ph)_2)_2C_6H_2$	Cl
5a	$PhCH_2$-	2,6-*i*-$Pr_2C_6H_3$	Cl
5b	$PhCH_2$-	4-CH_3-2,6-$(CH(Ph)_2)_2C_6H_2$	Cl
6a	Ph_2CH-	2,6-*i*-$Pr_2C_6H_3$	Cl
6b	Ph_2CH-	4-CH_3-2,6-$(CH(Ph)_2)_2C_6H_2$	Cl

Figure 4.9: Our library of different chiral complexes reported in Chapter 1 and 2

ketones. As discussed previously in this chapter, given the shortage of reported data involving asymmetric hydrosilylation reaction catalysed by Al based compounds, it was decided that exploring the activity of our complexes towards this reaction was worth investigating.

Initially, the most efficient catalysts from the optimisation experiments involving (i) the aryl groups at the achiral end (i.e. **3e**; Chapter 2) and (ii) the group attached to the chiral end (i.e. **4b**; Chapter 3) were tested for enantioinduction in a hydrosilylation reaction. Although the difference was not spectacular, **3e** was showing a better ability than **4b** (entries 1,2, Table 4.3)

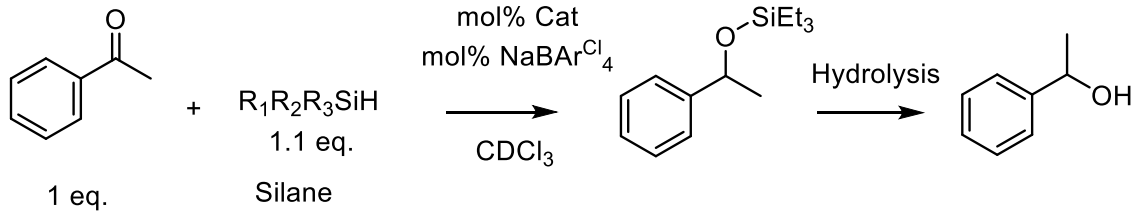

Table 4.3: Initial screening results for asymmetric hydrosilylation reaction

Entry	Cat.	Cat. Loading (mol %)	Silane	Time (h)	Temperature (°C)	Yield % (NMR)	ee (%)
1	**4b**	2.5	Et_3SiH	20	RT	> 98	2
2	**3e**	2.5	Et_3SiH	15	RT	> 98	6
3	**3e**	1	$PhSiH_3$	1	RT	> 99	25
4	**3e**	2.5	Ph_3SiH	48	RT	> 98	22
5	**3e**	2.5	Ph_2SiH_2	18	RT	> 98	17
6	**3e**	1	$PhMe_2SiH$	10	RT	> 98	10
7	**3e**	1	$PhSiH_3$	4	− 10	> 99	38
8	**3e**	2.5	Et_3SiH	24	− 10	> 98	27

Conversion was determined by NMR analysis. Hydrolysis was performed by stirring with NaOH/Methanol for multiple days. ee of hydrolysed product was determined by HPLC analysis using a chiral OD-H column 90:10 (hexane: *i*-PrOH) 0.65 mL/min, λ=254 nm, t_R~ 9 min t_R~10.0 min

for this particular purpose. Then, given their ability to induce enantioselectivity, bulkier silanes (instead of Et_3SiH) were also tested (Table 4.3) using **3e** as the catalyst.[39] In contract to some reported Lewis acidic compounds,[23,29] the catalytic system based on **3e** was able to execute the reaction in the presence of a vast range of different silylating reagents. It was observed that different primary, secondary and tertiary silanes exhibited different reaction times and efficiencies. Primary silane, $PhSiH_3$ showed the best efficiency (entry 3, Table 4.3), while the tertiary silanes were exhibiting increased reaction times (entries 2, 4, Table 4.3). The efficiency of secondary silanes was dependent on the bulkiness of the attached groups (entries 5,6, Table 4.3). Generally, with bulkier silanes, the %*ee* values increased (entries 3-6, Table 4.3). As mentioned, $PhSiH_3$ showed the best ability of enantioinduction (*ee* of 25%, entry 3, Table 4.3), but being a primary silane, an extremely fast reaction was observed. Therefore, it was decided to lower the reaction temperature in order to slow down the rate and potentially provide an adequate amount of time for the substrates to interact with the chiral complex i.e. for the chiral information to be "passed" from the complex to the substrate(s). This is a proven, reported technique to increase enantiomeric excess.[40,41] Although as expected, an increased value for *ee* of 38% was observed by bringing the reaction temperature to − 10°C (entry 7, Table 4.3), it was decided not to use this silane any further, as it was a well-studied silane and its use with other reported Lewis acids generated the *ee* value of 93% for the same reaction.[29] Nevertheless, a low temperature reaction was carried out for our far less investigated silane of choice, Et_3SiH, and to our delight about 27% *ee* was observed at − 10°C (entry 8, Table 4.3).

We then decided to use the same conditions to test the ability of enantioinduction with the rest of our collection of chiral catalysts (Table 4.4). All the chiral complexes were capable of catalysing the hydrosilylation reaction of acetophenone with Et_3SiH at low temperature. As a general trend, it was observed that the reaction times were increased when the *i*-Pr group at the chiral end was changed to *t*-Bu, -CH_2Ph and $CHPh_2$. On the other hand, when the steric demand

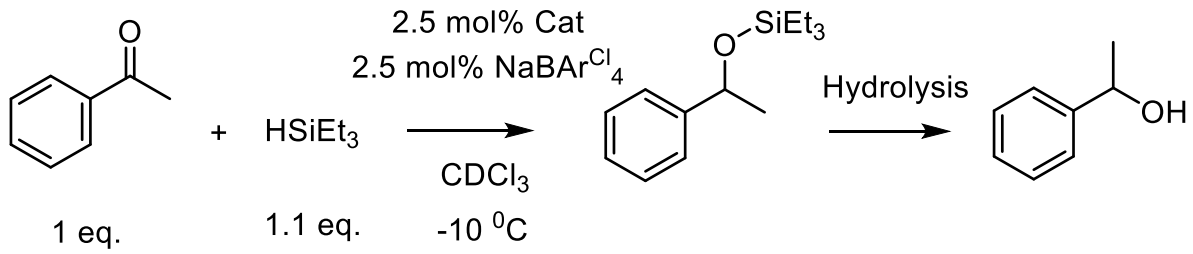

Table 4.4: Effect of different catalysts on the hydrosilylation of acetophenone at low temperature

Entry	Cat.	Time (h)	Yield % (NMR)	ee (%)
1	**3a**	24	> 98	2
2	**3b**	48	> 98	10
3	**3c**	24	> 98	4
4	**3d**	24	> 98	8
5	**3e**	24	> 98	27
6	**3f**	24	> 98	12
7	**4a**	48	> 98	44
8	**4b**	72	> 98	9
9	**5a**	5 days	> 96	13
10	**5b**	7 days	> 96	89
11	**6a**	10 days	> 95	67
12	**6b**	5 days	> 96	15

Conversion was determined by NMR analysis. Hydrolysis was performed by stirring with NaOH/Methanol for multiple days. ee of hydrolysed product was determined by HPLC analysis using a chiral OD-H column 90:10 (hexane: *i*-PrOH) 0.65 mL/min, λ=254 nm, t_R~ 9 min t_R~10.0 min

at the achiral end increased, no particular or notable increase in the *ee* values was observed (entries 1-6, Table 4.4). Specifically, enantiomeric excess values above 50% were observed

when **4a**, **5b** and **6a** (entries 7, 10, 11, Table 4.4) were used as the catalysts. Complex **5b**, containing -CH_2Ph at the chiral end and bulky 4-CH_3-2,6-$(CH(Ph)_2)_2C_6H_2$ at the achiral end, generated the best *ee* value of 89% with Et_3SiH. To best of our knowledge, this is the best *ee* value reported by a main group Lewis acid complex when Et_3SiH was used as the hydrosilylating reagent. Given the inability of boron-based complexes to effectively catalyse this reaction with Et_3SiH,[29] and no reported data on any Al based complexes catalysing asymmetric hydrosilylation reaction, this observation could be considered as breakthrough in main group asymmetric Lewis acid catalysis. Further studies to confirm the reproducibility and substrate scope of this study is currently being carried out in our laboratories.

4.4 Suggested mechanism for the hydrosilylation reaction

The mechanism for Lewis-acid initiated hydrosilylation of carbonyl species contains two competing pathways as activation (i.e. binding) of either the silane (via the H-Si bond) or the carbonyl (via the oxygen atom) substrate at the Lewis acid centre could occur (Figure 4.10). A vast majority of Lewis acid catalysed hydrosilylation reactions proceed via the former mechanism,[20-23] while only a couple of reports suggested the carbonyl activation pathway.[31,34]

We anticipated the hydrosilylation reactions examined in this work to proceed via the silane activation pathway, which, as stated before, is initiated via the Si-H bond activation by the Lewis acid compound. As discussed earlier, this was supported by the comparatively reduced catalytic efficiencies towards aldehyde substrates. Although it was presumed that aldehydes should have underwent more efficient hydrosilylation reactions than ketones, the opposite was actually observed. This could be explained by the higher tendency of aldehydes to bind to the aluminium centre compared to ketones. This further implied that aldehydes would be more detrimental to the overall hydrosilylation mechanism via the initial formation of an Al--H-Si interaction.[20] In other words, the presence of aldehydes, as opposed to ketones, would offer a

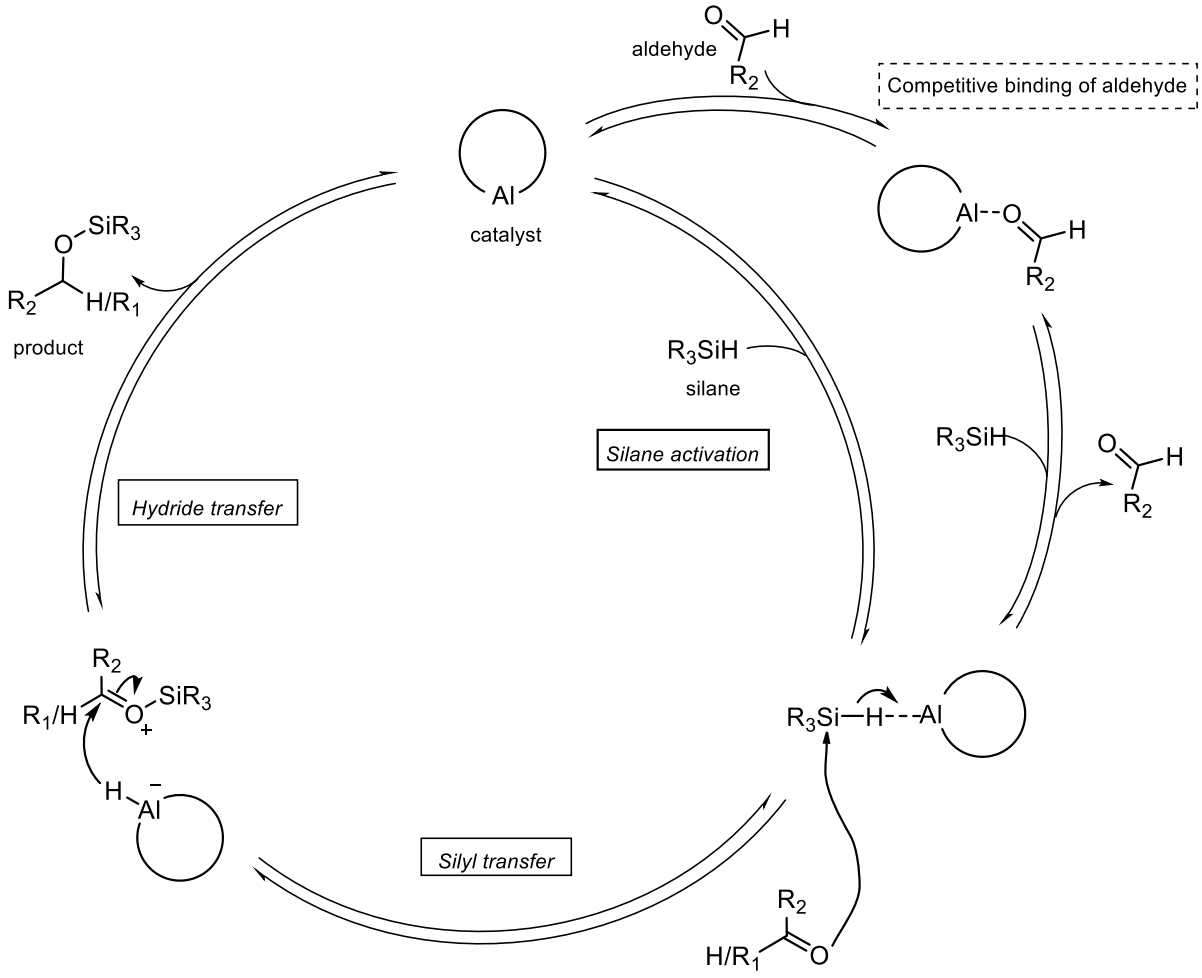

Figure 4.10: Suggested mechanism for hydrosilylation of ketones and aldehydes over the Al catalyst

higher degree of competition to the silane reagent with respect to binding to and activating at the aluminium centre, ultimately leading to lower substrate conversion percentages.

On the other hand, ketones are expected to be lesser competitors than aldehydes for binding to the aluminium centre in the presence of silanes resulting in better conversion rates for these carbonyl containing substrates.[22] Thus, as suggested in the catalytic cycle (Figure 4.10), direct activation of silane should be taken place without any competition at the binding site.

Therefore, the proposed catalytic cycle next proceeds to a silyl transfer step, where the activated silane is transferred on to the aldehyde or ketone. The cycle is competed via a final hydride transfer, where the free product, and free catalyst (which has now completed the reaction via transferring the H on to the substrate) is released. As already indicated, this type of mechanism has been reported to take place when other Lewis acid systems were used and it is consistent with our observations.[20,23]

4.5 Conclusion

In conclusion, our already published achiral catalytic systems were capable of efficiently catalysing hydrosilylation reactions of carbonyls and imines, using less reactive, industrially important silane Et_3SiH, while its analogous chiral catalytic systems, introduced in this thesis, were capable of driving asymmetric/enantioselective silylation of acetophenone with the same silylating agent.

All three different achiral complexes **1a**, **1b** and **1c** were catalytically active towards the hydrosilylation reaction of acetophenone with Et_3SiH. Complex **1c,** together with 1 equivalent of $NaBAr^{Cl}{}_4$ showed the best activity among all catalysts tested, exhibiting a TON of 40 and TOF of 8 h^{-1} which is comparative with other few Al based systems reported (see Figure 4.13). The system also showed excellent activity towards a range of different carbonyl substrates, including α, β-unsaturated ketones which are considered challenging. In addition, it also exhibits the best reported catalytic activity towards *N*-benzylideneaniline when compared to the known Al catalysts so far.

In addition, the catalyst showed reduced efficiency towards aldehydes compared to ketones, suggesting a mechanistic pathway starting with activation of the silane. The proposed catalytic cycle starts with activation of silane, followed by silyl transfer to the aldehyde/ketone, and completes with hydrogen transfer at the end.

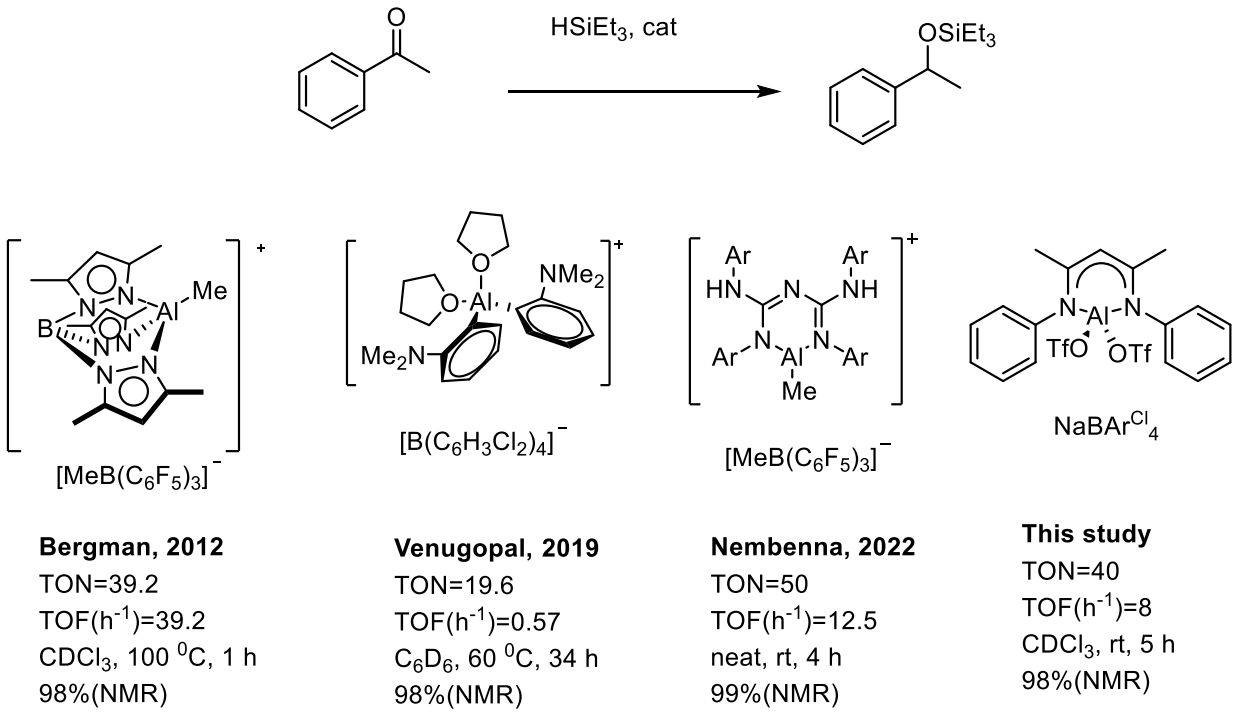

Figure 4.13: Comparison of catalytic activity of Al based systems reported up to date.

All asymmetric catalysts exhibited ability of driving the reaction between acetophenone and Et_3SiH at low temperature showing *ee* values ranging from 2-89%. In contrast to the observations in Chapter 2, better enantioinduction was not observed with increased steric demand at the achiral end. On the other hand, better enantioinduction was observed when the *i*-Pr group at the chiral end was changed to *t*-Bu, $-CH_2Ph$ and $CHPh_2$. Complex **5b** with $-CH_2Ph$ at the chiral end and bulky 4-CH_3-2,6-$(CH(Ph)_2)_2C_6H_2$ at the achiral end produced an *ee* value of 89% with Et_3SiH; the best %*ee* value reported by a main group Lewis acid complex with Et_3SiH.

Further studies to investigate hydrosilylation of imines using **1c** and asymmetric hydrosilylation of acetophenone with Et_3SiH by **5b** will be carried out in our laboratories in the future.

References

1 I. Ojima, in *The Chemistry of Organic Silicon Compounds*, John Wiley & Sons, Ltd, 1989, pp. 1479–1526.

2 I. Ojima, Z. Li and J. Zhu, in *The chemistry of organic silicon compounds Volume 2*, 1998, pp. 1687–1792.

3 V. M. Uvarov and D. A. de Vekki, *J. Organomet. Chem.*, 2020, 923, 121415.

4 B. Marciniec, *Hydrosilylation-A Comprehensive Review on Recent Advances*, Springer, 2008.

5 A. K. Franz and S. O. Wilson, *J. Med. Chem.*, 2013, **56**, 388–405.

6 F. De Buyl, *Int. J. Adhes. Adhes.*, 2001, **21**, 411–422.

7 L. D. de Almeida, H. Wang, K. Junge, X. Cui and M. Beller, *Angew. Chemie - Int. Ed.*, 2021, 60, 550–565.

8 N. Rabiee, S. Ahmadvand, S. Ahmadi, Y. Fatahi, R. Dinarvand, M. Bagherzadeh, M. Rabiee, M. Tahriri, L. Tayebi and M. R. Hamblin, *J. Drug Deliv. Sci. Technol.*, 2020, 59, 101879.

9 V. S. Shende, P. Singh and B. M. Bhanage, *Catal. Sci. Technol.*, 2018, 8, 955–969.

10 A. F. Abdel-Magid, in *Comprehensive Organic Synthesis: Second Edition*, Elsevier Ltd., 2014, vol. 8, pp. 1–84.

11 A. K. Roy, *Adv. Organomet. Chem.*, 2007, 55, 1–59.

12 G. A. Molander and W. H. Retsch, *J. Am. Chem. Soc.*, 1997, **119**, 8817–8825.

13 A. K. Dash, I. Gourevich, J. Q. Wang, J. Wang, M. Kapon and M. S. Eisen, *Organometallics*, 2001, **20**, 5084–5104.

14 S. Amrein and A. Studer, *Chem. Commun.*, 2002, **2**, 1592–1593.

15 O. Riant, N. Mostefaï and J. Courmarcel, *Synthesis (Stuttg).*, 2004, 2004, 2943–2958.

16 S. Díez-González and S. P. Nolan, *Org. Prep. Proced. Int.*, 2007, **39**, 523–559.

17 R. J. P. Corriu and J. J. E. Moreau, *J. Chem. Soc. Chem. Commun.*, 1973, 38–39.

18 R. D. Crouch, *Synth. Commun.*, 2013, **43**, 2265–2279.

19 H. Elsen, C. Fischer, C. Knüpfer, A. Escalona and S. Harder, *Chem. - A Eur. J.*, 2019, **25**, 16141–16147.

20 D. T. Hog and M. Oestreich, *European J. Org. Chem.*, 2009, 5047–5056.

21 D. J. Parks and W. E. Piers, *J. Am. Chem. Soc.*, 1996, **118**, 9440–9441.

22 P. H. Chen, C. P. Hsu, H. C. Tseng, Y. H. Liu and C. W. Chiu, *Chem. Commun.*, 2021, **57**, 13732–13735.

23 J. Koller and R. G. Bergman, *Organometallics*, 2012, **31**, 2530–2533.

24 W. E. Piers, A. J. V. Marwitz and L. G. Mercier, *Inorg. Chem.*, 2011, **50**, 12252–12262.

25 F. S. Tschernuth, T. Thorwart, L. Greb, F. Hanusch and S. Inoue, *Angew. Chemie - Int. Ed.*, 2021, **60**, 25799–25803.

26 R. L. Webster, E. E. Marlier, C. M. Seong, S. A. Brunclik, M. H. Nevins, E. L. Nolan, A. K. Olson, M. Osnaya, A. Reuter, M. E. Swanson, O. G. H. Wood, D. E. Janzen and B. Marciniec, *Hydrosilylation-A Comprehensive Review on Recent Advances*, Royal Society of Chemistry, 2008, vol. 46.

27 K. Yamamoto, T. Hayashi and M. Kumada, *J. Organomet. Chem.*, 1972, **46**, 65–67.

28 K. Yamamoto, T. Hayashi and M. Kumada, *J. Organomet. Chem.*, 1973, **54**, 45–47.

29 L. Sü, J. Hermeke and M. Oestreich, , DOI:10.1021/jacs.6b03443.

30 B. C. Kang, S. H. Shin, J. Yun and D. H. Ryu, *Org. Lett.*, 2017, **19**, 6316–6319.

31 R. Kannan, R. Chambenahalli, S. Kumar, A. Krishna, A. P. Andrews, E. D. Jemmis and A. Venugopal, *Chem. Commun.*, 2019, **55**, 14629–14632.

32 Z. Yang, M. Zhong, X. Ma, S. De, C. Anusha, P. Parameswaran and H. W. Roesky, *Angew. Chemie - Int. Ed.*, 2015, **54**, 10225–10229.

33 D. Vidović, in *Reference Module in Chemistry, Molecular Sciences and Chemical Engineering*, Elsevier, 2021.

34 N. Sarkar, R. K. Sahoo, S. Mukhopadhyay and S. Nembenna, *Eur. J. Inorg. Chem.*, 2022, **2022**, e202101030.

35 Z. Liu, J. H. Q. Lee, R. Ganguly and D. Vidović, *Chem. - A Eur. J.*, 2015, **21**, 11344–11348.

36 Z. Liu and D. Vidović, *J. Org. Chem.*, 2018, **83**, 5295–5300.

37 S. Zhai, C. Forsyth, Z. Liu and D. Vidović, *Organometallics*, 2022, **41**, 2562–2571.

38 D. Dissanayake, A. Draper, Z. Liu, J. J. Haven, C. Forsyth, T. Junkers and D. Vidović, *manuscript under revision.*

39 D. Wei, R. Buhaibeh, Y. Canac and J. B. Sortais, *Molecules*, , DOI:10.3390/molecules26092598.

40 T. Gatzenmeier, M. Turberg, D. Yepes, Y. Xie, F. Neese, G. Bistoni and B. List, *J. Am. Chem. Soc.*, 2018, **140**, 12671–12676.

41 S. Ghosh, S. Das, C. K. De, D. Yepes, F. Neese, G. Bistoni, M. Leutzsch and B. List, *Angew. Chemie - Int. Ed.*, 2020, **59**, 12347–12351.

Chapter 5

5. Future Directions

5.1 Possible future Directions

This study has enabled us to gain a thorough understanding about how steric factors and structural features of our complexes can affect the generation of enantioinduction values with respect to Diels alder reactions involving chalcones. From what we have learnt from Chapter 2, it was understood that increasing the steric bulk at the achiral end would create better enantioinduction. In addition, Chapter 3 finalised that *t*-Bu group with a quaternary C atom led to better enantioinduction as well. By combining these two observations, additional steric hindrance could be placed at the achiral end while a different quaternary C-containing group could be used in order to improve enantioinduction towards the DA reaction(s) in the future.

On the other hand, in Chapter 4 we have understood that our achiral aluminium based system can catalyse hydrosilylation reaction of imines efficiently at elevated temperature. As the obtained results showed better activity of our catalytic system compared to the published analogues, further optimising this reaction is also a possible future direction of this study.

Finally, we have obtained an excellent enantiomeric excess value (above 80%) for one of the complexes towards asymmetric hydrosilylation of acetophenone, which has never been achieved by an aluminium based catalyst. In addition, to the best of our knowledge, this kind of enantioselectivity has never been observed with Et_3SiH before, by any other system therefore, this is also a possible exciting future development arising from our study.

Chapter 6

Appendix

6. Experimental details

6.1 General experimental details

All air and moisture sensitive experiments were performed under an argon or nitrogen atmosphere using standard Schlenk line and glovebox techniques. All glassware involving such reactions were oven dried prior to usage. All the solvents used in air and moisture sensitive experiments were dried, degassed and stored over 4Å molecular sieves prior to use. All other solvents were used as received.

Deuterated solvents were purchased from Cambridge Isotope Laboratory and used either as received or after drying over 4 Å molecular sieves when needed. (*R*)-2- phenylglycinol, (L)-Valinol, 2-bromobenzaldehyde, 2-bromobenzonitrile, N-bromosuccinimide, potassium phosphate tribasic, aniline, 2,6-dimethylaniline, 2,6-diisopropylaniline, 2,4,6-trimethylaniline, $Pd(OAc)_2$, rac-BINAP, aluminum trichloride, silver triflate, sodium tert-butoxide, L-tert-leucine, L-phenylalanine, 3,3-diphenyl-L-alanine, Lithium Aluminium Hydride, and Anhydrous Zinc Chloride, were purchased from commercial sources and used as received.

All solid substrates used for DA (Diels Alder) (except for substituted chalcones) reactions such as trans-chalcone, 4-phenylbut-3-en-2-one, trans-methyl cinnamate etc. were obtained from commercial sources, kept under vacuum overnight and were transferred to the glovebox prior to use. All liquid DA substrates such as, 1,3-cyclohexadiene, methyl acrylate, cyclopent-2-en-1-one etc. were obtained from commercial sources, were dried with 4 Å molecular sieves overnight, distilled under vacuum, and were stored under N_2 environment before use. Cyclopentadiene was freshly cracked with a Vigreux column, and was stored under N_2 at -80°C and was used within a couple weeks of cracking.

2,6-bis(benzhydryl)-4-methyl-aniline, 2,6-bis(diphenylmethyl)-4-tertbutylaniline[1] and substituted chalcones[2] were synthesised using published methods and were dried under vacuum

at ~60-80 ℃ overnight prior to use. Due to the unavailability relevant chiral amino alcohols, L-tert-leucinol, L-phenylalaninol, 3,3-diphenyl-L-alaninol, were obtained by reducing the subsequent chiral amino acids, L-tert-leucine, L-phenylalanine, 3,3-diphenyl-L-alanine, respectively using $LiAlH_4$ following a simple procedure published.[3]

All liquid substrates used for hydrosilylation reactions such as, acetophenone, triethysilane, cyclohexanone etc. were purchased from commercial sources, were dried with 4 Å molecular sieves overnight, distilled under vacuum, and stored under N_2 prior to use. All solid substrates used for hydrosilylation reactions such as benzophenone, 9-fluorenone, 4-methoxyacetophenone etc. were purchased from commercial sources and were kept under vacuum overnight before transferring to the glove box for use.

Thin-layer chromatography (TLC) was performed on silica gel 60 F254 aluminum sheets. Column chromatography was performed on silica gel LC60A (40−63μm) using the indicated solvents.

Multinuclear NMR spectra were recorded at 298 K, unless otherwise stated, on a Bruker Avance III nanobay or a Bruker Avance III NMR spectrometer equipped with a 9.4 T magnet and 5 mm BBFO probe, operating at 400.2 MHz (^{1}H), 376.6 MHz (^{19}F), 104.3 MHz (^{27}Al) and 100.6 MHz (^{13}C) (BACS400 configuration). Chemical shifts (δ) are reported in ppm and were referenced to the residual solvent resonances for ^{1}H and ^{13}C NMR spectra.

Single Crystal X-ray diffraction was carried out on a Rigaku Synergy S diffractometer, fitted with a HyPix6000 hybrid photon counting detector. Collected data was processed using the proprietary software CrysAlisPro (Rigaku OD, Yarnton, UK, 2020).

Enantiomeric excesses were determined by analytical high-performance liquid chromatography (HPLC) analysis on an Agilent Technologies 1200 Infinity instrument with a chiral stationary phase using a Daicel Chiralcel OD-H or a Daicel Chiralcel OJ column.

High resolution mass spectrometry (HR-MS) was carried out at the Monash Analytical Platform, Australia (School of Chemistry, Monash University). Test compound/s were infused directly into the spectrometer (Agilent 6220 TOF MS system (Santa Clara, CA, USA) with a multimode ESI/APCI source) via a kdScientific infusion pump at a static flow rate of 650 µL/h. The spectrometer was operated in positive or negative mode using the following conditions: nebulizer pressure 35 psi, gas flow-rate 8 L/min, gas temperature 300°C, capillary voltage 2500/-2500 V, fragmentor 150 and skimmer 65 V. Instrument was operated in the extended dynamic range mode with data collected in m/z range 100–3200. It should be mentioned that triflate complexes (in solution) could not be identified by HRMS probably owing to their enhanced instability, as only m/z signals for ligand fragments were observed.

Gas liquid chromatography (GLC) was performed on an Agilent Technologies 7820 gas chromatograph equipped with a HP-5 capillary column using N_2 carrier gas, split 20:1 temperature program: start temperature 40°C, heating rate 10°C min^{-1}, end temperature 260°C held for 10 min.

Elemental analysis (EA) was conducted using a Perkin Elmer 2400 Series II CHNS/O Analyzer. The detector was calibrated using Acetanilide on the day of use. Unfortunately, due to the high sensitivity of the materials, only a few solid-state samples were suitable for this analysis. [4]

Optical rotation measurements were recorded on a POLAAR 2001 polarimeter. Solutions were prepared as specified. Rotation measurements were recorded at the sodium-D line (589 nm) at room temperature using a 1 dm cell. The specific optical rotation was calculated using Equation; $[\alpha]D = (100 \times \alpha) / (l \times c)$ where α is the observed optical rotation (°), l is the length of tube (dm), and *c* is the concentration (in g of solute per 100 mL of solution).

6.2 Synthesis of Ligands

General Procedure (GP) Synthesis of **2H, 3aH-3cH** have been previously reported and our data matched these reports.[5] Same method was followed for the synthesis of **3dH-6bH**. Typically, A mixture of 1: 1.5 equivalents of 2-bromobenzaldehyde and respective amino alcohol were stirred in toluene for 24 h at room temperature in the presence of powdered 4 Å molecular sieves. Next, 3 equiv. of potassium phosphate tribasic was added into the mixture and stirred for 5 minutes followed by addition of 1 equiv. of N- bromosuccinimide. The mixture was continued to stir until completion of reaction monitored by TLC and ^{1}HNMR. The crude reaction mixture was filtered and washed with saturated sodium bicarbonate and distilled water. The organic fraction was separated, concentrated through rotavapor and purified by column chromatography.

For synthesis of **5aH-6bH,** A mixture of 1eq. of 2-bromobenzonitrile, 1eq. of respective amino alcohol, L-phenylalaninol or 3,3-diphenyl-L-alaninol, and 0.05 eq. of anhydrous $ZnCl_2$ in chlorobenzene was refluxed at 130 ℃ for 72 h to give a colorless solution. The progress of the reaction was monitored by analysing small aliquots using TLC and 1H NMR spectroscopy. After removal of the solvent in vacuo, the residue was purified by column chromatography on silica gel with hexane and EtOAc.

Buchwald Hartwig coupling reaction. 1 equiv. of the product synthesised either way was then refluxed for 48 h with 1.2 equiv. of aromatic amine in the presence of with 10 mol% $Pd(OAc)_2$, 10 mol% *rac*-BINAP, and 1.4 equiv. of sodium tert-butoxide in dry degassed toluene under N_2. The product obtained was flittered, concentrated and purified by column chromatography to afford yellow oils or solids in yields of ~20-60%. Multinuclear NMR characterisation and single crystal X-ray data (of **2H**) was in accordance with reported values.[5]

3dH. Synthesised according to the general procedure using aromatic aniline, 2,4,6-trimethylaniline afforded an orange oil in 37% yield. ^{1}HNMR (400 MHz, $CDCl_3$): δ = 0.93 (d, 3H, (C*H*$_3$)$_2$CH, $^{3}J_{HH}$ = 6.7 Hz), 0.98 (d, 3H, (C*H*$_3$)$_2$CH, $^{3}J_{HH}$ = 6.7 Hz), 1.79 [m, 1H, (CH$_3$)$_2$C*H*], 2.15 (s, 6H, 2xArC*H*$_3$), 2.30 [s, 3H, ArC*H*$_3$], 4.03 [m, 1H, NC*H*(R)CH$_2$O], 4.16 [m, 1H, NCH(R)C*H*$_2$O], 4.30 [m, 1H, NC*H*(R)CH$_2$O], 6.22 (m, 1H, ArH), 6.60 (m, 1H, ArH), 6.93 (m, 2H, ArH), 7.11 (m, 1H, ArH), 7.76 (m, 1H, ArH), 9.88 (s, 1H, ArN*H*). ^{13}CNMR (100 MHz, $CDCl_3$): δ = 17.2 ([*C*H$_3$)$_2$CH]), 17.7 ([*C*H$_3$)$_2$CH]), 19.7 ([*C*H$_3$)$_2$*C*H]), 21.9 (Ar*C*H$_3$), 30.8 (Ar*C*H$_3$), 32.2 (Ar*C*H$_3$), 67.3 [NCH(R)*C*H$_2$O], 71.7 [N*C*H(R)CH$_2$O], 107.4, 110.6, 113.9, 128.1, 128.6, 129.8, 131.1, 134.4, 134.5, 135.2, 146.9 (CH$_{arom}$), 162.8 (C=N). HRMS (ESI) calculated for $C_{21}H_{26}N_2O$ $[M+H]^+$: 323.2118, found 323.2130.

3eH. Synthesised according to the general procedure using aromatic aniline, 2,6-bis(diphenylmethyl)-4-methyl-aniline afforded a white solid in 23% yield, which was stored under inert conditions until further use. ^{1}HNMR (400 MHz, $CDCl_3$) at 55°C : δ = 0.52 (d, 3H, (C*H*$_3$)$_2$CH, $^{3}J_{HH}$ = 6.3 Hz), 0.63 (d, 3H, (C*H*$_3$)$_2$CH, $^{3}J_{HH}$ = 6.6), 0.97 [m, 1H, (CH$_3$)$_2$C*H*], 2.18 [s, 3H, ArC*H*$_3$], 3.63 [m, 1H, NC*H*(R)CH$_2$O], 3.81 [m, 1H, NCH(R)C*H*$_2$O], 4.17 [m, 1H, NCH(R)C*H*$_2$O], 5.55 [s, 1H, C*H*(Ph)$_2$], 5.70 [s, 1H, C*H*(Ph)$_2$], 6.29 (m, 1H, ArH), 6.58 (m, 1H, ArH), 6.71 (m, 1H, ArH), 6.79 (m, 1H, ArH), 6.90-6.97 (m, 8H, ArH), 7.02 (m, 1H, ArH), 7.07-7.15 (m, 12H, ArH), 9.37 (s, 1H, ArN*H*). ^{13}CNMR (100 MHz, $CDCl_3$): δ = 18.8 ([*C*H$_3$)$_2$CH]), 21.8 (Ar*C*H$_3$), 33.0 ([CH$_3$)$_2$*C*H]), 51.7, 52.2 (Ar(Ph)$_2$*C*), 69.1 [NCH(R)*C*H$_2$O], 72.5 [N*C*H(R)CH$_2$O], 111.6-129.8, 143.9, 148.5 (CH$_{arom}$), 163.3 (C=N). HRMS (ESI) calculated for $C_{45}H_{43}N_2O$ $[M+H]^+$: 627.3375, found 627.3365. CHN elemental analysis calculated: C, 86.22; H, 6.75; N, 4.47. found: C, 85.16; H, 6.63; N, 4.26.

Crystallographic data for **3eH**: $C_{91}H_{85}Cl_3N_4O_2$, Fw 1372.97, Monoclinic, I2, a = 25.8439(2), b = 10.5505(1), c = 28.3697(2) Å, α = γ = 90 °, β = 101.6780(10), V = 7575.33(11) Å^3, Z = 4, ρ_c = 1.204 g/m^3, *F(000)* = 2904, θ range 4.223 to 77.497 °, 61556 reflections collected, 15643

independent reflections (R_{int} = 0.0337), which were used in all calculations; R1 = 0.0513, wR2 = 0.1285 for I>2σ(I) and wR1 = 0.0529, wR2 = 0.1295 for all unique reflections; maximum and minimum residual electron densities 0.820 and – 0.422 eÅ^3, Flack parameter 0.045(10).

3fH. Synthesised according to the general procedure using aromatic aniline, 2,6-2,6-bis(diphenylmethyl)-4-*tert*-butylaniline afforded a white solid in 18% yield, which was stored under inert conditions until further use. ^{1}HNMR (400 MHz, $CDCl_3$) at 55°C : δ = 0.48 (d, 3H, (C*H* $_3$)$_2$CH, $^3J_{HH}$ = 6.72 Hz), 0.62 (d, 3H, (C*H* $_3$)$_2$CH, $^3J_{HH}$ = 6.24 Hz), 1.09 [s, 9H, ArC*H* $_3$], 1.31 [m, 1H, (C*H* $_3$)$_2$C*H*], 3.58 [m, 1H, NC*H*(R)C*H*$_2$O], 3.81 [m, 1H, NC*H*(R)C*H*$_2$O], 4.19 [m, 1H, NC*H*(R)CH$_2$O], 5.56 [s, 1H, C*H*(Ph)$_2$], 5.69 [s, 1H, C*H*(Ph)$_2$], 6.34 (m, 1H, ArH), 6.91-6.98 (m, 10H, ArH), 7.06-7.19 (m, 13H, ArH), 7.67 (m, 1H, ArH), 9.53 (s, 1H, ArN*H*). ^{13}CNMR (100 MHz, $CDCl_3$): δ = 13.2 ([*C*H$_3$)$_2$CH]), 18.1 ([*C*H$_3$)$_2$CH]), 28.7 ([*C*H$_3$)$_2$*C*H]), 30.1 (Ar*C*H$_3$), 33.5 (Ar*C*H$_3$), 50.6 (Ar*C*H$_3$), 55.1 [NCH(R)*C*H$_2$O], 57.7 [N*C*H(R)CH$_2$O], 103.1-154.4 (CH$_{arom}$), 170.7 (C=N). HRMS (ESI) calculated for C$_{48}$H$_{49}$N$_2$O [M+H] $^+$: 669.3845, found 669.38462. CHN elemental analysis calculated C, 86.19; H, 7.23; N, 4.19. found: C, 81.62; H, 7.26; N, 2.52.

Crystallographic data for **3fH**: C$_{48}$H$_{48}$N$_2$O, Fw 668.88, Triclinic, P1, a = 10.4019(3), b = 13.7970(3), c = 15.2529(4) Å, α = 66.674(2), β = 77.295(2), γ = 77.259(2) °, V = 1939.00(9) Å^3, Z = 2, ρ_c = 1.146 g/m^3, *F(000)* = 716, θ range 7.056 to 155.478 °, 26609 reflections collected, 10453 independent reflections (R_{int} = 0.0568), which were used in all calculations; R1 = 0.0580, wR2 = 0.1528 for I>2σ(I) and R1 = 0.0654, wR2 = 0.1656 for all unique reflections; maximum and minimum residual electron densities 0.32 and – 0.26 eÅ^3, Flack parameter 0.0(1).

4aH. Synthesised according to the general procedure using aromatic aniline, 2,6-diisopropylaniline afforded a yellow solid in 55% yield. ^{1}HNMR (400 MHz, $CDCl_3$): δ = 0.92

(s, 9H, (C*H*$_3$)$_3$C), 1.18-1.15 (m, 12H, ArC*H*$_3$), 3.12 [m, 2H, Ar(CH$_3$)$_2$C*H*], 4.15 [m, 2H, NCH(R)C*H*$_2$O], 4.29 [m, 1H, NC*H*(R)CH$_2$O], 6.18 (m, 1H, ArH), 6.59 (m, 1H, ArH), 7.10 (m, 1H, ArH), 7.23 (m, 2H, ArH), 7.31 (m, 1H, ArH), 7.76 (m, 1H, ArH), 9.96 (s, 1H, ArN*H*). ^{13}CNMR (100 MHz, CDCl$_3$): δ = 22.9 ([*C*H$_3$)$_3$CH]), 24.8 ([CH$_3$)$_3$*C*H]), 24.9 (Ar*C*H$_3$), 25.9 (Ar*C*H$_3$), 28.4 (Ar*C*H(CH$_3$)$_2$), 32.9 (Ar*C*H(CH$_3$)$_2$), 67.0 [NCH(R)*C*H$_2$O], 76.4 [N*C*H(R)CH$_2$O], 108.8, 111.8, 114.8, 123.7, 127.2, 129.5, 132.1, 135.2, 147.7, 149.3 (CH$_{arom}$), 163.9 (C=N). HRMS (ESI) calculated for $C_{25}H_{34}N_2O$ $[M+H]^+$: 379.2744, found 379.2732. CHN elemental analysis calculated: C, 79.32; H, 9.05; N, 7.4. found: C, 79.44; H, 9.39; N, 7.4.

4bH. Synthesised according to the general procedure using aromatic aniline, 2,6-bis(diphenylmethyl)-4-methylaniline afforded a white solid in 43% yield, which was stored under inert conditions until further use. ^{1}HNMR (400 MHz, CDCl$_3$): δ = 0.49 (s, 9H, (C*H* $_3$)$_3$CH), 2.18 (s, 3H, ArC*H*$_3$), 3.58 [m, 1H, NC*H*(R)C*H*$_2$O], 3.93 [m, 1H, NC*H*(R)C*H*$_2$O], 4.11 [m, 1H, NC*H*(R)CH$_2$O], 5.53 [s, 1H, C*H*(Ph)$_2$], 5.72 [s, 1H, C*H*(Ph)$_2$], 6.36 (m, 1H, ArH), 6.61 (m, 1H, ArH), 6.68 (m, 1H, ArH), 6.78 (m, 1H, ArH), 6.91 (m, 8H, ArH), 7.15 (m, 13H, ArH), 7.67 (m, 1H, ArH), 9.61 (s, 1H, ArN*H*). ^{13}CNMR (100 MHz, CDCl$_3$): δ = 21.7 ([CH$_3$)$_2$*C*H]), 25.7 ([*C*H$_3$)$_2$CH]), 33.3 (Ar*C*H$_3$), 51.4 (Ph$_2$*C*H), 52.0 (Ph$_2$*C*H), 66.8 [NCH(R)*C*H$_2$O], 75.9 [N*C*H(R)CH$_2$O], 111.6-148.7 (CH$_{arom}$), 162.9 (C=N).

5aH. Synthesised according to the general procedure using aromatic aniline, 2,6-diisopropylaniline afforded a white solid in 58% yield. ^{1}HNMR (400 MHz, CDCl$_3$): δ = 1.12 (m, 9H, ArC*H*$_3$), 1.19 (m, 3H, ArC*H*$_3$), 0.97 [m, 1H, (ArCH$_3$)$_2$C*H*], 3.12 [m, 3H, [(ArCH$_3$)$_2$C*H*], 2x PhC*H*$_2$], 4.07 [m, 1H, NC*H*(R)CH$_2$O], 4.31 [m, 1H, NCH(R)C*H*$_2$O], 4.65 [m, 1H, NCH(R)C*H*$_2$O], 6.20 (m, 1H, ArH), 6.59 (m, 1H, ArH), 7.10 (m, 1H, ArH), 7.29 (m, 8H, ArH), 7.74 (m, 1H, ArH), 9.84 (s, 1H, ArN*H*). ^{13}CNMR (100 MHz, CDCl$_3$): δ = 22.9 (2xAr*C*H$_3$), 24.9 (2xAr*C*H$_3$), 28.8 ([ArCH$_3$)$_2$*C*H]), 32.2 ([ArCH$_3$)$_2$*C*H]), 42.2 (C*H*Ph), 68.1

[NCH(R)*C*H$_2$O], 70.1 [N*C*H(R)CH$_2$O], 108.2-149.5 (CH$_{arom}$), 164.4 (C=N). HRMS (ESI) calculated for $C_{28}H_{32}N_2O$ $[M+H]^+$: 413.2587, found 413.2577.

Crystallographic data for **5aH**: $C_{28}H_{32}N_2O$, Fw 412.55, trigonal, $P3_121$, a = 10.56220 (10), 10.56220 (10), c = 37.6815 (3), Å, α = β = 90 °, γ = 120, V = 3640.55 (7) Å^3, Z = 6, ρ_c = 1.129 g/m^3, *F(000)* = 1332, θ range 7.038 to 159.536˚, 50580 reflections collected, 5263 independent reflections (R_{int} = 0.0338), which were used in all calculations; R1 = 0.0340, wR2 = 0.0893 for I>2σ(I) and R1 = 0.0347, wR2 = 0.0899 for all unique reflections; maximum and minimum residual electron densities 0.28 and – 0.20 eÅ^3, Flack parameter 0.00(6).

5bH. Synthesised according to the general procedure using aromatic aniline, 2,6-bis(diphenylmethyl)-4-methyl-aniline afforded a brown oil in 37% yield, which was stored under inert conditions until further use. ^{1}HNMR (400 MHz, $CDCl_3$) 55°C: δ = 2.11 (s, 3H, ArC*H*$_3$), 2.52 (m, 1H, PhC*H*$_2$), 3.74 [m, 1H, NC*H*(R)CH$_2$O], 4.03 [m, 2H, NCH(R)C*H*$_2$O], 5.38 (m, 1H, PhC*H*$_2$), 5.50 [s, 1H, C*H*(Ph)$_2$], 5.60 [s, 1H, C*H*(Ph)$_2$], 6.22 (m, 1H, ArH), 6.33 (m, 1H, ArH), 6.49 (m, 1H, ArH), 6.64 (m, 2H, ArH), 6.89 (m, 11H, ArH), 7.01 (m, 6H, ArH), 7.11 (m, 3H, ArH), 7.18 (m, 6H, ArH), 7.58 (m, 1H, ArH), 9.27 (s, 1H, ArN*H*). ^{13}CNMR (100 MHz, $CDCl_3$): δ = 21.9 (Ar*C*H$_3$), 41.9 (Ph*C*H$_2$), 52.2 (Ar(Ph)$_2$*C*), 67.6 [NCH(R)*C*H$_2$O], 70.5 [N*C*H(R)CH$_2$O], 108.4-148.4 (CH$_{arom}$), 163.8 (C=N).

6aH. Synthesised according to the general procedure using aromatic aniline, 2,6-diisopropylaniline afforded a white solid in 60% yield. ^{1}HNMR (400 MHz, $CDCl_3$): δ = 0.98 (m, 6H, ArC*H*$_3$), 1.08 (m, 6H, ArC*H*$_3$), 2.98 [m, 2H, (ArCH$_3$)$_2$C*H*], 4.10 [m, 2H, NC*H*(R)CH$_2$O], 4.44 [m, 1H, NCH(R)C*H*$_2$O], 5.20 [m, 1H, Ph$_2$C*H*], 6.12 (m, 1H, ArH), 6.57 (m, 1H, ArH), 7.12 (m, 4H, ArH), 7.19 (m, 3H, ArH), 7.31 (m, 7H, ArH), 7.74 (m, 7H, ArH), 9.62 (s, 1H, ArN*H*). ^{13}CNMR (100 MHz, $CDCl_3$): δ = 22.7 (Ar*C*H$_3$), 24.7 ([ArCH$_3$)$_2$*C*H]), 28.4 (C*H*Ph), 57.2 [NCH(R)*C*H$_2$O], 70.0 [N*C*H(R)CH$_2$O], 112.2-149.7 (CH$_{arom}$), 164.8 (C=N).

Crystallographic data for **7aH**: $C_{68}H_{72}N_4O_2$, Fw 977.29, monoclinic, $P2_1$, a = 15.9991 (2), 10.05330 (10), c = 19.1215 (2), Å, α = γ = 90 °, β = 112.015(2), V = 2851.32 (7) $Å^3$, Z = 2, ρ_c = 1.138 g/m^3, *F(000)* = 1048.0, θ range 9.096 to 160.014˚, 59697 reflections collected, 12188 independent reflections (R_{int} = 0.0690), which were used in all calculations; R1 = 0.0498, wR2 = 0.1340 for I>2σ(I) and R1 = 0.0529, wR2 = 0.1368 for all unique reflections; maximum and minimum residual electron densities 0.46 and – 0.29 e$Å^3$, Flack parameter – 0.07(10).

6bH. Synthesised according to the general procedure using aromatic aniline, 2,6-bis(diphenylmethyl)-4-methyl-aniline afforded a yellow solid in 50% yield, which was stored under inert conditions until further use. ^{1}HNMR (400 MHz, $CDCl_3$): δ = 2.21 (s, 3H, ArC*H*$_3$), 3.82 [d, 1H, Ph_2C*H*], 3.90 [t, 1H, NCH(R)C*H*$_2$O], 4.29 [t, 1H, NCH(R)C*H*$_2$O], 4.79 [q, NC*H*(R)CH_2O], 5.49 (s, 1H, $(ArPh_2)_2$C*H*), 5.67 [s, 1H, $(ArPh_2)_2$C*H*], 6.48 (m, 1H, ArH), 6.70 (s, 1H, ArH), 6.79-6.85 (m, 2H, ArH), 6.85-6.90 (m, 6H, ArH), 6.90-7.05 (m, 7H, ArH), 7.05-7.16 (m, 12H, ArH), 7.16-7.25 (m, 6H, ArH), 7.59 (m, 1H, ArH), 9.52 (s, 1H, ArN*H*). ^{13}CNMR (100 MHz, $CDCl_3$): δ = 21.7 (Ar*C*H_3), 51.6, 52.1 ([$ArPh_2$*C*H]), 56.6 (C*H*Ph_2), 69.7 [NCH(R)*C*H_2O], 70.2 [N*C*H(R)CH_2O], 108.1-148.4 (*C*H_{arom}), 164.1 (C=N).

6.3 Synthesis of Aluminum dichloro complexes.

General procedure 1.0 equiv. of appropriate ligand **2H, 3aH-6bH** was dissolved in 20 mL of toluene, cooled down to -78 ˚C and 1.05 eq. of ^{n}BuLi (2.5 M in hexane) was added in a dropwise manner. The mixture was stirred for 1 h. After warming up to room temperature, 1.05 equiv. of $AlCl_3$ was added and the entire reaction mixture was left to stir over night. Next, the solution was filtered and the solvent was evaporated under reduced pressure. The residue was washed using cold hexane, and dried in vacuo overnight.

2AlCl$_2$. 0.26 g of **2H** (0.75 mmol), 0.32 mL of ^{n}BuLi (0.79 mmol) and 0.11 g of $AlCl_3$ (0.79 mmol) afforded 0.21 g of product as a dark yellow solid (yield 62%). ^{1}HNMR (400 MHz,

$CDCl_3$): δ = 2.05 (s, 3H, Ar*C*H_3), 2.12 (s, 3H, Ar*C*H_3), 4.67 (m, 1H, NCH(R)C*H*$_2$O), 5.05 (m, 1H, NCH(R)C*H*$_2$O), 5.58 (m, 1H, NC*H*(R)CH_2O), 6.15 (m, 1H, ArH), 6.63 (m, 1H, ArH), 7.02-7.05 (m, 4H, ArH), 7.19 (m, 2H, ArH), 7.35 (m, 3H, ArH), δ 7.84 (m, 1H, ArH). ^{13}CNMR (100 MHz, $CDCl_3$): δ = 18.8 (MePh), 66.1 (NCH(R)*C*H_2O), 76.0 (N*C*H(R)CH_2O), 116.3, 126.6, 127.9, 128.4, 129.1, 129.3, 129.7, 131.1, 136.9, 137.1, 137.2, 137.3, 156.5 (CH_{arom}), 171.8 (C=N). ^{27}AlNMR (104 Hz, $CDCl_3$): δ 104.0 (s). HRMS (ESI) calculated for $C_{23}H_{21}Al^{35}Cl_2N_2O$ $[M]^+$: 438.0841, found 437.1446

Crystallographic data for **2AlCl$_2$**: $C_{23}H_{21}AlCl_2N_2$ O, Fw 439.3, Monoclinic, I2/a, a = 16.0600 (2), b = 15.5021 (1), c = 18.4978 (2) Å, α = γ = 90 °, β = 112.814 (10), V = 4245.0 (11) Å^3, Z = 8, ρ_c = 1.375 g/m^3, *F(000)* = 1824, θ range 3.392 to 26.021 °, 21472 reflections collected, 4172 independent reflections (R_{int} = 0.0992), which were used in all calculations; R1 = 0.0688, wR2 = 0.1394 for I>2σ(I) and R1 = 0.1066, wR2 = 0.1549 for all unique reflections; maximum and minimum residual electron densities 0.460 and – 0.420 eÅ^3, Flack parameter – 3.5(10).

3aAlCl$_2$. 0.48 g of **3aH** (1.54 mmol), 0.62 mL of ^{n}BuLi (1.63 mmol) and 0.22 g of $AlCl_3$ (1.63 mmol) afforded 0.39 g of product as a dark yellow solid (yield 63%). ^{1}HNMR (400 MHz, $CDCl_3$): δ = 0.95 (d, 3H, CH(*C*H_3)$_2$, $^3J_{HH}$ = 6.85 Hz), 1.01 (d, 3H, CH(*C*H_3)$_2$, $^3J_{HH}$ = 7.09 Hz), 2.18 (s, 3H, ArMe), 2.20 (s, 3H, ArMe), 2.72 (m, 1H, $CHMe_2$), 4.59-4.73 (m, 3H, NCH(R)CH_2O), 6.22 (m, 1H, ArH), 6.66 (m, 1H, ArH), 7.14 (m, 2H, ArH), 7.24 (m, 2H, ArH), δ 7.82 (m, 1H, ArH). ^{13}CNMR (100 MHz, $CDCl_3$): δ = 13.8 ($CHMe_2$), 18.6 ($ArCH_3$), 19.1 ($ArCH_3$), 29.5 ($CHMe_2$), 67.1 (NCH(R)CH_2O), 68.5 (NCH(R)CH_2O), 104.3 171.7, 116.1, 116.2, 126.6, 128.2, 129.1, 130.9, 136.8, 136.9, 137.2, 139.4, 155.1 (CH_{arom}), 171.7 (C=N). ^{27}AlNMR (104 Hz, $CDCl_3$): δ 104.3 (s). $[\alpha]_D$ = – 46.0 (*c* = 1.0 g/100 mL, $CHCl_3$)

3bAlCl$_2$. 1.25 g of **3bH** (4.4 mmol), 1.86 mL of ^{n}BuLi (4.6 mmol) and 0.62 g of $AlCl_3$ (4.6 mmol) afforded 1.20 g of product as a dark yellow solid (yield 72 %). ^{1}HNMR (400 MHz,

$CDCl_3$): δ = 0.96 (d, 3H, (C*H* $_3$)$_2$CH, $^3J_{HH}$ = 6.72 Hz), 1.01 (d, 3H, $^3J_{HH}$ = 6.85 Hz), 2.66 [m, 1H, (C*H* $_3$)$_2$C*H*], 4.65 [m, 3H, NC*H*(R)C*H*$_2$O], 6.51 (m, 1H, ArH), 6.65 (m, 1H, ArH), 7.22-7.30 (m, 4H, ArH), 7.42-7.46 (m, 4 H, ArH), 7.79 (m, 1H, ArH). ^{13}CNMR (100 MHz, $CDCl_3$): δ = 14.0 (CH*C*H$_3$), 19.2, (CH*C*H$_3$), 29.7 (*C*HMe$_2$), 67.3 (NCH(R)CH$_2$O), 68.6 (NCH(R)CH$_2$O), 104.6, 116.1, 117.2, 126.2, 128.2, 128.8 130.1, 130.7, 136.4, 143.1, 156.3 (CH$_{arom}$), 171.8 (C=N). ^{27}AlNMR (104 Hz, $CDCl_3$): *δ* 104.1 (s).

Crystallographic data for **3bAlCl$_2$**: $C_{18}H_{19}AlCl_2N_2O$, Fw 377.23, Triclinic, P1, a = 8.05680(10), b = 9.7524(2), c = 12.7427 Å, α = 73.1720(10), β = 75.0700(10), γ = 72.673(2) °, V = 898.63 (3) Å^3, Z = 2, ρ$_c$ = 1.394 g/m^3, *F(000)* = 392, θ range3.401 to 31.961, 34610 reflections collected, 10032 independent reflections (R$_{int}$ = 0.0307), which were used in all calculations; R1 = 0.0277, wR2 = 0.0631 for I>2σ(I) and R1 = 0.0304, wR2 = 0.0643 for all unique reflections; maximum and minimum residual electron densities 0.242 and – 0.219 eÅ^3, Flack parameter – 0.005(16).

3cAlCl$_2$. 1.45 g of **3cH** (3.9 mmol), 1.66 mL of ^{n}BuLi (4.1 mmol) and 0.55 g of $AlCl_3$ (4.1 mmol) afforded 1.2 g of product as a brown solid (yield 66%). ^{1}HNMR (400 MHz, $CDCl_3$): δ = 0.90 (d, 3H, (C*H* $_3$)$_2$CH $^3J_{HH}$ = 6.85 Hz,), 0.95 (m, 6H, (C*H* $_3$)$_2$CH), 1.01 (d, 3H, (C*H* $_3$)$_2$CH, $^3J_{HH}$ = 7.09 Hz), 1.26 (m, 6H, (C*H* $_3$)$_2$CH), 2.73 [m, 1H, (C*H* $_3$)$_2$C*H*], 3.12 [m, 1H, (C*H* $_3$)$_2$C*H*], 3.24 [m, 1H, NC*H*(R)C*H*$_2$O], 4.68 [m, 3H, NC*H*(R)C*H*$_2$O], 6.27 (d, 1H, J = 8.68 Hz, ArH), 6.66 (m 1H, ArH), 7.25 (m, 4 H, ArH), 7.81 (m, 1H, ArH). ^{13}C NMR (100 MHz, $CDCl_3$): 13.8 (CHMe$_2$), 19.1 (ArCH$_3$), 24.1 (ArCH$_3$), 24.4 (CHMe$_2$), 25.5 (ArCH$_3$), 25.5 (ArCH$_3$), 28.0 (*C*HMe$_2$), 28.1 (*C*HMe$_2$), 29.5 (*C*HMe$_2$), 67.1 (NCH(R)CH$_2$O), 68.6 (NCH(R)CH$_2$O), 104.6, 116.2, 119.0, 124.7, 124.9, 127.4, 130.8, 135.9, 137.0, 147.2, 147.2, 156.7 (CH$_{arom}$), 171.6 (C=N). ^{27}Al NMR (104 Hz, $CDCl_3$): *δ* 104.8 (s). HRMS (ESI) calculated for $C_{24}H_{32}Al^{35}Cl_2N_2O$ $[M]^+$: 461.1702, found 461.1668 CHN elemental analysis calculated C, 62.48; H, 6.77; N, 6.07. found: C, 61.33; H, 7.02; N, 5.67

3dAlCl$_2$. 0.96 g of **3dH** (2.9 mmol), 1.25 mL of ^{n}BuLi (3.0 mmol) and 0.41 g of $AlCl_3$ (3.0 mmol) afforded 1.18 g of product as a yellow solid (yield 95 %). ^{1}HNMR (400 MHz, $CDCl_3$): δ = 0.94 (d, 3H, (C*H* $_3$)$_2$CH, $^3J_{HH}$ = 6.85 Hz), 1.01 (d, 3H, (C*H* $_3$)$_2$CH, $^3J_{HH}$ = 7.07 Hz), 2.14 (s, 6H, 2x ArC*H* $_3$), 2.30 [s, 3H, ArC*H* $_3$], 2.72 [m, 1H, (C*H* $_3$)$_2$C*H*], 4.65 [m, 3H, NC*H*(R)C*H*$_2$O], 6.24 (m, 1H, ArH), 6.65 (m, 1H, ArH), 6.97 (m, 2H, ArH), 7.23 (m, 1H, ArH), 7.80 (m, 1H, ArH), ^{13}CNMR (100 MHz, $CDCl_3$): δ = 13.9 (CH*C*H$_3$), 18.6 (CH*C*H$_3$), 19.1 (CH*C*H$_3$), 21.0, 29.5 (CHMe$_2$-mesityl), 67.2 (NCH(R)CH$_2$O), 68.5 (NCH(R)CH$_2$O), 116.0, 116.2, 129.9, 130.9, 133.6, 136.5, 136.8, 143.1, 143.8, 146.9, 147.9, 155.7 (CH$_{arom}$), 171.7 (C=N). ^{27}Al NMR (104 Hz, $CDCl_3$): *δ* 104.1 (s).

3eAlCl$_2$. 1.3 g of **3eH** (2.0 mmol), 0.87 mL of ^{n}BuLi (2.1 mmol) and 0.29 g of $AlCl_3$ (2.1 mmol) afforded 1.2 g of product as a yellow solid (yield 80 %)**.** ^{1}HNMR (400 MHz, $CDCl_3$) : δ = 0.95 (d, 3H, (C*H* $_3$)$_2$CH, $^3J_{HH}$ = 6.72 Hz), 1.00 (d, 3H, (C*H* $_3$)$_2$CH, $^3J_{HH}$ = 7.09 Hz,), 2.20 [s, 3H, ArC*H* $_3$], 2.68 [m, 1H, (C*H* $_3$)$_2$C*H*], 4.65 [m, 3H, NC*H*(R)C*H*$_2$O], 4.88 [m, 1H, NC*H*(R)C*H*$_2$O], 5.91 (m, 1H, ArH), 6.06 [s, 2H, C*H*(Ph)$_2$], 6.14 (m, 1H, ArH), 6.75-6.79 (m, 2H, ArH), 6.80-6.85 (m, 4H, ArH), 6.87-6.90 (m, 3H, ArH), 6.91-6.95 (m, 3H, ArH), 7.08-7.22 (m, 3H, ArH), 7.45 (m, 1H, ArH). ^{13}CNMR (100 MHz, $CDCl_3$): δ = 14.2 ([*C*H$_3$)$_2$CH]), 19.1 ([*C*H$_3$)$_2$CH]), 21.5 (Ar*C*H$_3$), 29.7 ([*C*H$_3$)$_2$*C*H]), 51.2 ([Ph)$_2$*C*H]), 51.5 ([Ph)$_2$*C*H]), 67.1 [NCH(R)*C*H$_2$O], 68.8 [N*C*H(R)CH$_2$O], 104.5-155.2 (CH$_{arom}$), 171.8 (C=N). ^{27}AlNMR (104 Hz, $CDCl_3$): *δ* = 104.4 (s). HRMS (ESI) calculated for $C_{45}H_{41}Al^{35}Cl^{37}ClN_2O$ $[M+H]^+$: 723.2484, found 723.2367.

Crystallographic data for **3eAlCl$_2$**: $C_{45}H_{41}AlCl_2N_2O$, Fw 723.68, Monoclinic, I2, a = 12.7756(2), b = 9.9253(2), c = 30.1239(5) Å, α = γ = 90 °, β = 98.056(2) °, V = 3782.07(12) Å^3, Z = 4, ρ_c = 1.271 g/m^3, *F(000)* = 1520, θ range3.221 to 32.037, 49969 reflections collected, 11268 independent reflections (R_{int} = 0.0352), which were used in all calculations; R1 = 0.0318, wR2 = 0.0778 for I>2σ(I) and R1 = 0.0360, wR2 = 0.0796 for all unique reflections;

maximum and minimum residual electron densities 0.234 and – 0.218 eÅ^3, Flack parameter – 0.032(14).

3fAlCl$_2$. 0.7 g of **3fH** (1.0 mmol), 0.44 mL of ^{n}BuLi (1.1 mmol) and 0.14 g of AlCl$_3$ (1.1 mmol) afforded 0.65 g of product as a yellow solid (yield 81 %). ^{1}HNMR (400 MHz, CDCl$_3$) : δ = 0.96 (d, 3H, (C*H* $_3$)$_2$CH, $^3J_{HH}$ = 6.60 Hz), 1.00 (d, 3H, (C*H* $_3$)$_2$CH $^3J_{HH}$ = 7.21 Hz), 1.11 [s, 9H, ArC*H* $_3$], 2.69 [m, 1H, (C*H* $_3$)$_2$C*H*], 4.62 [m, 3H, NC*H*(R)C*H*$_2$O], 4.87 [m, 1H, NC*H*(R)C*H*$_2$O], 5.95 [s, 1H, ArH], 6.06 [s, 2H, C*H*(Ph)$_2$], 6.15 (m, 1H, ArH), 6.73-6.86 (m, 4H, ArH), 6.86-6.95 (m, 6H, ArH), 6.98-7.09 (m, 4H, ArH), 7.09-7.15 (m, 4H, ArH), 7.15-7.24 (m, 6H, Ar*H*), 7.44 (m, 1H, ArH). ^{13}CNMR (100 MHz, CDCl$_3$): δ = 13.2 ([*C*H$_3$)$_2$CH]), 18.1 ([*C*H$_3$)$_2$CH]), 28.7 (Ar*C*H$_3$), 30.1 (Ar*C*H$_3$), 33.5 (Ar*C*H$_3$), 50.6 ([Ar*C*H$_3$)$_3$*C*H]), 50.6 ([*C*H$_3$)$_3$*C*H]), 66.1 ([Ph)$_2$*C*H]), 67.7 ([Ph)$_2$*C*H]), 103.1 [NCH(R)*C*H$_2$O], 115.1 [N*C*H(R)CH$_2$O], 119.0-154.4 (CH$_{arom}$), 170.7 (C=N). ^{27}AlNMR (104 Hz, CDCl$_3$): *δ* 104.0 (s). HRMS (ESI) calculated for C$_{48}$H$_{47}$Al^{35}Cl^{37}ClN$_2$O [M+H]$^+$: 765.2954, found 765.2834.

Crystallographic data for **3fAlCl$_2$**: C$_{54}$H$_{51}$AlCl$_2$F$_2$N$_2$O, Fw 879.85, Triclinic, P1, a = 10.05910(10), b = 10.2551(2), c = 12.5367(2) Å, α = 113.677(2), β = 95.1890(10), γ = 102.2070(10) °, V = 1135.18(3) Å^3, Z = 1, ρ$_c$ = 1.287 g/m^3, *F(000)* = 462, θ range 7.852 to 159.894, 45509 reflections collected, 9189 independent reflections (R$_{int}$ = 0.0388), which were used in all calculations; R1 = 0.0299, wR2 = 0.0793 for I>2σ(I) and R1 = 0.0306, wR2 = 0.0799 for all unique reflections; maximum and minimum residual electron densities 0.26 and – 0.24 eÅ^3, Flack parameter – 0.014(5).

4aAlCl$_2$. 1.07 g of **4aH** (2.6 mmol), 1.1 mL of ^{n}BuLi (2.7 mmol) and 0.37 g of AlCl$_3$ (2.7 mmol) afforded 0.69 g of product as a yellow solid (yield 55%). ^{1}HNMR (400 MHz, CDCl$_3$): δ = 0.92 (dd, 2H, ArC*H*$_3$, $^3J_{HH}$ = 6.7 Hz), 0.99 (m, 5H, ArC*H*$_3$, $^3J_{HH}$ = 6.4 Hz), 1.11 (s, 9H, (C*H*$_3$)$_3$C), 1.24 (m, 5H, ArC*H*$_3$, $^3J_{HH}$ = 6.4 Hz), 3.18 [m, 2H, Ar(CH$_3$)$_2$C*H*], 4.43 [m, 1H,

NCH(R)C*H*$_2$O], 4.71 [m, 2H, NC*H*(R)CH$_2$O], 6.29 (m, 1H, ArH), 6.65 (m, 1H, ArH), 7.24 (m, 3H, ArH), 7.32 (m, 1H, ArH), 7.82 (m, 1H, ArH). ^{13}CNMR (100 MHz, $CDCl_3$): δ = 24.2 ([*C*H$_3$)$_3$CH]), 24.2 ([CH$_3$)$_3$*C*H]), 25.2 ([*C*H$_3$)$_3$CH]), 26.3 (Ar*C*H$_3$), 28.0 (Ar*C*H$_3$), 28.3 (Ar*C*H(CH$_3$)$_2$), 34.8 (Ar*C*H(CH$_3$)$_2$), 71.0 [NCH(R)*C*H$_2$O], 72.1 [N*C*H(R)CH$_2$O], 104.9, 116.5, 118.7, 127.1, 128.8, 131.1, 136.3, 137.8, 147.4, 157.0 (CH$_{arom}$), 173.9 (C=N). ^{27}AlNMR (104 Hz, $CDCl_3$): *δ* 104.3. HRMS (ESI) calculated for $C_{25}H_{33}Al^{35}Cl^{37}ClN_2O$ [M+H] $^+$: 475.1858, found 475.1851, CHN elemental analysis calculated: C, 63.16; H, 7.0; N, 5.89. found: C, 61.98; H, 7.34; N, 5.56.

4bAlCl$_2$. 1.20 g of **4bH** (1.9 mmol), 0.78 mL of ^{n}BuLi (2.0 mmol) and 0.26 g of $AlCl_3$ (2.0 mmol) afforded 0.70 g of product as a yellow solid (yield 53%). ^{1}HNMR (400 MHz, $CDCl_3$): δ = 1.08 (s, 9H, (C*H* $_3$)$_3$CH), 2.19 (s, 3H, ArC*H*$_3$), 4.23 [m, 1H, NC*H*(R)C*H*$_2$O], 4.63-4.71 [m, 1H, NC*H*(R)C*H*$_2$O], 5.11 [m, 1H, NC*H*(R)CH$_2$O], 5.87 [s, 1H, C*H*(Ph)$_2$], 6.16 [s, 1H, C*H*(Ph)$_2$], 6.77 (m, 3H, ArH), 6.85-6.99 (m, 10H, ArH), 7.07 (m, 1H, ArH), 7.15 (m, 2H, ArH), 7.22 (m, 5H, ArH), 7.50 (m, 1H, ArH). ^{13}CNMR (100 MHz, $CDCl_3$): δ = 21.9 ([CH$_3$)$_2$*C*H]), 26.5 ([*C*H$_3$)$_2$CH]), 35.1 (Ar*C*H$_3$), 51.4 (Ph$_2$*C*H), 71.4 [NCH(R)*C*H$_2$O], 72.4 [N*C*H(R)CH$_2$O], 105.8.6-155.7 (CH$_{arom}$), 174.4 (C=N). ^{27}AlNMR (104 Hz, $CDCl_3$): *δ* 104.0. HRMS (ESI) calculated for $C_{46}H_{43}Al^{35}Cl_2N_2O$ [M] $^+$: 736.2562, found 736.2550. CHN elemental analysis calculated C, 74.38; H, 6.52; N, 3.62. found: C, 74.89; H, 5.88; N, 3.80.

Crystallographic data for **4bAlCl$_2$**: $C_{46}H_{43}AlCl_2N_2O$, Fw 737.70, monoclinoc, P2$_1$, a = 15.2370 (2), 17.2186 (2), c = 15.4659 (3), Å, α = 90, β = 105.529 °, γ = 90, V = 3909.51 (2) Å^3, Z = 4, ρ_c = 1.253 g/m^3, *F(000)* = 1552, θ range 6.668 to 62.026˚, 80470 reflections collected, 20379 independent reflections (R_{int} = 0.0328), which were used in all calculations; R1 = 0.0325, wR2 = 0.0814 for I>2σ(I) and R1 = 0.0382, wR2 = 0.0834 for all unique reflections; maximum and minimum residual electron densities 0.27 and – 0.27 eÅ^3, Flack parameter – 0.011(16).

5aAlCl$_2$. 0.76 g of **5aH** (1.8 mmol), 0.77 mL of ^{n}BuLi (1.9 mmol) and 0.25 g of $AlCl_3$ (1.9 mmol) afforded 0.51 g of product as a yellow solid (yield 55%). ^{1}HNMR (400 MHz, $CDCl_3$): δ = 0.94 (m, 6H, ArC*H*$_3$), 1.29 (m, 6H, ArC*H*$_3$), 3.02 [m, 1H, (ArCH$_3$)$_2$C*H*], 3.22 [m, 3H, [(ArCH$_3$)$_2$C*H*], 3.74 (m, 1H, PhC*H*$_2$), 4.54 [m, 1H, NC*H*(R)CH$_2$O], 4.62 [m, 1H, NCH(R)C*H*$_2$O], 4.95 [m, 1H, NCH(R)C*H*$_2$O], 6.27 (m, 1H, ArH), 6.63 (m, 1H, ArH), 7.14-7.38 (m, 10H, ArH), 7.75 (m, 1H, ArH). ^{13}CNMR (100 MHz, $CDCl_3$): δ = 24.4 (2xAr*C*H$_3$), 25.9 (2xAr*C*H$_3$), 28.1 ([ArCH$_3$)$_2$*C*H]), 40.4 (*C*H$_2$Ph), 63.2 [NCH(R)*C*H$_2$O], 73.2 [N*C*H(R)CH$_2$O], 104.5-157.0 (CH$_{arom}$), 172.0 (C=N). ^{27}AlNMR (104 Hz, $CDCl_3$): *δ* 104.8. CHN elemental analysis calculated: C, 66.01; H, 6.13; N, 5.50. found: C, 66.44; H, 6.55; N, 5.33.

5bAlCl$_2$. 0.31 g of **5bH** (0.45 mmol), 0.20 mL of ^{n}BuLi (0.48 mmol) and 0.064 g of $AlCl_3$ (0.48 mmol) afforded 0.17 g of product as a yellow solid (yield 50%). ^{1}HNMR (400 MHz, $CDCl_3$) 55°C: δ = 2.15 (s, 3H, ArC*H*$_3$), 2.92 (m, 1H, PhC*H*$_2$), 3.62 (m, 1H, PhC*H*$_2$), 4.50 [m, 2H, NC*H*(R)CH$_2$O], 4.86 [m, 1H, NCH(R)C*H*$_2$O], 5.52 (s, 1H, Ar-PhC*H*$_2$), 5.95 [m, 1H, ArH], 6.04 [s, 1H, Ar-C*H*(Ph)$_2$], 6.11 (m, 1H, ArH), 6.77 (m, 6H, ArH), 6.85 (m, 8H, ArH), 7.00 (m, 7H, ArH), 7.11 (m, 7H, ArH), 7.36 (m, 1H, ArH). ^{13}CNMR (100 MHz, $CDCl_3$): δ = 21.6 (Ar*C*H$_3$), 40.5 (Ph*C*H$_2$), 51.2 (Ar(Ph)$_2$*C*), 63.2 [NCH(R)*C*H$_2$O], 73.5 [N*C*H(R)CH$_2$O], 104.8-144.4 (CH$_{arom}$), 172.3 (C=N). ^{27}AlNMR (104 Hz, $CDCl_3$): *δ* 104.3. HRMS (ESI) calculated for $C_{49}H_{41}Al^{35}Cl_2N_2O$ $[M]^+$: 770.2406, found 770.5136. CHN elemental analysis calculated: C, 76.26; H, 5.36; N, 3.63. found: C, 74.28; H, 6.09; N, 3.03.

6aAlCl$_2$. 0.50 g of **6aH** (1.0 mmol), 0.43 mL of ^{n}BuLi (1.05 mmol) and 1.43 g of $AlCl_3$ (1.05 mmol) afforded 0.35 g of product as a yellow solid (yield 60%). ^{1}HNMR (400 MHz, $CDCl_3$): δ = 1.00 (m, 8H, ArC*H*$_3$), 1.26 (m, 3H, ArC*H*$_3$), 1.42 (m, 1H, ArC*H*$_3$), 2.89-3.39 [m, 2H, (ArCH$_3$)$_2$C*H*], 4.04-4.60 [m, 1H, NC*H*(R)CH$_2$O], 4.80-5.00 [m, 1H, NCH(R)C*H*$_2$O], 5.19-5.54 [m, 1H, NCH(R)C*H*$_2$O], 6.12-6.28 [m, 1H, Ph$_2$C*H*], 6.47-6.64 (m, 1H, ArH), 7.02-7.75

(m, 15H, ArH). ^{13}CNMR (100 MHz, $CDCl_3$): δ = 22.9 (Ar*C*H_3), 23.9 (Ar*C*H_3), 25.0 (Ar*C*H_3), 25.9 (Ar*C*H_3), 27.9 ([ArCH_3)$_2$*C*H]), 31.6 ([ArCH_3)$_2$*C*H]), 51.5 (C*H*Ph), 64.3 [NCH(R)*C*H_2O], 70.5 [N*C*H(R)CH_2O], 104.5-157.2 (CH_{arom}), 172.6 (C=N). ^{27}AlNMR (104 Hz, $CDCl_3$): δ 104.3. HRMS (ESI) calculated for $C_{34}H_{35}Al^{35}Cl^{37}ClN_2O$ $[M+H]^+$: 585.2015, found 585.1971. CHN elemental analysis calculated: C, 69.74; H, 6.03; N, 4.78. found: C, 70.6; H, 6.69; N, 4.80.

6bAlCl$_2$. 0.22 g of **6bH** (0.31 mmol), 0.13 mL of ^{n}BuLi (0.32 mmol) and 0.044 g of $AlCl_3$ (0.32 mmol) afforded 0.10 g of product as a yellow solid (yield 38%). ^{1}HNMR (400 MHz, $CDCl_3$): ^{1}HNMR (400 MHz, $CDCl_3$): δ = 2.23 (s, 3H, ArC*H*$_3$), 4.62 [m, 1H, Ph$_2$C*H*], 4.92 [t, 1H, NCH(R)C*H*$_2$O], 5.03 [m, 1H, NCH(R)C*H*$_2$O], 5.30 (s, 1H, (ArPh$_2$C*H*), 5.69 [m, NC*H*(R)CH_2O], 5.80 [s, 1H, (ArPh$_2$)$_2$C*H*], 6.41 (m, 2H, ArH), 6.73 (m, 2H, ArH), 6.79-6.85 (m, 2H, ArH), 6.94 (m, 7H, ArH), 7.00 (m, 4H, ArH), 7.13 (m, 8H, ArH), 7.19 (m, 2H, ArH), 7.30-7.40 (m, 5H, ArH). ^{13}CNMR (100 MHz, $CDCl_3$): δ = 21.7 (Ar*C*H_3), 31.8 (Ph$_2$C*H*), 51.2, 52.0 (ArPh$_2$*C*H), 64.8 [NCH(R)*C*H_2O], 70.6 [N*C*H(R)CH_2O], 116.1-155.5 (CH_{arom}), 172.7 (C=N). ^{27}AlNMR (104 Hz, $CDCl_3$): δ 104.6.

6.4 Synthesis of Aluminum bistriflate complexes.

General Procedure 1.0 eq. of respective dichloro complex, **3AlCl$_2$** and 2.1eq. of AgOTf were mixed in DCM/ Difluoro benzene and stirred overnight in the absence of light. The reaction mixture was then filtered and concentrated in vacuo to obtain a solid. This sticky solid was washed with dry hexane and dried under reduced pressure to obtain a solid.

3aAl(OTf)$_2$. 1.0 g of **3aAlCl$_2$** (2.4 mmol) and 1.3 g of AgOTf (5.2 mmol) afforded 0.67 g of a brown solid (yield 43%). ^{1}HNMR (400 MHz, $CDCl_3$): δ = 0.86 (d, 3H, CH(CH_3)$_2$, $^3J_{HH}$ = 6.79 Hz), 0.98 (d, 3H, , CH(CH_3)$_2$, $^3J_{HH}$ = 6.97 Hz), 1.97 (s, 3H, ArMe), 2.13 (s, 3H, ArMe), 2.35 (m, 1H, $CHMe_2$), 4.63-4.31 (m, 3H, NCH(R)CH_2O), 6.28 (m, 1H, ArH), 6.76 (m, 1H, ArH),

7.12 (m, 3H, ArH), 7.30 (m, 1H, ArH), 7.86 (m, 1H, ArH). ^{13}CNMR (100 MHz, $CDCl_3$): 12.9 ($CHMe_2$), 16.6 ($ArCH_3$), 17.8 ($ArCH_3$, 29.0 ($CHMe_2$), 30.6 ($CHMe_2$), 65.6 (NCH(R)CH_2O), 68.6 (NCH(R)CH_2O), 103.4, 115.5, 117.0, 126.5, 128.4, 128.6, 130.5, 135.4, 136.2, 137.2, 154.0 (CH_{arom}), 173.1 (C=N). ^{27}AlNMR (104 Hz, $CDCl_3$): δ = – 22.60 (s). ^{19}FNMR (376 Hz, $CDCl_3$, 25°C): δ = – 77.2. [α]D = − 28.0° (c = 0.05 g/mL, $CHCl_3$). HRMS (ESI) calculated for ligand fragment $C_{18}H_{24}N_2O$ (**3aH**+H)$^+$: calc 309.1961, found 309.1944

3bAlOTf$_2$. 1.0 g **3bAlCl$_2$** (2.6 mmol) and 1.4 g of AgOTf (5.5 mmol) afforded 1.27 g of a yellow solid (yield 84%).^{1}HNMR (400 MHz, $CDCl_3$): δ = 0.97 (d, 3H, (C*H* $_3$)$_2$CH, $^3J_{HH}$ = 6.85 Hz), 1.06 (d, 3H, (C*H* $_3$)$_2$CH, $^3J_{HH}$ = 6.85 Hz), 2.42 [m, 1H, (C*H* $_3$)$_2$C*H*], 4.64-4.86 [3 H, m, NC*H*(R)C*H*$_2$O], 6.64 (1 H, m, ArH), 6.82 (m, 1H, ArH), 6.92 (m, 1H, ArH), 7.08 (m, 1 H, ArH), 7.23 (m, 2H, ArH), 7.35 (m, 2H, ArH), 7.48 (m, 1H, ArH), 7.88 (m, 1H, ArH). ^{13}CNMR (100 MHz, $CDCl_3$): δ = 14.0 (CH*C*H$_3$), 19.1 (CH*C*H$_3$), 30.0 (*C*HMe$_2$), 66.9 (NCH(R)CH_2O), 69.4 (NCH(R)CH_2O), 104.6, 117.5, 117.9, 124.9, 127.3, 128.1, 130.5, 131.2, 137.7, 140.4, 147.5, 156.8 (CH_{arom}), 174.2 (C=N). ^{19}FNMR (376 Hz, $CDCl_3$, 25°C): δ – 77.2. ^{27}Al NMR (400 Hz, $CDCl_3$): δ – 22.6 (s). HRMS (ESI) calculated for ligand fragment $C_{18}H_{19}N_2O$ (**3bH**)$^+$: calc 279.1492, found 279.1448

3cAlOTf$_2$. 1.0 g **3cAlCl$_2$** (2.1 mmol) and 1.2 g of AgOTf (4.4 mmol) afforded 1.3 g of a brown solid (yield 87%). ^{1}HNMR (400 MHz, $CDCl_3$): δ = 0.79 (d, 3H, (C*H* $_3$)$_2$CH $^3J_{HH}$ = 6.85 Hz,), 0.90 (d, 3H, (C*H* $_3$)$_2$CH, $^3J_{HH}$ = 6.85 Hz), 1.05 [d, 3H, (C*H* $_3$)$_2$CH, $^3J_{HH}$ = 7.09 Hz], 1.16 [m, 6H, (C*H* $_3$)$_2$CH], 1.24 [m, 3H, (C*H* $_3$)$_2$CH], 2.32 [m, 1H, (C*H* $_3$)$_2$C*H*], 2.70 [m, 1H, (C*H* $_3$)$_2$C*H*], 3.11 [m, 1H, NC*H*(R)C*H*$_2$O], 4.76 [m, 3H, NC*H*(R)C*H*$_2$O], 6.45 (d, 1H, ArH), 6.83 (t, 1H, ArH), 7.21-7.24 (m, 1H, ArH), 7.27-7.31 (m, 1H, ArH), 7.34-7.39 (m, 2H, ArH), 7.93 (d, 1H, ArH). ^{13}CNMR (100 MHz, $CDCl_3$): δ = 14.0 ($CHMe_2$), 18.6 ($ArCH_3$), 22.9 ($ArCH_3$), 23.2 ($CHMe_2$), 24.9 ($ArCH_3$), 25.4 ($ArCH_3$), 27.9 (*C*HMe$_2$), 28.5 (*C*HMe$_2$), 30.7 (*C*HMe$_2$), 66.3 (NCH(R)CH_2O), 70.2 (NCH(R)CH_2O), 104.6, 118.2, 118.9, 124.7, 125.3,

128.1, 131.5, 135.1, 137.5, 145.8, 147.0, 156.5 (CH_{arom}), 174.0 (C=N). ^{19}FNMR (376 Hz, $CDCl_3$, 25°C): δ – 77.0. ^{27}AlNMR (104 Hz, $CDCl_3$): δ – 23.0 (s). HRMS (ESI) calculated for ligand fragment $C_{24}H_{32}N_2O$ **(3cH**+H)$^+$: calc 365.2587, found 365.2594

3dAlOTf$_2$. 1.0 g **3dAlCl$_2$** (2.3 mmol) and 1.2 g of AgOTf (4.8 mmol) afforded 1.20 g of a dark yellow solid (yield 81%). ^{1}HNMR (400 MHz, $CDCl_3$): δ = 0.92 (d, 3H, $^3J_{HH}$ = 6.85 Hz, (C*H* $_3$)$_2$CH), 1.04 (d, 3H, $^3J_{HH}$ = 7.09 Hz, (C*H* $_3$)$_2$CH), 2.00 (s, 3H, ArC*H* $_3$), 2.13 [s, 3H, ArC*H* $_3$], 2.31 [s, 3H, ArC*H* $_3$], 2.43 [m, 1H, (C*H* $_3$)$_2$C*H*], 4.74 [m, 2H, NC*H*(R)C*H*$_2$O], 4.87 [m, 1H, NC*H*(R)C*H*$_2$O], 6.31 (m, 1H, ArH), 6.81 (m, 1H, ArH), 6.99 (m, 3H, ArH), 7.34 (m, 1H, ArH), 7.86 (m, 1H, ArH). ^{13}CNMR (100 MHz, $CDCl_3$): δ = 12.8 (CH*C*H$_3$), 16.6 (CH*C*H$_3$), 17.8 (CH*C*H$_3$), 19.9, 22.3 29.0 (CHMe$_2$-mesityl), 65.6 (NCH(R)CH$_2$O), 68.5 (NCH(R)CH$_2$O), 103.4, 115.5, 116.4, 129.6, 129.2, 130.4, 134.7, 134.9, 137.0, 140.9, 149.2, 154.4 (CH_{arom}), 172.9 (C=N). ^{19}FNMR (376 Hz, $CDCl_3$): δ – 77.1(impurity peaks present*). ^{27}Al NMR (104 Hz, $CDCl_3$): δ – 22.2 (s) (impurity peak present*). HRMS (ESI) calculated for ligand fragment $C_{23}H_{25}N_2O$ **(3dH**-H)$^-$: calc 344.1894, found 344.9762

3eAlOTf$_2$ 1.0 g **3eAlCl$_2$** (1.3 mmol) and 0.74 g of AgOTf (2.9 mmol) afforded 1.10 g of a yellow solid (yield 83%). DCM was replaced by 1,2-difluorobenzene.^{1}HNMR (400 MHz, $CDCl_3$) : δ = 0.91 (m, 3H, (C*H* $_3$)$_2$CH), 1.05 (m, 3H, (C*H* $_3$)$_2$CH), 2.25 [m, 3H, ArC*H* $_3$], 2.29 [m, 1H, (C*H* $_3$)$_2$C*H*], 4.69-4.74 [m, 2H, NC*H*(R)C*H*$_2$O], 4.85 [m, 1H, NC*H*(R)C*H*$_2$O], 5.11-7.69 aromatic protons and C*H*Ph$_2$ were considerably overlapped and not resolved. ^{13}CNMR (100 MHz, $CDCl_3$): δ = 14.3 ([*C*H$_3$)$_2$CH]), 18.9 ([*C*H$_3$)$_2$CH]), 21.6 (Ar*C*H$_3$), 31.4 ([*C*H$_3$)$_2$*C*H]), 51.3 ([Ph)$_2$*C*H]), 52.4 ([Ph)$_2$*C*H]), 66.4 [NCH(R)*C*H$_2$O], 70.5 [N*C*H(R)CH$_2$O], 103.8-155.8 (CH_{arom}), 174.6 (C=N). ^{19}F NMR (400 Hz, $CDCl_3$, 25°C): δ – 76.4. ^{27}AlNMR (104 Hz, $CDCl_3$): not observed. HRMS (ESI) calculated for ligand fragment $C_{45}H_{42}AlN_2O$ **(3eH**-H)-: calc 626.3224, found 625.3192.

3fAlOTf$_2$ 0.6 g **3fAlCl$_2$** (0.82 mmol) and 0.44 g of AgOTf (1.7) mmol) afforded 0.6 g of a yellow solid (yield 73%). DCM was replaced by 1,2-difluorobenzene. ^{1}HNMR (400 MHz, $CDCl_3$): δ = 0.89 (m, 3H, (C*H* $_3$)$_2$CH), 0.94 (m, 3H, (C*H* $_3$)$_2$CH), 1.06 [s, 9H, ArC*H* $_3$], 2.33 [m, 1H, (C*H* $_3$)$_2$C*H*], 4.71 [m, 2H, NC*H*(R)C*H*$_2$O], 4.84 [m, 1H, NC*H*(R)C*H*$_2$O], 4.98 [m, 1H, NC*H*(R)C*H*$_2$O], 5.47 [s, 1H, C*H*(Ph)$_2$], 5.86 [s, 1H, C*H*(Ph)$_2$], 5.99 (m, 1H, ArH), 6.30 [m, 1H, ArH], 6.51 (m, 2H, ArH), 6.79-7.26 (m, 22 H, ArH), 7.61 (d, 1H, ArH). ^{13}CNMR (100 MHz, $CDCl_3$): δ = 15.1 ([*C*H$_3$)$_2$CH]), 16.5 ([*C*H$_3$)$_2$CH]), 29.7 (Ar*C*H$_3$), 33.7 (Ar*C*H$_3$), 34.8 (Ar*C*H$_3$), 51.9 ([Ar*C*H$_3$)$_3$*C*H]), 55.4 ([*C*H$_3$)$_3$*C*H]), 60.2 ([Ph)$_2$*C*H]), 61.8 ([Ph)$_2$*C*H]), 98.7 [NCH(R)*C*H$_2$O], 105.0 [N*C*H(R)CH$_2$O], 125.2-161.3 (CH$_{arom}$), 171.0 (C=N). ^{27}AlNMR (104 Hz, $CDCl_3$): *δ* – 22.8 (s). ^{19}FNMR (400 Hz, $CDCl_3$): *δ* – 75.9. HRMS (ESI) calculated for ligand fragment $C_{48}H_{48}AlN_2O$ (**3fH**)-: calc 668.3772, found 669.3674.

6.5 General procedure for asymmetric Diels Alder reactions.

Catalyst, $NaBAr^{Cl}{}_4$ (1:1 ratio) and dienophile (1 eq.) were measured in to a J. Young NMR tube under an inert atmosphere. The diene (2.1 eq) was dissolved in 1 mL of $CDCl_3$ and was then transferred in to the catalyst mixture. The reaction mixture was left for the relevant time and was concentrated under reduced pressure, purified using flash column chromatography, and analysed using appropriate methods. Analytical and spectroscopic data reported below are in accordance with those reported.[2,6]

Bicyclo[2.2.1]hept-5-ene-2-carboxylic acid methyl ester *(Entry 1, Table 2.4)*. Prepared according to GP from methyl acrylate and cyclopentadiene with a yield of ~ 80%, separated using flash column chromatography using cyclohexane: ethyl acetate (50/1) as eluent. ^{1}H NMR (400 MHz, $CDCl_3$, 25 °C): δ = 1.33−1.44 (m, 3H), 1.91 (m, 1H), 2.23 (m, 1H), 2.93-3.05 (m, 2H), 3.69 (s, 3H), 6.10 (m, 2H). ^{13}C NMR (100 MHz, $CDCl_3$): δ 30.1, 41.6, 42.3, 45.6, 50.1, 50.9, 135.5, 137.9, 175.1. $[\alpha]_D$ + 15 (*c* = 1 g/100 mL, $CHCl_3$).

Phenyl-(3-phenylbicyclo[2.2.1]hept-5-en-2-yl)methanone *(Entry 2, Table 2.4)*. Prepared according to GP from chalcone and cyclopentadiene with ~ 88% yield, separated using flash column chromatography using cyclohexane/ethyl acetate (50/1) as eluent. ^{1}H NMR (400 MHz, $CDCl_3$, 25 °C): δ 1.55 (m, 1H) 1.93 (d, 1H), 3.04 (m, 1H), 3.24 (m, 1H), 3.40 (m, 1H), 3.81 (m, 1H), 5.78 (m, 1H), 6.37 (m, 1H), 7.03-7.08 (m, 1H), 7.12-7.20 (m, 4H), 7.25-7.35 (m, 2H), 7.37-7.45 (m, 1H), 7.81-7.87 (m, 2H). ^{13}C NMR (100 MHz, $CDCl_3$): δ 47.8, 48.0, 48.7, 48.9, 54.6, 125.8, 126.8, 128.5, 128.6, 128.7, 128.9, 132.9, 133.0, 136.7, 139.8, 145.3, 200.0. $[\alpha]_D$ + 53 (*c* = 1 g/100 mL, $CHCl_3$)

1-(3-Phenylbicyclo[2.2.1]hept-5-en-2-yl)ethanone (*Entry 3, Table 2.4*). Prepared according to GP from 4-phenylbut-3-en-2-one and cyclopentadiene with a yield of ~ 90% after flash column chromatography on silica gel using cyclohexane/ethyl acetate (20/1) as eluent. ^{1}H NMR (400 MHz, $CDCl_3$, 25 °C): δ 1.55 (m, 1H), 1.78 (m, 1H), 2.09 (s, 3H), 2.95 (m, 1H), 3.01 (m, 1H), 3.12 (m, 1H), 3.27 (m, 1H), 5.94 (dd, $^{3}J_{HH}$ = 5.7, 2.6 Hz, 1H), 6.36 (dd, $^{3}J_{HH}$ = 5.7, 3.4 Hz, 1H), 7.01−7.17 (m, 2H), 7.19−7.25 (m, 5H). ^{13}C NMR (100 MHz, $CDCl_3$): δ 29.0, 44.4, 46.6, 47.8, 49.7, 60.2, 126.1, 127.7, 128.7, 133.3, 139.8, 143.8, 209.1. $[\alpha]_D$ + 16 (c = 0.5 g/100 mL, $CHCl_3$)

3-phenylbicyclo[2.2.1]hept-5-ene-2-carboxylate (*Entry 4, Table 2.4*). Prepared according to GP from trans methyl cinnamate and cyclopentadiene with a yield of ~ 70% after flash column chromatography on silica gel using cyclohexane/ethyl acetate (20/1) as eluent. ^{1}H NMR (400 MHz, $CDCl_3$, 25 °C) δ 1.59 (m,1H), 1.85 (d, $^{3}J_{HH}$ = 8.4 Hz, 1H), 3.00-3.03 (m, 2H), 3.10 (m, 1H), 3.28 (m, 1H), 3.67 (s, 3H), 6.12 (m, 1H), 6.42 (m, 1H), 7.10-7.38 (m, 5H). ^{13}C NMR (100 MHz, $CDCl_3$) δ 45.5, 46.3, 47.8, 52.0, 52.5, 77.1, 77.3, 126.1, 127.2, 128.4, 134.6, 139.5, 144.8, 175.0. $[\alpha]_D$ + 16 (c = 0.1 g/100 mL, $CHCl_3$). HPLC (Daicel Chiralcel OJ, 20°C, MeOH/H_2O 97/3, flow rate: 1 mL/min, λ = 220 nm): t_R = 15.4 min, t_R = 16.9 min.

Tricyclo[5.2.1.02,7]undec-9-en-3-one (*Entry 5, Table 2.4*). Prepared according to GP from cyclohex-2-en-1-one and cyclopentadiene with a yield of 59% yield after flash column chromatography on silica gel using cyclohexane/ ethyl acetate (20/1) as eluent. ^{1}H NMR (400 MHz, $CDCl_3$, 25 °C): δ 0.77 (m, 1H), 1.32 (m, 1H), 1.44 (m, 1H), 1.68−1.73 (m, 1H), 1.77−1.83 (m, 1H), 1.87−1.95 (m, 2H), 2.29−2.34 (m, 1H), 2.64−2.71 (m, 2H), 2.88 (m, 1H), 3.27 (m, 1H), 6.02 (dd, $^{3}J_{HH}$ = 5.6, 2.9 Hz, 1H), 6.18 (dd, $^{3}J_{HH}$ = 6.1, 3.0 Hz, 1H). ^{13}C NMR (100 MHz, $CDCl_3$): δ 22.2, 28.6, 40.0, 42.6, 44.4, 47.7, 49.4, 60.1, 135.5, 137.8, 216.8. $[\alpha]_D$ + 17 (c = 0.05 g/100 mL, $CHCl_3$).

Tricyclo[5.2.1.02,6]dec-8-en-3-one (*Entry 6, Table 2.4*). Prepared according to GP from cyclopent-2-en-1-one and cyclopentadiene with a yield of 50% yield after flash column chromatography on silica gel using cyclohexane/ ethyl acetate (20/1) as eluent. ^{1}H NMR (400 MHz, $CDCl_3$, 25 °C): δ 1.31 (m, 1H), 1.36−1.46 (m, 2H), 1.82−2.00 (m, 2H), 2.01−2.09 (m, 1H), 2.70− 2.78 (m, 1H), 2.80−2.93 (m, 2H), 3.08 (m, 1H), 6.00 (dd, $^{3}J_{HH}$ = 5.7, 2.8 Hz, 1H), 6.11 (dd, $^{3}J_{HH}$ = 5.7, 2.9 Hz, 1H). ^{13}C NMR (100 MHz, $CDCl_3$): δ 23.1, 39.7, 41.2, 47.5, 47.9, 51.4, 55.5, 133.9, 136.9, 221.5. $[\alpha]_D$ + 15 (c = 0.5 g/100 mL, $CHCl_3$).

Bicyclo[2.2.2]oct-5-ene-2-carboxylic acid methyl ester (*Entry 7, Table 2.4*). Prepared according to GP from methyl acrylate and cyclohexa-1,3-diene with a yield of 65% after flash column chromatography on silica gel using cyclohexane/ethyl acetate (50/1) as eluent. ^{1}H NMR (400 MHz, $CDCl_3$, 25 °C): δ 1.17−1.32 (m, 2H), 1.42−1.55 (m, 2H), 1.56−1.64 (m, 1H), 1.69−1.77 (m, 1H), 2.54−2.66 (m, 2H), 2.90 (m, 1H), 3.61 (s, 3H), 6.12 (m, 1H), 6.30 (m, 1H). ^{13}C NMR (100 MHz, $CDCl_3$): δ 24.5, 25.5, 29.5, 30.1, 32.6, 42.6, 52.1, 132.5, 136.3, 177.1. $[\alpha]_D$ + 15 (c = 1.0 g/100 mL, $CHCl_3$).

3-phenylbicyclo[2.2.2]oct-5-en-2-yl-methanone *(Entry 8, Table 2.4).* Prepared using GP from chalcone and 1,3-cyclohexadiene, white solid obtained with a yield of ~ 70%, separated

using flash column chromatography using cyclohexane: ethyl acetate (50/1) as eluent. ^{1}H NMR (400 MHz, $CDCl_3$, 25 °C): δ = 1.13 (m, 1H) 1.50 (m, 1H), 1.87 (m, 2H), 2.67 (m, 1H), 2.98 (m, 1H), 3.48 (m, 1H), 3.81 (m, 1H), 6.11 (m, 1H), 6.55 (m, 1H), 7.20 (m, 1H), 7.39 (m, 4H), 7.49 (m, 2H), 7.15 (m, 1H), 7.86 (m, 2H). ^{13}CNMR (100 MHz, $CDCl_3$): δ = 18.5, 26.5, 34.6, 36.5, 44.8, 51.0, 126.2, 128.1, 128.5, 128.5, 130.7, 132.7, 136.3, 136.5, 142.9, 200.8. $[\alpha]_D$ + 19 (c = 1.0 g/100 mL, $CHCl_3$). HPLC (Daicel Chiralcel OD-H, 20°C, n-hexane/i-PrOH 98.5/1.5, flow rate: 0.65 mL/min, λ = 254 nm): t_R = 10.0 min, t_R = 12.0 min.

1-(-3-Phenylbicyclo[2.2.2]oct-5-en-2-yl)ethan-1-one (*Entry 9, Table 2.4*). Prepared according to GP from 4-phenylbut-3-en-2-one and cyclohexa-1,3-diene with a yield of 60% after flash column chromatography on silica gel using cyclohexane/ethyl acetate (20/1) as eluent. ^{1}H NMR (400 MHz, $CDCl_3$, 25 °C): δ 1.04 (m, 1H), 1.38−1.48 (m, 1H), 1.65−1.75 (m, 2H), 2.03 (s, 3H), 2.52−2.56 (m, 1H), 2.90−2.93 (m, 1H), 3.02 (m, 1H), 3.00−3.12 (m, 1H), 6.25 (m, 1H), 6.40 (m, 1H), 7.22 (m, 1H), 7.27−7.38 (m, 4H). ^{13}C NMR (100 MHz, $CDCl_3$): δ 18.4, 26.8, 30.0, 31.7, 37.3, 45.8, 56.7, 127.5, 128.2, 128.4, 130.6, 136.2, 145.8, 209.0. $[\alpha]_D$ + 51 (c = 0.5 g/100 mL, $CHCl_3$)

3-phenylbicyclo[2.2.2]oct-5-en-2-yl-(p-tolyl)methanone *(Entry 2, Table 3.3).* Prepared using GP from (E)-3-phenyl-1-(p-tolyl)prop-2-en-1-one and 1,3-cyclohexadiene, yield ~ 70%, separated using flash column chromatography using cyclohexane: ethylacetate (50/1) as eluent. . ^{1}HNMR (400 MHz, $CDCl_3$, 25 °C): δ = 1.12 (m, 1H) 1.47 (m, 1H), 1.86 (m, 2H), 2.44 (s, 3H), 2.67 (m, 1H), 2.96 (m, 1H), 3.47 (m, 1H), 3.77 (m, 1H), 6.11 (m, 1H), 6.55 (m, 1H), 7.18 (m, 3H), 7.29 (m, 2H), 7.65 (m, 1H), 7.77 (m, 1H), 7.95 (m, 1H$^{)}$. ^{13}CNMR (100 MHz, $CDCl_3$): δ = 18.5, 21.6, 23.6, 26.5, 34.8, 43.0, 44.7, 51.0, 122.1, 128.4, 128.7, 129.0, 129.4, 130.4, 135.0, 135.7, 136.5, 143.6, 144.4, 190.1. HPLC (Daicel Chiralcel OD-H, 20°C, n-hexane/i-PrOH 98.5/1.5, flow rate: 0.65 mL/min, λ= 254 nm): t_R= 11.8 min, t_R= 14.2 min.

3-phenylbicyclo[2.2.2]oct-5-en-2-yl-(o-tolyl)methanone *(Entry 4, Table 3.3).* Prepared using GP from (E)-3-phenyl-1-(o-tolyl)prop-2-en-1-one and 1,3-cyclohexadiene, yield ~ 70%, separated using flash column chromatography using cyclohexane: ethyl acetate (50/1) as eluent. ^{1}HNMR (400 MHz, $CDCl_3$, 25 °C): δ = 1.14 (m, 1H) 1.47 (m, 1H), 1.85 (m, 2H), 2.31 (s, 3H) 2.63 (m, 1H), 2.97 (m, 1H), 3.42 (m, 1H), 3.76 (m, 1H), 6.13 (m, 1H), 6.57 (m, 1H), 7.23 (m, 3H), 7.29 (m, 3H), 7.63 (m, 2H). ^{13}CNMR (100 $_3$Hz, $CDCl_3$): δ = 18.6, 21.2, 26.3, 34.4, 36.5, 45.0, 51.3, 125.6, 126.3, 128.2, 128.5, 129.0, 131.0, 133.5, 136.1, 136.5, 138.3, 148.0, 204.4. HPLC (Daicel Chiralcel OD-H, 20°C, n-hexane/i-PrOH 98.5/1.5, flow rate: 0.65 mL/min, λ = 254 nm): t_R = 11.9 min, t_R = 14.9 min.

3-phenylbicyclo[2.2.2]oct-5-en-2-yl-(m-tolyl)methanone *(Entry 3, Table 3.3).* Prepared using GP from (E)-3-phenyl-1-(m-tolyl)prop-2-en-1-one and 1,3-cyclohexadiene, yield ~ 70%, separated using flash column chromatography using cyclohexane: ethyl acetate (50/1) as eluent. ^{1}HNMR (400 MHz, $CDCl_3$, 25 °C): δ = 1.13 (m, 1H) 1.50 (m, 1H), 1.86 (m, 2H), 2.30 (s, 3H) 2.66 (m, 1H), 2.99 (m, 1H), 3.41 (m, 1H), 3.78 (m, 1H), 6.15 (m, 1H), 6.55 (m, 1H), 7.21 (m, 1H), 7.29 (m, 6H), 7.60 (m, 1H), 7.65 (m, 1H). ^{13}CNMR (100 MHz, $CDCl_3$): δ = 18.6, 26.4, 33.4, 36.9, 44.7, 54.9, 55.3, 111.1, 120.7, 125.9, 128.1, 128.2, 129.2, 130.0, 131.2, 132.3, 136.5, 143.3, 157.2, 204.4. HPLC (Daicel Chiralcel OD-H, 20°C, n-hexane/i-PrOH 98.5/1.5, flow rate: 0.65 mL/min, λ = 254 nm): t_R = 10.1 min, t_R = 12.5 min.

2-Methoxyphenyl-3-phenylbicyclo[2.2.2]oct-5-en-2-yl-methanone *(Entry 5, Table 3.3).* Prepared using GP from (E)-1-(2-methoxyphenyl)-3-phenylprop-2-en-1-one and 1,3-cyclohexadiene, yield ~ 70%, separated using flash column chromatography using cyclohexane: ethyl acetate (50/1) as eluent. ^{1}HNMR (400 MHz, $CDCl_3$, 25 °C): δ = 1.05 (m, 1H) 1.41 (m, 1H), 1.75 (m, 2H), 2.60 (s, 1H) 2.96 (m, 1H), 3.40 (m, 1H), 3.70 (m, 3H), 3.90 (m, 1H), 6.11 (m, 1H), 6.53 (m, 1H), 6.82 (1H), 6.95 (1H), 7.18 (m, 1H), 7.28 (m, 4H), 7.36 (m, 1H), 7.41 (m, 1H). ^{13}CNMR (100 MHz, $CDCl_3$): δ = 18.6, 21.3, 26.3, 34.4, 36.5, 45.0,

51.3, 125.6, 126.2, 128.3 (3C), 129.2, 131.0, 133.4, 136.0, 136.5, 138.2, 143.0, 201.1. HPLC (Daicel Chiralcel OD-H, 20°C, n-hexane/i-PrOH 98.5/1.5, flow rate: 0.65 mL/min, λ = 254 nm): t_R = 17.0 min, t_R = 21.2 min.

Naphthalen-2-yl(-3-phenylbicyclo[2.2.2]oct-5-en-2-yl)methanone *(Entry 7, Table 3.3).* Prepared using GP from (E)-1-(2-methoxyphenyl)-3-phenylprop-2-en-1-one and 1,3-cyclohexadiene, yield ~ 70%, separated using flash column chromatography using cyclohexane: ethyl acetate (50/1) as eluent. ^{1}HNMR (400 MHz, $CDCl_3$, 25 °C): δ = 1.16 (m, 1H) 1.56 (m, 1H), 1.91 (m, 2H), 2.67 (s, 1H) 3.06 (m, 1H), 3.43 (m, 1H), 3.93 (m, 1H, 6.21 (m, 1H), 6.56 (m, 1H), 7.25 (2H), 7.34 (3H), 7.48 (m, 1H), 7.55 (m, 1H), 7.73 (m, 1H), 7.83 (m, 1H), 7.95 (m, 1H), 8.24(m,1H). ^{13}CNMR (100 MHz, $CDCl_3$): δ = 18.7, 26.3, 34.3, 36.6, 45.4, 51.6, 124.5, 126.3, 127.6, 128.5, 129.5, 130.1, 131.4, 132.4, 133.6, 135.4, 135.8, 143.0, 204.4. HPLC (Daicel Chiralcel OD-H, 20°C, n-hexane/i-PrOH 98.5/1.5, flow rate: 0.65 mL/min, λ = 254 nm): t_R = 21.2 min, t_R = 26.3 min.

1,1'-Biphenyl]-4-yl(-3-phenylbicyclo[2.2.2]oct-5-en-2-yl)methanone *(Entry 6, Table 3.3).* Prepared using GP from (E)-1-([1,1'-biphenyl]-4-yl)-3-phenylprop-2-en-1-one and 1,3-cyclohexadiene, yield ~ 70%, separated using flash column chromatography using cyclohexane: ethyl acetate (50/1) as eluent. ^{1}HNMR (400 MHz, $CDCl_3$, 25 °C): δ = 1.14 (m, 1H), 1.50 (m, 1H), 1.88 (m, 2H), 2.70 (m, 1H), 3.02 (m, 1H), 3.50 (m, 1H), 3.83 (m, 1H), 6.15 (m, 1H), 6.57 (m, 1H), 7.21 (m, 1H), 7.32 (m, 4H), 7.38 (m, 1H), 7.45 (m, 2H), 7.60 (m, 4H), 7.94 (m, 2H). ^{13}CNMR (100 MHz, $CDCl_3$): δ = 18.9, 26.8, 35.1, 37.1, 45.1, 51.3, 126.5, 127.5, 127.6, 128.6, 128.8, 129.3, 129.4, 131.2, 135.7, 136.6, 140.3, 143.3, 145.6, 200.5. HPLC (Daicel Chiralcel OD-H, 20°C, n-hexane/i-PrOH 98.5/1.5, flow rate: 0.65 mL/min, λ = 254 nm): t_R = 14.2 min, t_R = 16.0 min.

6.6 General procedure for hydrosilylation reactions

In a typical experiment, a J. Young NMR tube was charged with the catalyst, $NaBAr^{Cl}{}_4$, and the internal standard, 1, 3, 5-trismethoxybenzene inside the glove box. The mixture is then dissolved in $CDCl_3$. Next, the respective substrate (1.0 mmol) and $HSiEt_3$/ other silane (1.1 mmol) were added to the catalyst mixture. The NMR tube was then sealed with a Teflon cap and the reaction progress was followed by ^1H NMR spectroscopy until quantitative conversion of the substrate was achieved. Once the completion was achieved, the reaction mixture was extracted with hexane, and the resulting extraction was dried using a rotary evaporator and the samples were analysed. Some non-sensitive products were further purified using a short silica column and chromatographed using a mixture of hexane basified with triethyl amine (NEt_3). The solvent was removed under reduced pressure to yield the pure silyl ethers.

Triethyl(1-phenylethoxy)silane *(Entries 1-7, Table 4.1).* Prepared using GP from acetophenone and triethyl silane with a yield of ~ 98 % as light-yellow oil. ^1H NMR ($CDCl_3$, 400 MHz, 25 °C): δ = 0.68-0.81 (m, 6H), 1.09 (t, $^3J_{HH}$ = 7.9 Hz, 9H), 1.60 (d, $^3J_{HH}$ = 6.4 Hz, 3H), 5.01 (q, $^3J_{HH}$ = 6.3 Hz, 1H), 7.31-7.38 (m, 1H), 7.40-7.47 (m, 2H), 7.47-7.53 (m, 2H). ^{13}CNMR (100 MHz, $CDCl_3$): δ = 4.5, 6.4, 26.8, 70.4, 124.8, 126.1, 127.8, 146.2.

(Benzhydryloxy)triethylsilane *(Entry 2, Table 4.2).* Prepared using GP from benzophenone and triethyl silane with a yield of ~ 97 % as a colorless oil. ^1H NMR ($CDCl_3$, 400 MHz, 25 °C): δ = 0.46 (q, $^3J_{HH}$ = 7.9 Hz, 6H), 0.85 (t, $^3J_{HH}$ = 8.0 Hz, 9H), 5.94 (s, 1H), 7.05– 7.09 (m, 2H), 7.13-7.17 (m, 8H). ^{13}C NMR (100 MHz, $CDCl_3$): δ = 4.9, 6.8, 64.0, 126.4, 126.9, 128.2, 145.3.

Triethyl((4-phenylbut-3-en-2-yl)oxy)silane *(Entry 3, Table 4.2).* Prepared using GP from 4-phenylbut-3-en-2-one and triethyl silane with a yield of ~ 98 % as a yellow solid. ^1H NMR ($CDCl_3$, 400 MHz, 25 °C): δ = 0.89 (q, $^3J_{HH}$ = 7.5 Hz, 6H), 1.27 (t, $^3J_{HH}$ = 8.0 Hz, 9H), 1.53

(d, $^{3}J_{HH}$ = 6.2 Hz, 3H), 3.21 (m, 1H), 6.21 (m, 1H), 6.42 (m, 1H), 7.19– 7.25 (m, 1H), 7.33-7.39 (m, 4H). ^{13}C NMR (100 MHz, $CDCl_3$): δ = 8.3, 14.1, 22.6, 31.5, 125.4, 128.4, 128.5, 128.7, 128.8, 129.7, 128.0, 136.8.

(1,3-(diphenylallyl)oxy)triethylsilane *(Entry 4, Table 4.2)*. Prepared using GP from trans-chalcone and triethyl silane with a yield of ~ 98 % as a white solid. ^{1}H NMR ($CDCl_3$, 400 MHz, 25 °C): δ = 0.46 (m, 6H), 0.85 (t, $^{3}J_{HH}$ = 8.0 Hz, 9H), 5.57 (m, 1H), 4.43 (m, 1H), 6.27 (m, 1H), 6.35 (m, 1H), 7.17– 7.24 (m, 4H), 7.30-7.40 (m, 1H). ^{13}C NMR (100 MHz, $CDCl_3$): δ = 6.7, 11.3, 78.6, 126.4, 127.0, 127.4, 127.8, 128.5, 128.5, 128.7, 128.9, 130.0, 130.0, 131.2, 140.1

(Cyclohexyloxy)triethylsilane *(Entry 5, Table 4.2)*. Prepared using GP from cyclohexanone and triethyl silane with a yield of ~ 95 % as a colourless oil. ^{1}H NMR ($CDCl_3$, 400 MHz, 25 °C): δ = 0.60 (m, 6H), 0.96 (t, $^{3}J_{HH}$ = 8.0 Hz, 9H), 1.17-1.29 (m, 5H), 1.50 (m, 1H), 1.6-1.72 (m, 4H), 3.55 (m, 1H). ^{13}C NMR (100 MHz, $CDCl_3$): δ = 6.8, 11.2, 23.8, 23.8, 27.0, 35.6, 35.6, 77.8.

(Cyclopentyloxy)triethylsilane *(Entry 6, Table 4.2)*. Prepared using GP from cyclopentanone and triethyl silane with a yield of ~ 96 % as a colourless oil. ^{1}H NMR ($CDCl_3$, 400 MHz, 25 °C): δ = 0.67 (m, 6H), 0.94 (t, $^{3}J_{HH}$ = 8.0 Hz, 9H), 1.60-1.62 (m, 4H), 1.71-1.82 (m, 4H), 7.51-7.56 (m, 2H), 7.88-7.90 (m, 2H). ^{13}C NMR (100 MHz, $CDCl_3$): δ = 6.8, 11.3, 24.0, 24.2, 38.3, 38.5, 78.6.

((9H-fluoren-9-yl)oxy)triethylsilane *(Entry 7, Table 4.2)*. Prepared using GP from 9-fluorenone and triethyl silane with a yield of ~ 97 % as a yellow solid. ^{1}H NMR ($CDCl_3$, 400 MHz, 25 °C): δ = 0.67 (m, 6H), 0.94 (t, $^{3}J_{HH}$ = 8.0 Hz, 9H), 5.92 (s, 1H), 7.27-7.36 (m, 4H), 3.61 (m, 1H). ^{13}C NMR (100 MHz, $CDCl_3$): δ = 6.8, 11.2, 85.6, 125.9, 126.1, 126.2, 126.4, 126.8,126.9, 128.0, 128.1, 141.8, 141.9, 150.0, 151.1.

(1-([1,1'-biphenyl]-4-yl)ethoxy)triethylsilane *(Entry 8, Table 4.2)*. Prepared using GP from 1-([1,1'-biphenyl]-4-yl)ethan-1-one and triethyl silane with a yield of ~ 95 % as a light-yellow solid. ^{1}H NMR ($CDCl_3$, 400 MHz, 25 °C): δ = 0.57 (m, 6H), 0.90 (t, $^{3}J_{HH}$ = 8.0 Hz, 9H), 1.42 (d, $^{3}J_{HH}$ = 6.5 Hz, 3H), 4.86 (q, $^{3}J_{HH}$ = 6.2 Hz, 1H), 7.21-7.25 (m, 2H), 7.31-7.36 (m, 3H), 7.47-7.53 (m, 4H). ^{13}C NMR (100 MHz, $CDCl_3$): δ = 6.8, 11.2, 23.9, 75.5, 127.9 (x3), 128.1 (x2), 129.0 (x2), 139.4, 139.6 141.8, 141.7.

(1-(2-bromophenyl)ethoxy)triethylsilane *(Entry 9, Table 4.2)*. Prepared using GP from 2'-bromoacetophenone and triethyl silane with a yield of ~ 98 % as a colourless oil. ^{1}H NMR (400 MHz, $CDCl_3$, 25 °C): δ = 0.55 (q, J = 8.0 Hz, 6H), 0.89 (t, $^{3}J_{HH}$ = 8.0 Hz, 9H), 1.36 (d, $^{3}J_{HH}$ = 6.4 Hz, 3H), 4.80 (q, $^{3}J_{HH}$ = 6.4 Hz, 1H), 7.19 (m, 2H), 7.40 (m, 2H). ^{13}C NMR (100 MHz, $CDCl_3$): δ = 5.0, 6.2, 24.8, 70.2, 121.0, 127.1, 127.8, 128.4, 132.5, 145.3.

Triethyl(1-(p-tolyl)ethoxy)silane *(Entry 10, Table 4.2)*. Prepared using GP from 4'-methylacetophenone and triethyl silane with a yield of ~ 98 % as a white solid. ^{1}H NMR (400 MHz, $CDCl_3$, 25 °C): δ = 0.54 (q, $^{3}J_{HH}$ = 8.0 Hz, 6H), 0.89 (t, $^{3}J_{HH}$ = 8.0 Hz, 9H), 1.37 (d, $^{3}J_{HH}$ = 6.4 Hz, 3H), 2.31 (s, 3H), 4.80 (q, $^{3}J_{HH}$ = 6.3 Hz, 1H), 7.08 (m, 2H), 7.19 (m, 2H). ^{13}C NMR (100 MHz, $CDCl_3$): δ = 5.2, 6.8, 21.2, 23.9, 74.8, 125.0, 125.2, 128.2, 128.5, 137.5, 138.9.

Triethyl(1-(4-methoxyphenyl)ethoxy)silane *(Entry 11, Table 4.2)*. Prepared using GP from 4'-methoxyacetophenone and triethyl silane with a yield of ~ 96 % as a light-yellow solid. ^{1}H NMR (400 MHz, $CDCl_3$, 25 °C): δ = 0.51 (q, $^{3}J_{HH}$ = 8.0 Hz, 6H), 0.82 (t, $^{3}J_{HH}$ = 8.0 Hz, 9H), 1.67 (d, $^{3}J_{HH}$ = 6.4 Hz, 3H), 2.31 (s, 3H), 3.79 (s, 3H), 4.56 (q, $^{3}J_{HH}$ = 6.3 Hz, 1H), 6.89 (m, 2H), 7.17 (m, 2H). ^{13}C NMR (100 MHz, $CDCl_3$): δ = 5.9, 10.2, 23.9, 57.8, 115.2, 115.674.8, 126.7, 126.8 133.5, 160.1.

(Benzyloxy)triethylsilane *(Entry 12, Table 4.2*). Prepared using GP from benzaldehyde and triethyl silane with a yield of ~ 98 % as a colourless oil. ^{1}H NMR (400 MHz, $CDCl_3$, 25 °C): δ

= 0.51 (q, $^{3}J_{HH}$ = 8.0 Hz, 6H), 0.82 (t, $^{3}J_{HH}$ = 8.0 Hz, 9H), 4.69 (s, 2H), 7.09 – 7.39 (m, 5H). ^{13}C NMR (100 MHz, $CDCl_3$): δ = 5.5, 8.9, 65.0, 127.3, 127.5, 128.5, 128.6, 140.6.

((2,6-dimethylbenzyl)oxy)triethylsilane *(Entry 13, Table 4.2*). Prepared using GP from 2,3-dimethylbenzaldehyde and triethyl silane with a yield of ~ 98 % as a colourless oil. ^{1}H NMR (400 MHz, $CDCl_3$, 25 °C): δ = 0.63 (q, $^{3}J_{HH}$ = 8.0 Hz, 6H), 0.96 (t, $^{3}J_{HH}$ = 8.0 Hz, 9H), 2.37 (s, 6H), 4.69 (s, 2H), 6.89 – 7.11 (m, 3H). ^{13}C NMR (100 MHz, $CDCl_3$): δ = 10.5, 14.2, 20.5, 64.5, 127.3, 127.5, 127.6, 135.5, 140.0, 140.2.

((2-bromobenzyl)oxy)triethylsilane *(Entry 14, Table 4.2*). Prepared using GP from 2-bromobenzaldehyde and triethyl silane with a yield of ~ 98 % as a yellow oil. ^{1}H NMR (400 MHz, $CDCl_3$, 25 °C): δ = 0.61 (q, $^{3}J_{HH}$ = 8.0 Hz, 6H), 0.91 (t, $^{3}J_{HH}$ = 8.0 Hz, 9H), 4.67 (s, 2H), 7.00 (m, 1H), 7.19 (m, 1H), 7.35 (m, 1H), 7.48 (m, 1H). ^{13}C NMR (100 MHz, $CDCl_3$): δ = 8.9, 11.2, 64.7, 126.8, 127.8, 129.5, 129.3, 132.5, 138.9.

(Cinnamyloxy)triethylsilane (*Entry 15, Table 4.2*). Prepared using GP from cinnamaldehyde and triethyl silane with a yield of ~ 98 % as a pale-yellow oil. ^{1}H NMR (400 MHz, $CDCl_3$, 25 °C): δ = 0.56 (q, J = 8.0 Hz, 6H), 0.90 (t, $^{3}J_{HH}$ = 8.0 Hz, 9H), 4.24 (dd, $^{3}J_{HH}$ = 5.2, 1.6 Hz, 2H), 6.21 (m, 1H), 6.49 (m, 1H), 7.09 (m, 1H), 7.18 (m, 2H), 7.27 (m, 2H). ^{13}C NMR (100 MHz, $CDCl_3$): δ = 8.9, 11.0, 60.2, 122.5, 126.8, 128.3, 128.5, 128.6, 128.8, 129.5, 133.5, 136.9.

N-benzyl-1,1,1-triethyl-N-phenylsilanamine (*Entry 15, Table 4.2*). Prepared using GP from N-benzylideneaniline and triethyl silane with a yield of ~ 99 %. ^{1}H NMR (400 MHz, $CDCl_3$, 25 °C): δ = 0.80 (q, $^{3}J_{HH}$ = 8.0 Hz, 6H), 0.94 (t, $^{3}J_{HH}$ = 8.0 Hz, 9H), 4.51 (s, 2H), 6.72 (t, $^{3}J_{HH}$ = 7.3 Hz, 1H), 6.87 (d, $^{3}J_{HH}$ = 7.8 Hz, 2H), 7.04-7.11(m, 3H), 7.18 (d, $^{3}J_{HH}$ = 4.6 Hz, 4H). ^{13}C NMR (100 MHz, $CDCl_3$): δ = 5.9, 8.0, 59.9, 117.2 (x2), 118.5 (x2), 120.9, 126.4, 126.6, 126.8, 128.3, 128.5, 141.8, 150.1.

6.7 General procedure for asymmetric hydrosilylation reactions

In a typical experiment, a J. Young NMR tube was charged with the catalyst and $NaBAr^{Cl}{}_4$ inside the glove box. The mixture is then dissolved in $CDCl_3$. Next, 1.0 mmol of acetophenone and 1.1 mmol of $HSiEt_3$ were added to the catalyst mixture. The NMR tube was then sealed with a Teflon cap and the reaction progress was followed by ^1H NMR spectroscopy until quantitative conversion of the substrate was achieved. Once the completion was achieved, the reaction mixture was transferred to a vial with Et_2O, 1M NaOH and methanol, capped and was kept stirring at RT for about 2 weeks. The resulting solution was extracted with Et_2O and dried with anhydrous $MgSO_4$. The solvent was removed under reduced pressure to yield the alcohol product.

1-phenylethan-1-ol (*Table 4.3*). ^1H NMR (400 MHz, $CDCl_3$, 25 °C): δ = 1.42 (d, $^3J_{HH}$ = 6.5 Hz, 3H), 1.71 (s, 1H), 4.82 (q, $^3J_{HH}$ = 6.5 Hz, 1H), 7.18-7.22 (m, 1H), 7.25-7.31 (m, 4H). ^{13}C NMR (100 MHz, $CDCl_3$): δ = 23.0, 70.1, 127.3, 127.4, 127.8, 128.9, 129.0, 146.5. (Daicel Chiralcel OD-H, 20°C, n-hexane/i-PrOH 90/10, flow rate: 0.65 mL/min, λ = 254 nm): t_R = 8.8 min, t_R = 9.9 min.

References

1 S. Dai, S. Zhou, W. Zhang and C. Chen, *Macromolecules*, 2016, **49**, 8855–8862.

2 P. Shaykhutdinova and M. Oestreich, *Organometallics*, 2016, **35**, 2768–2771.

3 S. Nair, J. R. Zeevaart and R. Hunter, *Arkivoc*, 2020, **2020**, 90–102.

4 R. E. H. Kuveke, L. Barwise, Y. Van Ingen, K. Vashisth, N. Roberts, S. S. Chitnis, J. L. Dutton, C. D. Martin and R. L. Melen, *ACS Cent. Sci.*, 2022, **8**, 855–863.

5 P. I. Binda, S. Abbina and G. Du, *Synthesis (Stuttg).*, 2011, **2011**, 2609–2618.

6 V. H. G. Rohde, M. F. Müller and M. Oestreich, *Organometallics*, 2015, **34**, 3358–3373.